Applications of Quantum Operations with Indefinite Time Direction

A Thesis

submitted to
Indian Institute of Science Education and Research Pune
in partial fulfillment of the requirements for the
BS-MS Dual Degree Program

by

Gaurang Agrawal

Indian Institute of Science Education and Research, Pune
Dr Homi Bhabha Road
Pashan, Pune 411008, India.

May, 2025

Supervisor: Prof. Aditi Sen De

Certificate

This is to certify that this dissertation entitled **Applications of Quantum Operations with Indefinite Time Direction** towards the partial fulfilment of the BS-MS degree at the Indian Institute of Science Education and Research, Pune represents study/work carried out by Gaurang Agrawal at Harish-Chandra Research Institute, Prayagraj (Allahabad) under the supervision of Prof. Aditi Sen De, Professor, Department of Physics, during academic year 2024 - 2025.

Aditi Sen(De)

Prof. Aditi Sen De

Committee:
Supervisor: Prof. Aditi Sen De
Expert: Prof. T. S. Mahesh

This thesis is dedicated to my family and friends.

Declaration

I hereby declare that the matter embodied in the report entitled **Applications of Quantum Operations with Indefinite Time Direction** are the results of the work carried out by me at Harish-Chandra Research Institute, Prayagraj (Allahabad), under the supervision of Prof. Aditi Sen De and the same has not been submitted elsewhere for any other degree. Whenever others contribute, every effort is made to indicate this clearly, with due reference to the literature and acknowledgement of collaborative research and discussions.

Gaurang Agrawal
20201049

List of Publications

Parts of this thesis are based on our preprint [1] that was prepared during my MS thesis project. The preprint is available on arXiv.

1. Gaurang Agrawal, Pritam Halder, and Aditi Sen De. Indefinite Time Directed Quantum Metrology. arXiv, February 2025.

Acknowledgements

I am deeply indebted to my advisor, Prof. Aditi Sen De, whose unwavering support, guidance, and mentorship have shaped not only this work but my entire journey in academic research. Her wisdom, patience, and nurturing approach to mentorship have been foundational in cultivating the scholar I am today. The Aditi group, under her leadership, has become more than a research team, it has been a family, and for that, I am eternally grateful.

I extend my sincere gratitude to Prof. Deepak Dhar, who enabled me to pursue numerous intriguing projects and research ideas. His unwavering commitment and dedication to supporting his students are truly unparalleled. The invaluable advice he shared during my early presentations is something I will always carry with me.

I am profoundly grateful to Dr. Matt Wilson for introducing me to the exhilarating landscape of categorical quantum mechanics and higher-order quantum theory. He guided me from wondering how researchers develop cool formalisms and ideas to creating my own. His insightful perspectives and collaborative spirit are qualities I will carry forward into our future works.

Many thanks to Sachin, Ritesh, Debargya, and Dhruv, the individuals closest to me during this journey for making this place feel like home. I will forever cherish the laughs,banters and late night walks.

Special thanks to my seniors at HRI Pritam, Tanoy, Ganesh, and Ayan for patiently addressing all my queries, no matter how trivial. I am particularly grateful to Pritam for his constant guidance throughout this thesis. I also extend heartfelt thanks to Pratham, Ritopriyo, and Stavya for their advice, friendship, and unwavering camaraderie.

Finally, I would like to thank my parents, my sister, and Baba for the endless moments of joy, love, and care. None of this would have been possible without all of you.

Abstract

This thesis investigates higher-order quantum operations, particularly those exhibiting the property of indefinite time direction (ITD) and their applications to quantum metrology and capacity enhancement. We begin by surveying higher-order quantum theory and examining indefinite causal order (ICO). We focus on the quantum switch, a well-established higher-order operation that implements a causal superposition of two quantum channels. Then we introduce quantum operations with indefinite time directions and the quantum time flip supermap. We go on to introduce classical and quantum metrology and ICO-assisted metrology, which eventually leads to a brief tour of optimal metrology where we illustrate known semidefinite programming algorithms for optimizing metrological protocols.

Our work makes two primary contributions: First, we introduce a novel framework for quantum metrology using indefinite time direction operations. We develop a universal protocol that achieves Heisenberg-limited precision for parameter estimations of unitaries, demonstrating its effectiveness in phase and axis estimation tasks. Notably, we prove that this quantum advantage does not require entanglement, establish the optimality of symmetric pure product states, and show that our approach remains effective even with simplified measurement strategies and under realistic noise conditions.

Second, we explore the enhancement of classical communication capacity through the combined application of ICO and ITD operations. In order to accomplish this, we survey existing literature in quantum capacity and capacity enhancement with various supermaps, including quantum switch, SDPPs, half-switch and quantum time flip. Finally, by composing quantum switch and quantum time flip supermaps, we demonstrate capacity enhancements (Holevo bound) exceeding those achievable with either operation alone. We interpret the obtained results and discuss potential future research directions, including optimizing indefinite time-directed metrology and identifying justifications for the additional capacity enhancement, as well as figuring out optimal protocols when both flip and switch are available.

Our results contribute to the growing understanding of higher-order quantum operations and their practical applications in quantum technologies, highlighting how these operations enable novel approaches to fundamental information processing tasks.

Contents

Front Matter ii

List of Figures xx

List of Tables xxii

1 Introduction 1

2 Indefiniteness in Causal Order and Time Direction 3

2.1 Higher-Order Quantum Operations 5

2.2 Indefinite Causal Order 8

2.3 Indefinite Time Direction 11

3 Quantum Metrology 14

3.1 Metrology 14

3.1.1 Classical Case 14

3.1.2 Quantum Case 16

3.1.3 Multiparameter estimation 17

3.2 Indefinite Causal Order in Metrology 18

3.3 Optimal Metrology 20

4 Indefinite Time Directed Metrology 23

4.1 Introduction 23

4.2 Framework for Indefinite time directed metrology (ITDM) 26

4.2.1 Time-flipped encoding stratgey 27

4.2.2 Quantum Fisher information in ITDM 27

4.3 Estimating phases with ITDM 30

4.3.1 Classical Fisher Information by projective measurement on control qubit 32
4.4 Entanglement can not beat N^2-scaling 35
4.5 Advantage in noisy Unitary encoding 37
4.5.1 Comparison of NITDM with “switched” and regular strategy in single qubit 38
4.5.2 Advantage in multiqubit strategy 41

5 Capacity Enhancement with Supermaps 44

5.1 Quantifying Quantum Communication 44
5.1.1 Capacity Enhancement with Quantum Switch 46
5.1.2 Capacity Enhancement with SDPPs 49
5.1.3 Capacity Enhancement by Coherent Control 49
5.2 Communication as a Resource Theory 50
5.3 Capacity Enhancement with Quantum Time Flip 52
5.4 Capacity Enhancement with the Combination of Flip and Switch 53

6 Conclusion 57

7 Appendix 60

7.1 Calculation of QFI for a general Product state 60
7.2 Proof of Theorem 1 61
7.3 Proof of $A + B \leq 1$ in Theorem 3 62
7.4 Axis Estimation with ITDM 63
7.5 Spectrum of $U_\theta^\dagger U_\theta^T$ 64
7.6 FI for small values of θ 65
7.7 Proof of Theorem 6 66
7.8 Demonstration of advantage in $N = 1$ for nonoptimal encoding 70
7.9 θ-averaged performance of single qubit-NITDM 72
7.10 θ-averaged performance of multiqubit-NITDM 74

List of Figures

2.1 Composition of quantum combs. 6

2.2 A process matrix W acting on the quantum operations of Alice and Bob. . . 9

2.3 A global process M acting on the quantum operation of Alice. 12

3.1 ICO metrology protocol from Ref. [2]. 18

3.2 Obtainable Fisher information using quantum Switch and conventional non-switch method on a single probe. 19

3.3 Optimal Quantum Fisher information for different sets of strategies. 22

4.1 ITDM scheme. 26

4.2 QFI obtained by the optimal states using 3-qubit probe states for difference axis. 37

4.3 Fisher information with respect to noise parameter q. Comparison between time-flipped, "switched" and regular strategies. 40

4.4 Fisher information with respect to number or qubits N for different values of noise parameter q. Competition between Flip and regular strategy. 42

5.1 Employing quantum switch for capacity enhancement. 47

5.2 Capacity of regular depolarising channel and causally activated depolarising channel. 48

5.3 Half Switch Circuit. 50

5.4 Flip capacity enhancement protocol. 52

5.5 Capacity of regular depolarising channel DPC, DPC under quantum switch and DPC under quantum time flip. 53

5.6 Switch $\circ$ Flip and Flip $\circ$ Switch strategies for capacity enhancement. 54

5.7 Capacities enhancement due to different quantum supermaps. 55

7.1 Value of $x + y$ against noise strength q, and paramater θ 71
7.2 Fisher information, $\mathcal{F}_{\theta}^{q}, \mathcal{F}_{\theta}^{q,S}$ and QFI, $\mathcal{Q}_{\theta}^{q,R}$ with respect to noise parameter q. Comparison between Flip, Switch, and regular strategies for $n_2 \neq 1$. . . . 72
7.3 Comparison between Flip and switch strategy on average. Variation of $\langle \mathcal{F}_{\theta}^{q} \rangle - \langle \mathcal{F}_{\theta}^{q,S} \rangle$ against n_2 and noise strength q. 73
7.4 Advantage of average performance of multi-qubit NITDM and regular strategy. 73

List of Tables

7.1 Given two values of q, the maximum value of both θ-averaged FI, $\max_N \langle \mathcal{F}_\theta^q \rangle$ and θ-averaged FI per qubit, $\langle \tilde{\mathcal{F}}_\theta^q \rangle / \tilde{N}$, and the corresponding number of qubits for each maximum value are listed from Fig. 7.4. 74

Chapter 1

Introduction

While traditional formulations of quantum theory revolve around quantum states and channels, in recent times, there has been an ever-growing interest towards higher-order quantum operations, i.e., operations which input or output a quantum channel or other higher-order quantum operations. A well known example of such operations is that of a quantum switch [3], which takes in a pair of channels and outputs a causal superposition of the two. While being a particularly fascinating example among the various possible higher-order operations particularly for its indefinite causal ordered (ICO) nature [4, 5], over the years quantum switch has found plenty of applications and has shown a number of advantages in state and channel discrimination [6–9], communication [10–17], thermodynamics [18–21] and metrology [2, 22–29] with many experimental realizations of itself [30–33] and the proposed advantages [27, 28, 34–38]. A detailed description of the experiments and applications of quantum switch and indefinite causal order was given in [39]. These experiments and applications have shown the potential of higher-order quantum maps towards quantum technologies.

More recently, a new broader class of such idiosyncratic higher-order operations has been discovered, which are called quantum operations with indefinite time (ITD) or input-output direction [40, 41]. These can not be written as convex combinations of any definite time directed operations. Like Hadamard gates, which allow us to access and ask new questions to quantum states, these supermaps allow us to posit new questions, protocols and strategies to know about quantum channels. The paradigmatic example of such operations is quantum time flip [40, 42], which takes as an input a single instance of a bistochastic channel $\mathcal{C}$ and outputs a channel with a superposition of the original channel with its input-output reversed counterpart $\mathcal{T}(\mathcal{C})(\rho_c \otimes \rho) = \sum_i T_i(\rho_c \otimes \rho)T_i^\dagger$ with $T_i(\mathcal{C}) = |0\rangle\langle 0| \otimes \mathcal{C}_i + |1\rangle\langle 1| \otimes \Theta(\mathcal{C}_i)$

where $\mathcal{C}_i$, are the Kraus operators of the input channel and T_i are the Kraus operators of the output channel and Θ is the time reversal operator. Similar to quantum switch, quantum time flip has shown promising applications in certain discrimination tasks [40, 43], Communication [42], non-Markovinity [44], and metrology [45] some of which have been demonstrated experimentally [43, 45–47]

In this work, we explore these newfound operations in detail and introduce their novel applications to quantum metrology and quantum communications. In particular, we introduce a novel framework for the applications of quantum operations with indefinite input-output direction towards quantum metrology. We exploit the properties of quantum time flip to access a channel from both directions and devise a universal protocol to achieve Heisenberg limit for parameter-dependent bistochastic channels. Here, by universal, we mean that the same protocol is applicable to achieve the said advantages with arbitrary bistochastic channels with arbitrary parametrizations. We ascertain the applicability of our method by employing it for phase estimation and axis estimation tasks. By doing so, we show that entanglement is not a necessary resource for what we call Indefinite time directed metrology (ITDM). Among product states, we prove the optimality of symmetric pure product states and show that a higher scaling of quantum Fisher information is not attainable even with entanglement. We also present a more practical setting where measurement is done on the single control qubit in the fixed $|\pm\rangle$ basis and show that the attained Fisher Information can still achieve the Heisenberg limit. Finally, we analyze our strategy under the limit of small parameters, derive its behaviour under depolarizing noise and present various cases where our strategy is advantageous.

On the communications front, we access the classical capacity enhancement provided by ITD and ICO strategies in conjunction. Following the work of [42], which demonstrated the advantages of quantum time flip in classical capacity enhancement and sought investigation of cases where both ICO and ITD are employed for capacity enhancement. We employ compositions of quantum switch and quantum time flip supermaps and demonstrate that the capacity enhancement provided in such cases is higher than what is provided by any number of switches and flips alone. We explore the reasons behind this advantage and suggest future research directions. Lastly, other possible applications of ITD operations in various tasks, such as channel discrimination and query complexity, are discussed.

Chapter 2

Indefiniteness in Causal Order and Time Direction

The quantum description of systems A, B, and the transformations between them $A \to B$ is given by quantum states and channels. Mathematically these states are linear operators on the Hilbert spaces $\mathcal{H}_A$, and $\mathcal{H}_B$ known as density matrices $\rho_A \in \mathcal{L}(\mathcal{H}_A)$, which are hermitian $\rho_A = \rho_A^\dagger$, positive $\rho_A \geq 0$, and normalized $\mathrm{Tr}[\rho_A] = 1$, while the quantum channels $\mathcal{C}$ are completely positive $\mathcal{I}_E \otimes \mathcal{C}(\rho_{EA}) \geq 0$ and trace preserving $\mathrm{Tr}[\mathcal{C}(\rho_A)] = \mathrm{Tr}[\rho_A]$ (CPTP) maps between these quantum states. The action of quantum channels on the density matrix can be evaluated by the Choi matrix [48] or Kraus decomposition [49] of the channel. If we denote the set of linear maps from $\mathcal{L}(\mathcal{H}_A)$ to $\mathcal{L}(\mathcal{H}_B)$ (a set which contains all quantum channels), as $\mathcal{L}(\mathcal{L}(\mathcal{H}_A), \mathcal{L}(\mathcal{H}_B))$, then there exists isomorphisms CJ and CJ^{-1} between the spaces $\mathcal{L}(\mathcal{L}(\mathcal{H}_A), \mathcal{L}(\mathcal{H}_B))$ and $\mathcal{L}(\mathcal{H}_A \otimes \mathcal{H}_B)$, given by

$$\mathrm{CJ} \ : \ \mathcal{C} \mapsto C \qquad C = \mathcal{I}_A \otimes \mathcal{C}(|n\rangle\rangle\langle\langle n|) \tag{2.1}$$

$$\mathrm{CJ}^{-1} \ : \ C \mapsto \mathcal{C} \qquad \mathcal{C}(\rho_A) = \mathrm{Tr}_A[(\rho_A^T \otimes I_B)C], \tag{2.2}$$

where $|n\rangle\rangle = \sum_i^{d_A} |i\rangle \otimes |i\rangle$ is an unnormalized maximally entangled state, I_B is identity on Hilbert space $\mathcal{H}_B$, and ρ^T denotes the transpose operator with respect to the basis $|i\rangle$. These isomorphisms hold additional properties, such as

$$\mathcal{I}_E \otimes \mathcal{C}(\rho_{EA}) \geq 0 \quad \forall\ \rho_{EA} \quad \Longleftrightarrow \quad C \geq 0 \tag{2.3}$$

$$\mathcal{C}(\rho)^\dagger = \mathcal{C}(\rho^\dagger) \quad \Longleftrightarrow \quad C^\dagger = C \tag{2.4}$$

$$\mathrm{Tr}[\mathcal{C}(\rho)] = \mathrm{Tr}[\rho] \quad \forall \rho \in \mathcal{L}(\mathcal{H}_A) \quad \Longleftrightarrow \quad \mathrm{Tr}_B[C] = I_A \tag{2.5}$$

$$\text{CJ: } \mathcal{C} \circ \mathcal{D} \quad \mapsto \quad C * D \tag{2.6}$$

where $*$ is the link product [50], with $C * D = Tr_{C \cup D}[(I_{D-C} \otimes C)^{T_{C\cup D}}(D \otimes I_{C-D})]$ and $C \cup D$ being systems common in C and D, and $C - D$ being systems in C and not in D. Furthermore, isomorphisms analogous to above, can also be established for pure quantum theory by CJ: $\mathcal{C} \mapsto C \quad C = \mathcal{I} \otimes \mathcal{U}|n\rangle\rangle$ with similar identities and link product properties. From the above results, known as Choi isomorphism, any quantum channel between systems $A \to B$ can be represented by a matrix known as its Choi matrix $\in \mathcal{L}(\mathcal{H}_A \otimes \mathcal{H}_B)$. If one finds the eigenvectors of this Choi matrix $|C\rangle_i$ and writes them in the form $|C\rangle_i = \mathcal{I}_A \otimes K_i\,|n\rangle\rangle$ then one obtains the Kraus operators of the channel K_i. Writing the Choi matrix in terms of these Kraus operators, it is clear that $C = \mathcal{I}_A \otimes \sum_i K_i(|n\rangle\rangle\langle\langle n|)K_i^\dagger$, and thus the channel can be given in terms of these as, $\mathcal{C}(\rho_A) = \sum_i K_i \rho_A K_i^\dagger$. The system evolves by the Kraus K_i by the probability $\mathrm{Tr}\left[K_i \rho_A K_i^\dagger\right]$. The experimenter could also forget or miss some information on which of the Kraus evolution has occurred and get a probabilistic mixture, i.e., $\sum_i K_{i,\sigma}\rho_A K_{i,\sigma}^\dagger$, which would instead signify a completely positive trace non increasing (CPTNI) evolution known as a quantum operation. Physically, these Kraus operators tell us what happens to the local open system when a global closed system (system + environment) evolves. Notably, the combined system evolves as

$$\rho_A \otimes |0\rangle\langle 0|_E \to K_0 \rho_A K_0^\dagger \otimes |0\rangle\langle 0|_E + K_1 \rho_A K_1^\dagger \otimes |1\rangle\langle 1|_E + ... + K_r \rho_A K_r^\dagger \otimes |r\rangle\langle r|_E\,, \tag{2.7}$$

which is an isometry. Completing this isometry on the dimensions of the environment shows that the evolution of a closed system must be unitary. A result known as the Stinespring dilation.

This completes a basic description of quantum theory in finite dimensions from the perspective of open system evolution. However, this is clearly not all that is possible. We considered states of quantum systems and transformations between these states, but we could have gone on and asked about the transformations between these transformations, the transformations thereof and all other 'sorts of transformation'. We could also wonder about the transformations from quantum channels to states and vice-versa. Vitally, such transformations do not limit themselves to mere mathematical curiosity. The task of quantum metrology is to convert a parameterized channel to an optimal state to be measured in order to extract information on that parameter. How to best communicate with quantum resources can be formalized as a resource theory in which the resources are the transformations between quantum channels. In general, whenever a theory is comfortable in talking about certain kinds of maps, the maps between these maps and so one tend to have important ramifications for the theory itself. Hence we ask: What are all such transformations? What is their mathematical structure? Do they have any interesting properties and ramifications for quantum theory? We answer these in the following section.

2.1 Higher-Order Quantum Operations

A general all-encompassing term for 'sorts of transformation' in the above discussion is that of a type. While type theory in itself is an important branch of mathematics, here we shall only discuss quantum types. We provide an inductive description of quantum types in line with Ref. [51]. We correspond every finite-dimensional quantum system to an elementary type A, the tensor product of two of such systems to type AB, and the type of system $\mathbb{C}^1$ to I. With these, we define the set of elementary types as Eletypes and our alphabet (set of all symbols) as $\aleph = \text{Eletypes} \cup \{(\} \cup \{)\} \cup \{\rightarrow\}$. Finally, we can define the set of quantum types as the smallest subset of the set of words (ordered sets with elements picked from the alphabet) of the alphabet $\aleph$ satisfying

1. Eletypes $\subset \aleph$
2. if $A, B \in$ Types then $(A \rightarrow B) \in$ Types

With the set of quantum types in hand, we can now formally discuss what sort of transformation is of concern. For instance, a d dimensional quantum state in the system A, which can be seen as a quantum channel from $\mathbb{C}^1$ to $\mathbb{C}^d$ now has type $I \rightarrow A$. While, the transformation between channels, i.e., a superchannel which takes a channel between systems A, B and converts it to a channel between systems C, D has a type $(A \rightarrow B) \rightarrow (C \rightarrow D)$. In general one can also talk about exotic types such as $A \rightarrow (B \rightarrow (C \rightarrow (D \rightarrow E)))$ and wonder about their quantum mechanical description. Since the elementary types are linear operators, by Choi isomorphisms, all of these types are also linear operators. The Choi characterization and other theorems on these types are available in Ref. [51]. Of course this is not the only possible type theory for quantum transformations. One can also conceive of a richer type theory with additional symbols for considering channels that are composed but must be non-signalling. Such a type theory with its category-theoretic description can be found in Ref. [52].

Certain kinds of quantum types are interesting. We can inductively define the notion of quantum combs, where the nth quantum comb takes the n-1th quantum comb as an input and outputs a channel. Formally, we define them as

1. $\mathrm{C}_1 = A \to B$
2. $\mathrm{C}_n = (\mathrm{C}_{n-1}) \to (A \to B)$

these quantum transformations, first introduced in [50, 53] contain quantum states, channels, and superchannels and mathematically formalize the transformations practically possible in gate-based quantum computing. Operationally, due to the quantum comb - memory channel realization theorem [53] which states that any quantum comb can be realized as a memory channel and vice versa, these combs come with a notion of circuit with holes, e.g., one can think of a n - quantum comb as a quantum circuit with n teeth and $n-1$ holes, where another quantum circuit with $n-1$ teeth and $n-2$ holes may slot in to output a quantum channel, see Fig. 2.1.

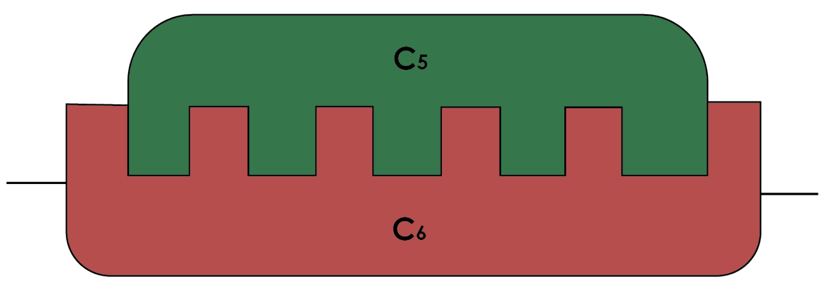

Figure 2.1: **Composition of quantum combs** A quantum comb C_6 which operationally corresponds to a quantum circuits with 5 holes takes as an input a quantum comb C_5 and outputs a quantum channel.

Before moving further, we shall first define signalling conditions. Physically, these are quantum information theoretic conditions to argue about cause-effect relations. We say that Alice can signal to Bob if she can affect Bob. Like many other definitions in quantum information theory, this is done by defining what non-signalling is. We say that Bob, denoted as B with input and output systems B_1, B_2, can not signal to Alice, denoted as A with input and output systems A_1, A_2 if, for the combined channel between their labs $\Phi : (A_1B_1) \to (A_2B_2)$ there exists a channel $\Phi' : A_1 \to A_2$ such that $Tr_{B_2}(\Phi) = \Phi' \otimes I_{B_1}$. Where Φ and Φ' are the Choi matrices of the respective channels. This depicts that when Alice's output is isolated, Bob's input can not affect her output. We denote Bob can not signal to Alice $A \leq B$. This is also known as one-way signalling, as there is at most one direction in which the signal can travel. This condition can be generalized; there can be N parties where the output of A_{ith} party is independent of the inputs of $A_{i+1}, A_{i+2}, \ldots, A_N$. By the above convention, this can be written as $A_1 \leq A_2 \leq \cdots \leq A_N$. Among any two parties, there can be cases where both parties may signal to each other: two-way signalling, one party is not able to signal to the other party: one-way signalling and no party is able to signal to each other: non-signalling. Interestingly, along with product channels $\Phi_A \otimes \Phi_B$, non-signalling may also contain cases where Alice and Bob possess shared entanglement. This is another way to say that shared entanglement does not enable faster than light communication since the involved transformations are still non-signalling. This signalling business may be seen as a bridge between general relativity and quantum theory.

Now, we shall return to quantum combs. Apart from their type-theoretic description, quantum combs can also be defined as circuits with certain causal / signalling relations. It can be shown that quantum combs are those quantum circuits with one-way signalling relations across their input-output pairs. These quantum combs, which are realizable as circuits with holes, depict an important physical principle: There exist quantum transformations which may not perform transformations from channel to channel but from a subset of channels to channel. A quantum comb C_3 strictly takes as input one-way signalling channels, C_2 and outputs a quantum channel. Moreover, this type has more elements than those of superchannels since superchannels may also take as input a one-way signalling channel and ouptut a channel. One can think of C_3 as superchannels C_2 with a restricted input space. Such a possibility raises an immediate question. What is the biggest possible set of realizable supermaps? Can we consider more restrictions? How about quantum transformations from product channels to channels? From non-signalling channels to channels? From unital product channels to channels? We shall answer these in the subsequent sections.

2.2 Indefinite Causal Order

One can define second-order causal SOC_n transformations [54] as those which take n product channels as input and output valid quantum channels. These have type $(A_1 \to A_2)(B_1 \to B_2)\ldots(N_1 \to N_2) \to (K_1 \to K_2)$. Since these can also be seen as quantum transformations from channels to channels but with an even more restricted input set, these sets of transformations are even bigger than quantum combs and contain all the previously named transformations. Alongside these, we may want to define transformations that take n non-signalling channels as input and output valid quantum channels. While these can not be assigned a proper type structure with the previously defined type theory, which does not have any symbol to ascertain the non-signalling behaviour, the type theory defined in Ref. [52] can accommodate and argue about such transformations as well. Fascinatingly [52] shows that this and the previously defined SOC_n transformations are type equivalent, e.g., any map which is an element of one type is also an element of the other.

In particular, since this type contains elements which do not lie in quantum combs, such quantum transformations can not be executed by standard gate-based quantum computing. This gives an immediate reason to study SOC_n from the point of view of quantum computation as they allow for quantum computations which are not possible otherwise. Indeed, instances of SOC_n have shown advantages in quantum query complexity and more recently have been shown to be unsimulable with even exponential queries to standard quantum circuits [55–61].

At the same time, the possibility of such transformation also raises deep questions about the very foundations of physics. General relativity defines events as points in spacetime where an event can only influence/signal to the other if the other lies in its causal future or future light cone. If these events are experiments performed by agents on their respective systems A, B, etc., this means that events must form a partial order. If point a lies in the future light cone of point b, then b does not lie in the future light cone of a (anti-symmetric), and if b lies in the future light cone of a and c lies in the future light cone of b, then c also lies in the future light cone of a (transitive). Since any partial order can be totalized, that is, it can be embedded in a total order, causal relations, according to general relativity, must be embeddable in a total order. At the same time, according to quantum theory, there is a possibility of operations other than quantum combs. That is, there are types such as SOC_n which contain operations not embeddable in any total order. Quantum theory, therefore, predicts the existence of operations with no global definite causal order. Such operations are called operations with indefinite causal order (ICO).

Originally ICO was defined along with the process matrix framework [4, 5]. In their original paper, Oreshkov, Costa, and Brukner argues for indefinite causal order in this manner: Suppose there are two distant agents Alice and Bob who perform experiments in their own respective labs. To be consistent with physical observations, we assume that in their labs, that is locally, Alice and Bob observe local definite causal order and quantum operations M_A and M_B. However, globally a definite causal order is not assumed and hence, it is possible that an operation is performed which takes Alice's and Bob's quantum operations as input and outputs a channel and such an operation would exhibit indefinite causal order. In their work Ref. [4] is restricted to output channels in $\mathbb{C}^1 \to \mathbb{C}^1$, that is their global operations takes a pair of quantum operations and outputs the probability of the overall process to happen, given those input quantum operations. Here, the rest of the global process $\mathcal{W}$, (see Fig. 2.2) is denoted by a process matrix which has a Choi W and the output probability is calculated via the generalised Born Rule, $P(M_A, M_B) = Tr\Big[W(M_A \otimes M_B)\Big]$. Even under these constraints they are able to come up with processes which can not be written as a probabilistic combination of a quantum combs and hence do not possess a definite causal order (see Fig. 2.2). Formally along the lines of the literature in entanglement theory such process are called causally inseparable.

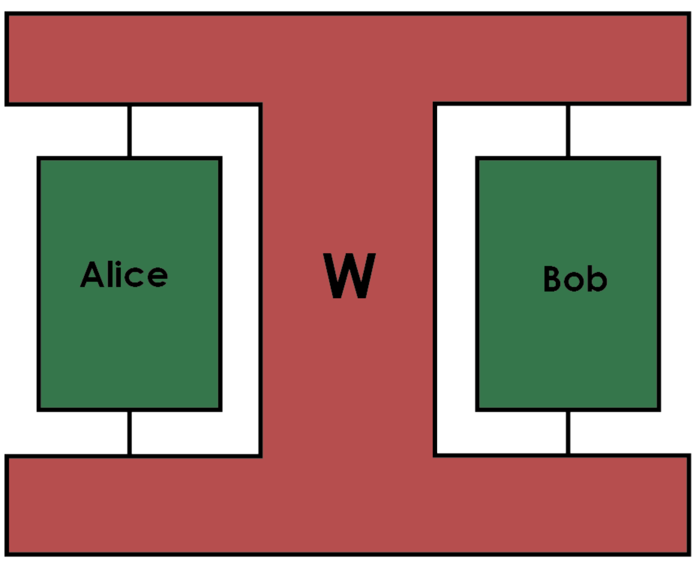

Figure 2.2: **A process matrix W acting on the quantum operations of Alice and Bob.** The process matrix W, takes as input the product of quantum operations of Alice and Bob and outputs the probability of the overall process.

To show that they indeed possess a process with indefinite causal order in Ref. [4] causal inequalities were devised. In particular a game, now known as the OCB game was proposed, where Alice and Bob possess random bits a and b. Bob is in possession of another random bit b' which determines the their goal. If $b' = 0$ then Bob has to communicate his bit b to Alice, if $b' = 1$ then Alice has to communicate her bit to Bob. It can be shown that using processes with definite causal order, it is not possible to win this game by a probability of more than 3/4. However, there is a quantum processes with indefinite causal order, the OCB process employing which, the game can be won by a probability of $\frac{2+\sqrt{2}}{4}$.

Ref. [4, 5], also provide the constrains on process matrices. In particular, for two party process matrix W, it must satisfy the following constraints.

$$\begin{aligned} W &\geq 0 \\ \mathrm{Tr}[W] &= d_{A_2} d_{B_2} \\ {}_{B_1B_2}W &= {}_{A_2B_1B_2}W \\ {}_{A_1A_2}W &= {}_{B_2A_1A_2}W \\ W &= {}_{B_2}W + {}_{A_2}W - {}_{A_2B_2}W, \end{aligned} \tag{2.8}$$

where A_1, A_2, B_1, B_2 are inputs and outputs of Alice and Bob respectively and the left subscript denotes a discard prepare channel ${}_iW = \frac{\mathbb{1}}{d_i} \otimes \mathrm{Tr}_i[W]$.

The framework can be modified, as is considered in subsequent works, see e.g., [62] to supermaps which output channels with arbitrary dimensions. A process is then defined as a bilinear supermap which takes a pair of local quantum channels $\mathcal{M}_A$ and $\mathcal{M}_B$ to a quantum channel $\mathcal{M}_C$. This has a Choi operator $W \in \mathcal{L}(\mathcal{H}_{C_1} \otimes \mathcal{H}_{A_1} \otimes \mathcal{H}_{A_2} \otimes \mathcal{H}_{B_1} \otimes \mathcal{H}_{B_2} \otimes \mathcal{H}_{C_2})$ such that $M_c = \mathrm{Tr}_{A_1A_2B_1B_2}\left[W^{T_{A_1A_2B_1B_2}}(M_A \otimes M_B)\right]$.

In Ref. [3], Chiribella et al. gave the description of one such quantum process, known as the quantum switch. A quantum switch supermap takes as an input a pair of channels $\mathcal{C}_A$ and $\mathcal{C}_B$ and outputs a quantum channel $\mathcal{S}$ such that $\mathcal{S}(\rho \otimes \rho_c) = \sum_i S_i \rho \otimes \rho_c S_i^\dagger$, and $S_i = C_{Ai}C_{Bi} \otimes |0\rangle\langle 0| + C_{Bi}C_{Ai} \otimes |1\rangle\langle 1|$ where, S_i are the Kraus operators of the output channel and C_{Ai}, C_{Bi} are the Kraus operators of the input channels. Operationally quantum switch outputs a composition of channels $\mathcal{C}_A$ and $\mathcal{C}_B$ with their causal order controlled by ρ_c. If $\rho_c = |0\rangle\langle 0|$ then $\mathcal{C}_A$ appears after $\mathcal{C}_B$, if $\rho_c = |1\rangle\langle 1|$ then $\mathcal{C}_A$ appears before $\mathcal{C}_B$ and when ρ_c is in a superposed state, say $\rho_c = |+\rangle\langle+|$, then the causal orders are superposed as well. This is sometimes phrased as 'causal order of channels being entangled with the control qubit'.

Apart from a significant theoretical interest, quantum switch has also presented significant advantages in various quantum information tasks, not possible by definite causally ordered strategies. In quantum metrology, enabling super-Heisenberg scaling and noise mitigation [2, 22–29], in state and channel discrimination, enabling perfect channel discrimination which is not possible via combs [6–9], enhancing communication capacity of depolarsing channel [10–17, 34–36], thermodynamical tasks including charging, refrigeration, work extraction, and activation of thermal states [18–21, 37, 38, 63]. Experimental implementations quantum switch and many of such protocols have also been realized [15, 17, 27, 28, 30–33, 35, 36, 39]. A thorough analysis of such experimental realisations and their implications were provided in Ref. [39].

2.3 Indefinite Time Direction

More recently, an even broader class of supermaps has been proposed, which are called quantum operations with indefinite time direction or indefinite input-output direction [40]. These are defined as quantum transformations from a probabilistic (convex) combination of the product of N bistochastic quantum channels to quantum channels. With even more constraints on the input channels, the set of these supermaps is even bigger and contains processes which can not be written as a probabilistic combination of processes with definite time direction.

To work more formally with time directions, an input-output inversion operator Θ is defined. Θ takes as input a quantum channel $\mathcal{A}: A_1 \to A_2$ and outputs a time reversed / input-output reversed channel $\Theta(\mathcal{A}): A_2 \to A_1$. In particular, it must satisfy the following properties.

Order reversing: $\Theta(\mathcal{A}\mathcal{B}) = \Theta(\mathcal{B})\Theta(\mathcal{A})$

Identity preserving: $\Theta(\mathcal{I}) = \mathcal{I}$

Distinctness preserving: $\mathcal{A} \neq \mathcal{B} \Rightarrow \Theta(\mathcal{A}) \neq \Theta(\mathcal{B})$

Compatibility with random mixtures: $\Theta(p\mathcal{A} + (1-p)\mathcal{B}) = p\Theta(\mathcal{A}) + (1-p)\Theta(\mathcal{B})$, Finally, after applying the time reversal operator on the channel, the output must also be a valid channel. Such channels are termed as bidirectional. In Ref. [40], it has been shown that the set of bidirectional processes coincides with bistochastic or unital channels. Hence, the input is constrained to probabilistic mixtures of products of unital channels. Moreover, the input-output inversion map Θ is shown to be unitarily equivalent to either $\mathcal{A}^\dagger : \mathcal{A}^\dagger(\rho) = \sum K_{Ai}^\dagger \rho K_{Ai}$ or $\mathcal{A}^T : \mathcal{A}^T(\rho) = \sum K_{Ai}^T \rho \bar{K_{Ai}}$. With input-output inversion in hand, it has been shown that a supermap which takes such a bistochastic channel and outputs valid channels may have quantum operations which can not be written as probabilistic combinations of forward and backward processes

$$\begin{aligned} M &\neq p\mathcal{S}_{fwd} + (1-p)\mathcal{S}_{bwd} \\ \mathcal{S}_{fwd}(\mathcal{A}) &= \Phi_2(\mathcal{A} \otimes \mathcal{I}_{aux})\Phi_1 \\ \mathcal{S}_{bwd}(\mathcal{A}) &= \Phi_1(\Theta(\mathcal{A}) \otimes \mathcal{I}_{aux'})\Phi_2. \end{aligned} \tag{2.9}$$

That is, we have quantum operations with indefinite time directions.

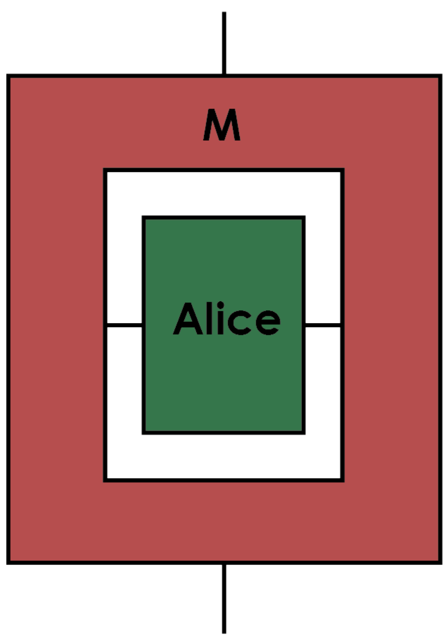

Figure 2.3: **A global process M acting on the quantum operation of Alice.** The process M takes as input the the quantum operation of Alice and outputs another channel. The process M may be indefinite time directed e.g., a quantum time flip.

Since, such operations do not have a fixed ordering of temporal direction, the notion of indefinite time direction may involve a coherent superposition of forward and backward time direction. A paradigmatic example of such indefinite time directed processes is the quantum time flip supermap. It takes input as a channel $\mathcal{A}$ and outputs channel $\mathcal{F}_{\mathcal{A}} : \mathcal{F}_{\mathcal{A}}(\rho \otimes \rho_c) = \sum_i F_i \rho F_i^{\dagger}$, where $F_i = K_{Ai} \otimes |0\rangle \langle 0| + \Theta(K_{Ai}) \otimes |1\rangle \langle 1|$. Where, K_{Ai} are the Kraus operators of channel $\mathcal{A}$. Operationally, depending on the control qubit ρ_c, the quantum time flip outputs the channel in the forward time direction $\mathcal{A}$, backward time direction $\Theta(\mathcal{A})$ or a superposition of both. Just like a quantum switch, this is sometimes phrased as time direction of the channel being entangled with the control qubit'.

Quantum operations with indefinite time directions have also shown advantages in channel discrimination [40], capacity enhancement [42], and quantum metrology in continuous variable regime [45]. There have also been experiments demonstrating that such operations are physically viable [43, 46]. However, apart from these, applications of such operations have been largely undiscovered. It is this gap we fill in this thesis by proposing potential advantages of quantum operations with indefinite time directions in discrete dimensional quantum metrology, for which we propose a novel encoding scheme which we name time-flip encoding under a framework of indefinite time directed quantum metrology. The preprint of our work is available on arXiv [1]. Furthermore we discuss the applications of time flip and switch in conjunction for capacity enhancement in quantum communication protocols.

Chapter 3

Quantum Metrology

Here, we briefly introduce quantum metrology [64–70] and elaborate on the use of ICO. We end the chapter by introducing the notion of optimal metrology, which quantifies the power of the particular framework under use.

3.1 Metrology

3.1.1 Classical Case

Metrology is the science of measurement. The parameter θ that we typically wish to measure, say, magnetic field, charge, number of particles, and position, influence the states and transformations of physical systems. From these parameter-dependent transformations Λ_θ, the parameters are to be extracted. Classically, if we have N uses of such a transformation available, then N probe states (systems) are initialised and evolved under these transformations. This makes the probe state parameter dependent. These probes are then measured to obtain data $\mathbf{x} = \{x_1, \ldots, x_2\}$ with probability $p(\mathbf{x}|\theta)$. Since the observed data contains information on the parameter, an estimator function $\hat{\theta}(\mathbf{x})$ is constructed, which estimates the value of θ from the given data. The goal of metrology is, therefore, to create the most precise estimator. There can be multiple ways to determine what a precise estimator is, especially in Bayesian metrology, which has several loss functions. In frequentist metrology where θ is not a random variable itself, a precise estimator is one with the least variance, that is $\Delta^2\hat{\theta} = \int dx(\hat{\theta}(x) - \theta)^2 p_\theta(x)$ is minimised. Along with being precise, we demand one more condition on our estimator: accuracy. We want our estimator to return the true value on average, that is $\langle\hat{\theta}\rangle = \int dx\hat{\theta}(x)p_\theta(x) = \theta$, where θ is the true parameter value. Operationally, this condition leads to better outcomes when experiments are repeated and is known as the unbiased estimator condition.

However, an estimator may not exist that minimises the variance everywhere. In such cases, different estimators may perform better at different regions of parameter values. Typically, we deal with situations where we know the parameter value to be around some θ_0, and the task is to estimate it precisely around an interval of θ_0. As such, it is more beneficial to introduce a weaker condition of local unbiasedness that is $\langle\hat{\theta}\rangle_{\theta=\theta_0} = \int dx\hat{\theta}(x)p_{\theta_0}(x) = \theta_0$ and $\frac{d\langle\hat{\theta}\rangle}{d\theta}_{\theta=\theta_0} = \int dx\hat{\theta}(x)\frac{dp_{\theta_0}(x)}{d\theta}_{\theta=\theta_0} = 1$, where, the last condition implies the deviation of only first order around the expected value θ_0.

Under this condition, the variance of the estimator is lower bounded by a quantity that solely depends on the probability function. From the second local unbiasedness condition, we write

$$
\begin{aligned}
\left[\int dx(\hat{\theta}(x)-\theta)\frac{dp_{\theta_0}(x)}{d\theta}\right]^2 &= 1 \\
\text{using Cauchy-Schwarz on functions } \frac{1}{\sqrt{p_\theta(x)}}\frac{dp_{\theta_0}(x)}{d\theta} \qquad & \text{and } \sqrt{p_\theta(x)}(\hat{\theta}(x)-\theta) \\
\int dx\left(\frac{1}{\sqrt{p_\theta(x)}}\frac{dp_{\theta_0}(x)}{d\theta}\right)^2 \cdot \int dx\left(\sqrt{p_\theta(x)}(\hat{\theta}(x)-\theta)\right)^2 &\geq 1 \\
\Rightarrow \int dx\frac{1}{p_\theta(x)}\left(\frac{dp_{\theta_0}(x)}{d\theta}\right)^2 \cdot \Delta^2\hat{\theta} &\geq 1 \\
\Rightarrow \Delta^2\hat{\theta} \geq \frac{1}{F}, \text{ where } F &= \int dx\frac{1}{p_\theta(x)}\left(\frac{dp_{\theta_0}(x)}{d\theta}\right)^2 . \qquad (3.1)
\end{aligned}
$$

The quantity F is defined as the Fisher information, and its inverse $1/F$ lower bounds the variance, also known as the Cramer-Rao bound. Hence, under these constraints the goal of metrology is to increase the Fisher information. Since standard error grows as $1/\sqrt{N}$, it can be shown that using the classical strategy of repeated experiments, with N usage of the probe or N experiments, F can grow at most linearly with N.

3.1.2 Quantum Case

In the quantum case, instead of being classical, the probes and transformations are now quantum states and quantum channels. Quantum metrology is particularly beneficial because quantum correlations can be utilised to better estimate these parameters. Like the classical case, a typical quantum metrological protocol consists of the probe preparation step, the evolution of the probe under the parametrised channel and measurement to obtain the statistics from which to infer the parameter. However, now quantum mechanical properties such as entanglement and quantum supermaps can be utilised for better metrology. Right now, we will discuss the role of entanglement. We will eventually employ supermaps by applying quantum switch and time flip to attain better precision.

Once the measurement has been performed and a probability function has been received, the precision on the estimator $\Delta^2\hat{\theta}$ can be lower bounded by a function that depends on the probability, just like in the classical case. However, there can be multiple POVMs and, thus, multiple probability functions for a given encoding. This raises a need to optimise the available measurements. It can be shown that the optimal measurements correspond to those done in the eigenbasis of the symmetric logarithmic derivative or SLD operator which is defined implicitly. If ρ_θ is the encoded probe then $\frac{d\rho_\theta}{d\theta} = (\lambda_\theta\rho_\theta + \rho_\theta\lambda_\theta)/2$ defines the SLD operator λ_θ. After measurement on its eigenbasis, the optimal achievable Fisher information is given by $Q = \mathrm{Tr}(\rho_\theta\lambda_\theta^2)$, which is also known as the quantum Fisher information QFI. Therefore, when optimised on all measurements, the achievable precision is lower bounded by $\Delta^2\hat{\theta} \geq \frac{1}{Q}$. This is known as the quantum Cramer-Rao (QCR) bound.

QFI follows several interesting properties. We list a few of them here:

- Additivity: QFI is additive under the tensor product of encoded states, e.g., if the encoded state is $\rho_\theta^a \otimes \rho_\theta^b$ then the QFI is $Q_a + Q_b$, where Q_a and Q_b are QFIs of the subsystem states.

- Purification: QFI of encoded state ρ_θ can be evaluate as a simple expression of the minimisation over purifications. $Q = \min_{|\Psi_\theta\rangle} 4(\langle\dot{\Psi}_\theta|\dot{\Psi}_\theta\rangle - |\langle\dot{\Psi}_\theta|\Psi_\theta\rangle|^2)$, where $|\Psi_\theta\rangle$ is purification of ρ_θ. This also gives a simple expression of QFI for a pure encoded state.

- Saturability: The lower bound using QFI is obtainable by measurements in the eigenbasis of the SLD. Although, it is not a unique measurement that maximises the Fisher information.

- Convexity: QFI is convex on the set of encoded states $Q(p\rho_\theta^a + (1-p)\rho_\theta^b) \leq pQ(\rho_\theta^a) + (1-p)Q(\rho_\theta^b)$.
- Metric: QFI defines a natural matrix on the space of encoded states by $ds^2 = \frac{1}{4}Q(\rho_\theta)d\theta^2$. This relates the fidelity and QFI by $Q(\rho_\theta) = \lim_{d\theta\to 0} 8(1-\sqrt{\mathcal{F}(\rho_\theta, \rho_{\theta+d\theta})})/d\theta^2$.
- Concavity under CPTP: QFI reduces by the action of the channels $Q(\mathcal{C}(\rho_\theta)) \leq Q(\rho_\theta)$.

Now, we provide one example to demonstrate the applicability of quantum metrology. Suppose we wish to estimate the phase of a unitary transformation $U_\theta = e^{-i\frac{\theta}{2}\sigma_z}$ with N usage of this unitary. A particularly useful strategy to estimate this phase is to prepare an initial GHZ state $\frac{|0\rangle^{\otimes N}+|1\rangle^{\otimes N}}{2}$. Evolve this GHZ state under $U_\theta^{\otimes N}$ to obtain $\frac{e^{-iN\frac{\theta}{2}}|0\rangle^{\otimes N}+e^{+iN\frac{\theta}{2}}|1\rangle^{\otimes N}}{2}$. This state is now measured in the $|\pm\rangle$ basis which provides statistics $p(\pm|\theta) = \frac{1\pm\cos N\theta}{2}$ for which the Fisher information comes out to be N^2 which is also the QFI. While other sequential strategies can provide similar QFI, this is particularly beneficial because it can be performed over systems with low coherence times. However, such a strategy does not give optimal results when noise is employed in the circuit. For instance, if there is a bitflip noise involved in the protocol, then it can be shown that error correction protocols, which involve an error-correcting channel after each usage of the parametrised channel, outperform any parallel protocol. The error correction protocols can broadly be seen as utilising quantum combs for the N usage of the parametrised channel.

3.1.3 Multiparameter estimation

The above discussion was relevant to single parameter estimation. Like above, multiparameter estimations of parameters $\theta = (\theta_1, \theta_2, \ldots, \theta_k)$ can be done and their precision, quantified by the covariance matrix $\mathbf{C}_{ij} = \int dx p_\theta(x)(\hat{\theta}_i(x) - \theta_i)(\hat{\theta}_j(x) - \theta_j)$ can be lower bounded through the Fisher information matrix $\mathbf{C} \geq \mathbf{F}^{-1}$, where $\mathbf{F}_{ij} = \int dx \frac{1}{p_\theta(x)} \frac{\partial p_\theta(x)}{\partial \theta_i} \frac{\partial p_\theta(x)}{\partial \theta_j}$. Similarly, for the quantum case, the quantum Fisher information matrix can be obtained as $\mathbf{Q}_{ij} = \mathrm{Tr}[\rho_\theta(\Lambda_{\theta,i}\Lambda_{\theta,j} + \Lambda_{\theta,j}\Lambda_{\theta,i})]$. However, unlike single parameter cases, multiparameter QCR is not saturable in general since SLDs corresponding to optimal measurements of different parameters do not necessarily commute.

3.2 Indefinite Causal Order in Metrology

While quantum metrology has had an immense amount of literature on optimising measurement and state preparation protocol, a third option is to modify the evolution step by applying appropriate supermaps over the parametrised channel. In particular, it will be interesting to evaluate the potential advantages of using the quantum supermaps, which exhibit the properties of indefinite causal order and indefinite time direction, and ask if they can provide some novel advantages to quantum metrology. In this section, we will observe two use cases of ICO in quantum metrology from the works of [2, 28] and [23] with further use cases discussed in the next section.

While quantum correlations can be utilised to obtain Heisenberg scaling, that is, the growth of Fisher information proportional to N^2, can we go to higher powers of N? In Ref. [2], the authors utilise the quantum switch operation to get super-Heisenberg scaling N^4 of Fisher information. Since it can be shown that such scaling is not obtainable in discrete regimes [71], they utilise a combination of discrete and continuous variable systems. The metrological task at hand is to estimate products of the average of position and momentum displacements $(\overline{x \cdot p})$ from displacement channels $D_{p_k} = e^{ip_k X}$, and $D_{x_k} = e^{-ix_k P}$. The quantum circuit in Fig. 3.1 is constructed, employing a quantum switch with a discrete 2-level control and continuous target system.

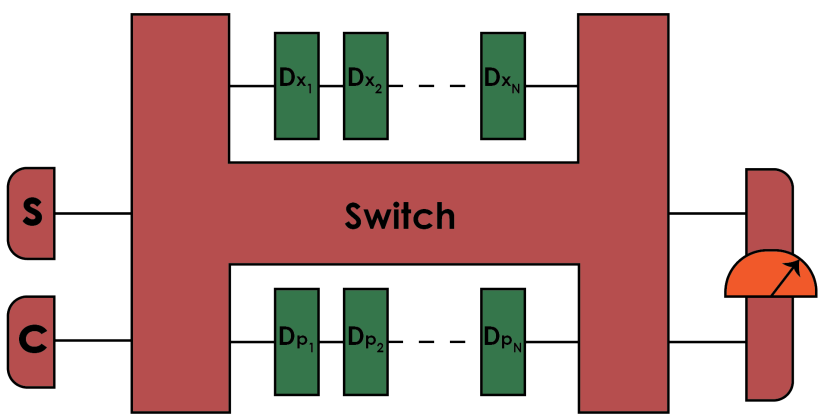

Figure 3.1: **ICO metrology protocol from Ref. [2].** The quantum switch takes the sequence of position displacement operators in one slot and the momentum displacement operators in the other slot. The control **C** is fixed in the $|+\rangle$ state, and therefore, a causal superposition of orders of position and momentum displacements is created, which acts on the initial state **S**.

The switched channel has the form $\mathcal{C} = |0\rangle\langle 0| \otimes \prod_{i=1}^{N} D_{p_i} \prod_{i=1}^{N} D_{x_i} + |1\rangle\langle 1| \otimes \prod_{i=1}^{N} D_{x_i} \prod_{i=1}^{N} D_{p_i}$. Using the Weyl relations $e^{ip_iX}e^{-ix_kP} = e^{ixpI}e^{-ix_kP}e^{ip_iX}$ the above form simplifies to $\mathcal{C} = (|0\rangle\langle 0| + e^{iN^2\bar{x}\bar{p}I}|1\rangle\langle 1|)/2 \otimes \prod_{i=1}^{N} D_{p_i} \prod_{i=1}^{N} D_{x_i}$. Measuring in $|\pm\rangle$ basis in the control now gives a Fisher information of N^4, hence obtaining the super-Heisenberg scaling.

On the other hand, in Ref. [23], the authors show that using the same circuit as above albeit in the discrete dimensions for the phase estimation task for unitary $e^{-i\theta\vec{n}\cdot\vec{\sigma}}$ in the presence of depolarising noise, one can obtain Fisher information value that is independent of the probe state. This implies that non-zero Fisher information is obtainable for arbitrary noisy state and even white noise probes. In particular, if we write the qubit state in the form $\rho = (I + \vec{s}\cdot\vec{\sigma})/2$ and the depolarising channel as $\mathcal{N}(\rho) = \alpha\rho + (1-\alpha)I/2$ which acts on the unitary as defined above and put the noisy channel, along with its copy in the quantum switch supermap the achievable Fisher information, when measured in the control qubit is $[\alpha(1-\alpha)\sin\theta]^2/(1-[\alpha(1-\alpha)\cos\theta+(1+\alpha)^2/4]^2)$ which is independent of the state of probe. The derivation can be done via a general method presented in the next chapter, through which we reproduce the results to obtain the Fig. 3.2.

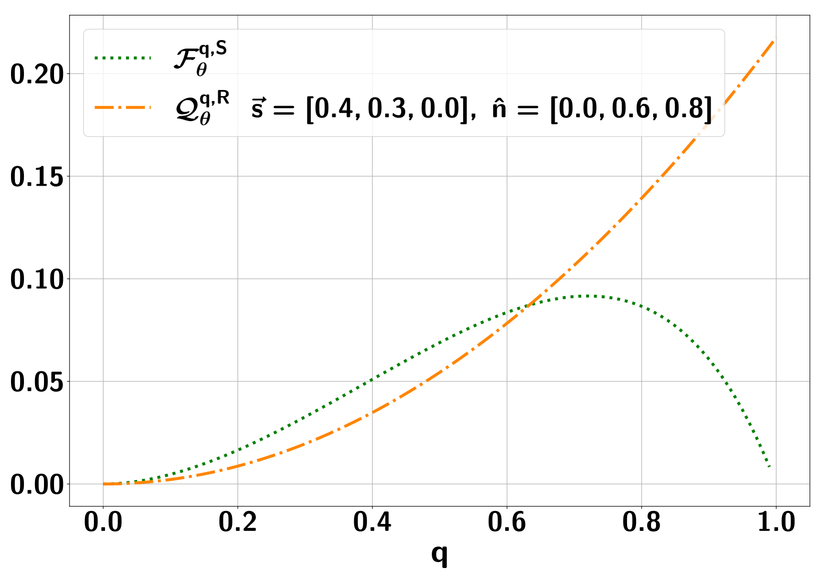

Figure 3.2: **Obtainable Fisher information using quantum Switch and conventional non-switch method on a single probe.** The probe and unitary axis are fixed to the values according to the legend. The Fisher information is independent for the switch case and dependent for the regular probe. The advantage of switch encoding in a high noise regime can be seen.

Apart from these, there have been several other contributions to the field of ICO metrology. Since ICO with process matrix formalism provides a much bigger set of available super operations/strategies than regular quantum combs and parallel methods, evaluating if it can provide higher Fisher information than the optimal FI attainable via combs is instructive. This question of optimal metrology is the one we consider in the next section.

3.3 Optimal Metrology

Since using the SLD operator more or less solves the optimal measurement problem, we can club the state preparation and evolution steps into one. In all the quantum metrological protocols, the parametrized channel is converted to an encoded state. Hence, optimal metrology can be summarised as finding the most optimal supermap or quantum type $(A \to B) \to C$ which converts the parametrized channel to an encoded state. In Ref. [22], sets of such types are termed as strategy sets. If $\mathcal{Q}(\mathcal{C}_\theta, P)$ is a function which calculates the quantum Fisher information of the encoded state when strategy P acts the channel $\mathcal{C}_\theta$ then the aforementioned problem can be more formally written as finding $\max_{P \in Strat} \mathcal{Q}(C_\phi, P)$. This maximization can be done via semi-definite programming algorithms, which were provided in Ref. [22] with further details in Ref. [29].

In particular, their algorithm utilizes the maximization over purification method. As elucidated in the quantum metrology section, for an encoded state ρ_θ the QFI can be obtained as $Q = \min_{|\Psi_\theta\rangle} 4(\langle\dot{\Psi}_\theta|\dot{\Psi}_\theta\rangle - |\langle\dot{\Psi}_\theta|\Psi_\theta\rangle|^2)$. This expression can actually be simplified since for every purification $|\Psi_\theta\rangle$, one can also obtain purification $e^{i\gamma\theta}|\Psi_\theta\rangle$, with $\gamma = -i\langle\dot{\Psi}_\theta|\Psi_\theta\rangle$ which has the same QFI but the $|\langle\dot{\Psi}_\theta|\Psi_\theta\rangle|^2$ term is zero. Hence, $Q = \min_{|\Psi_\theta\rangle} 4\langle\dot{\Psi}_\theta|\dot{\Psi}_\theta\rangle$. The quantum channels involved can be written in terms of quantum states from Choi isomorphism. Utilising the link product from the first chapter we write $\mathcal{Q}^{max} = \max_{P \in Strat} \mathcal{Q}(C_\theta * P)$. Here, C_θ might be a quantum comb of N parametrized channels; for example, there might be correlated noise between the transformations. Following [29, 42, 72] the problem can be rewritten as

$$\mathcal{Q}^{max} = 4 \max_{P} \min_{|\Psi_\theta^N\rangle_{A_1^N A_2^N R}} \langle\dot{\Psi}_\theta^N|\dot{\Psi}_\theta^N\rangle, \tag{3.2}$$

where $|\Psi_\theta^N\rangle$ is the purification of Choi state $C_\theta * P$ with global input A_1^N global output A_2^N

and R as ancilla for purification. this is now equal to

$$\mathcal{Q}^{max} \quad = \quad 4 \max_{P} \min_{\{K_{\theta,i}^N\}} \sum_i \langle \dot{K}_{\theta,i}^N * P | \dot{K}_{\theta,i}^N * P \rangle, \tag{3.3}$$

which is the expansion of the above equation using Kraus of $C_\theta * P$, given by link product. This becomes

$$\begin{aligned} \mathcal{Q}^{max} \quad &= \quad 4 \max_{P} \min_{\{K_{\theta,i}^N\}} \mathrm{Tr}\left[\sum_i |\dot{K}_{\theta,i}^N\rangle\langle \dot{K}_{\theta,i}^N| \right], \\ &= \quad 4 \max_{P} \min_{h} \mathrm{Tr}\Big[(\Omega(h) \otimes \mathcal{I}_{A_2^N})(P \otimes \mathcal{I}_{A_1^N}) \Big] \end{aligned} \tag{3.4}$$

where the last inequality [73] is the result of performing local metrology due to which instead of optimizing over all Kraus operators, optimization on single parameter family of Kraus operators with $\dot{K}_{\theta,i}(h) = \dot{K}_{\theta,i}(h)^{loc} - i \sum_j h_{ji} K_{\theta,i}^{loc}$ where $K_{\theta,i}^{loc}$ is some fixed Kraus representation and $\Omega(h) = \sum_i |\dot{K}_{\theta,i}^N(h)\rangle\langle \dot{K}_{\theta,i}^N(h)|^T$. Lastly, defining $\bar{\Omega}(h) = \mathrm{Tr}_{A_1^N}[\Omega(h)]$ and $\bar{P} = \mathrm{Tr}_{A_2^N}[P]$ and using minmax theorem since the optimization is convex with one parameter and concave with the other. We get,

$$\mathcal{Q}^{max} \quad = \quad 4 \max_{\bar{P}} \min_{h} \mathrm{Tr}\big[\bar{\Omega}(h)\bar{P}\big] = 4 \min_{h} \max_{\bar{P}} \mathrm{Tr}\big[\bar{\Omega}(h)\bar{P}\big] \tag{3.5}$$

The maximization can now be formalized as an SDP problem. Utilising the dual of this SDP makes a double minimization SDP.

$$\begin{aligned} \mathcal{Q}^{max} =& 4 \min_{\lambda, \mathcal{O}^i, h} \lambda, \\ & \text{s.t. } A^i \geq 0,\ \mathcal{O}^i \in DF(S)^i,\ i = 1, \ldots, K, \end{aligned} \tag{3.6}$$

$$A = \begin{pmatrix} \lambda I & B^\dagger \\ B & \mathcal{O}^i \end{pmatrix} \tag{3.7}$$

with

$$B = \left(\left| \dot{K}_{\theta,1}(h) \right\rangle, \cdots, \left| \dot{K}_{\theta,r}(h) \right\rangle \right) \tag{3.8}$$

and $DF(S)^i$ is the dual affine space of operators S^i which are affine spaces with the convex hull $\bar{P}$.

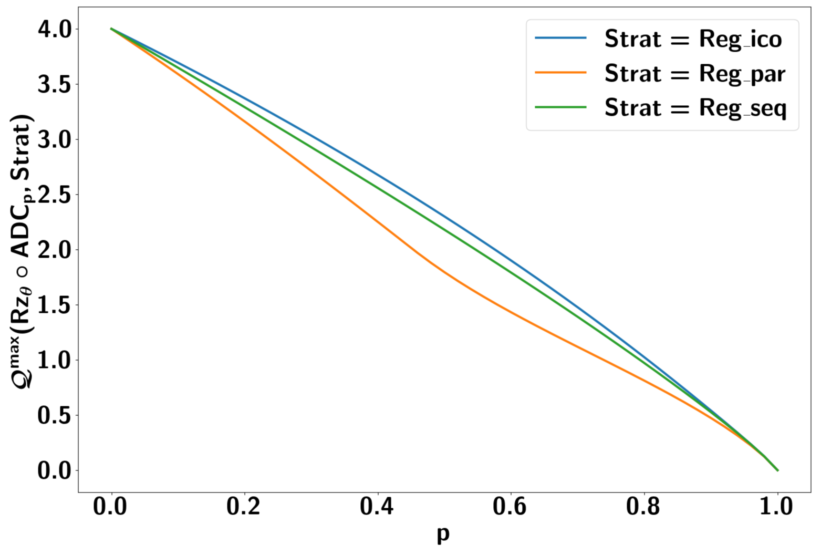

Figure 3.3: **Optimal Quantum Fisher information for different sets of strategies.** Notably two uses of noisy channel $Rz_\theta = e^{-i\theta\sigma_z/2}$ with amplitude damping noise of strength p and parameter value $\theta = \pi/2$ are utilized under strategy sets involving indefinite causal order (ICO), Parallel (entanglement), and sequential also known as adaptive or quantum combs strategy. An advantage of the ICO strategy can be seen.

We numerically perform this SDP to reproduce the results of Ref. [29, 42] (see Fig. 3.3). This algorithm, while being extremely useful, is not very scalable. Typically, it is not possible to go beyond four uses of channels because the size of matrices and the number of parameters grow exponentially fast. In this domain therefore, it is also instructive to find upper bounds on the achievable QFI and figure out how optimal QFI per usage of channel scales. This was considered in Ref. [71], which derived upper bounds on optimal metrology. This is also done via SDP methods by optimizing over all Kraus operators. The results show higher upper bounds of Causal superposition (subset of ICO) over adaptive or quantum combs strategy and higher upper bounds of adaptive over parallel ones in finite usage N, as is observed in the figure above. In the asymptotic regime, where the upper bounds are saturable, all three classes converge, signifying that ICO and adaptive schemes are only as good as parallel ones in high usage limits.

Chapter 4

Indefinite Time Directed Metrology

The contents of this chapter follow our recent arXiv preprint [1].

4.1 Introduction

Quantum metrology [64–70] aims to collect information about observable parameters of a system with high precision. These parameters often include phase shifts of evolving quantum systems, accumulated in multiple scenarios such as biological sensing [74, 75], dark matter search [76, 77], gravitational wave detection [78–80], atomic clock [81–84], magnetometry [85, 86] and quantum imaging [87–89]. The metrological protocol involves measuring a quantum state that encodes the parameter of interest, to obtain information about its value. An unbiased estimator is employed to process the measurement data and extract an estimate of the parameter with its precision satisfying the Cramér-Rao inequality [90]. This inequality establishes a lower bound on the precision, quantified in terms of the variance of the estimate, which is constrained by the inverse of the classical Fisher information (FI). By optimizing the FI over all possible measurement strategies, one obtains the quantum Fisher information (QFI), which represents the ultimate precision limit and saturates the Cramér-Rao bound. Using an uncorrelated probe system in parameter estimation protocols can extract QFI which scales at most linearly with the number of subsystems of the probe, hence attaining standard quantum limit (SQL) in terms of precision. However, by leveraging nonclassical resources such as entangled or spin-squeezed probe state [66, 67, 91–94], the sensitivity can be enhanced where scaling of QFI can be elevated to quadratic from linear with the number of subsystems of the probe, thereby achieving the Heisenberg limit (HL) in precision.

In conventional metrological protocols, as outlined above, the encoding operation is performed within a classical framework that adheres to a well-defined causal order and a fixed temporal direction. Recently, however, there has been a surge of interest in exploring metrological advantages [2, 22–29] (ranging from HL to super-Heisenberg limit) with the aid of indefinite causal order (ICO)[4, 5, 30–33, 39]. The operation with ICO can take multiple casually ordered transformations as input and outputs superposition of them controlled by a quantum degree of freedom [95], e.g., the quantum switch [3]. Experimental implementations of such protocols have also been realized [27, 28]. In recent years, along with sensitivity enhancements, ICO has exhibited advantages across various domains including state and channel discrimination [6–9], communication capacity and complexity [10–17, 34–36], thermodynamical tasks including charging, refrigeration, work extraction, and activation of thermal states [18–21, 37, 38, 63].

Notably, indefinite causal ordered processes are a particular kind of higher-order quantum transformation that inputs or outputs a quantum channel or other quantum operations [51]. Lately, a new broader class of such idiosyncratic higher-order operations has been discovered, which are called quantum operations with indefinite time direction or indefinite input-output direction [40] as they do not have a fixed temporal direction. The notion of indefinite time direction involves a coherent superposition of forward and backward time direction. In the backward time direction, the roles of input and output port are interchanged, defining quantum processes which receive the input in the future and output in the past timeline. Indefinite time direction can be realized in bidirectional quantum devices [40, 42] which include crystals that rotate the polarization of single photons such as half-wave plates, and quarter-wave plates. Analogous to the quantum switch in the context of ICO, the quantum time flip [40, 42], a paradigmatic example of indefinite time directed processes, has shown promising advantages in certain operator discrimination tasks [40], communication capacity [42], emergence of dynamical memory effect in memoryless phase-covariant processes [44]. Furthermore, its feasibility has been established through experimental implementations [43, 46]. Additionally, foundational queries such as the thermodynamic "arrow of time" and thermodynamic work in the quantum superpositions of forward and backward time evolution have been investigated in [41, 47]. Despite these advancements, the potential applications of the quantum time flip in quantum technologies remain largely unexplored, especially in comparison to the ICO-based processess.

Recently, in the context of quantum metrology, Xia et al. [45] conducted an experimental study by demonstrating that the estimation of the optical Kerr effect-induced phase shift, using coherent states and the rotation of light beams, utilizing Hermite-Laguerre-Gaussian beams, respectively, can achieve Heisenberg-limited precision, with photon number and orbital angular momentum serving as the fundamental resources for precision enhancement. However, to date, no studies have explored the usage of time-flip in discrete-variable regimes, where the fundamental resource is the number of subsystems in the probe system for enhancing precision.

In this work, we introduce a novel framework that consists of encoding operations with indefinite input-output direction in quantum metrology. By exploiting the properties of quantum time flip we devise a protocol that enables Heisenberg-limited precision in the estimation of an arbitrary single parameter of unitary channels, hence the name indefinite time directed metrology (ITDM). We prove that initializing the probe as pure product states where all the subsystems align in the same direction, referred to as symmetric product probe states attains the maximum value of QFI with time-flipped encoding procedure. Specifically, without preparing entangled probe states, the optimal symmetric product probe states can attain Heisenberg-limited precision. Consequently, we establish the fact that entanglement is not a prerequisite for attaining HL precision and cannot provide a scaling advantage beyond the HL when the temporal direction of the encoding process is rendered indefinite through quantum control. We elucidate the no advantage condition (NAC) and quantitatively assess the advantage conferred by time-flipping in our study.

We explicitly demonstrate these advantages for phase-shift and axis estimation of a unitary. Furthermore, in the case of phase estimation, we devise a measurement strategy that operates exclusively on the control qubit yielding an FI that exhibits Heisenberg scaling. Interestingly, the parameter dependency of the optimal input probe state and FI is removed when the value of the parameter that is to be estimated is small. In such a parameter regime, FI can saturate to QFI by employing a particular symmetric product probe state and an optimally chosen control qubit, irrespective of the direction of the encoding axis. Furthermore, in the case of a single qubit noisy ITDM (NITDM) where noise affects the encoding strategy and input probes, our protocol showcases the advantage of the time-flipped strategy over the existing quantum "switched" strategy [23] and regular strategy within specific parameter values and noise regimes. Additionally, we provide a brief discussion on the impact of noise in multi-qubit NITDM and explore a potential strategy for achieving a higher FI compared to the regular approach, highlighting the need for further investigation in this direction.

4.2 Framework for Indefinite time directed metrology (ITDM)

Quantum "time flip (TF)" is defined on the set of bidirectional quantum processes which can operate either in forward or backward time directions. A quantum channel $\mathcal{C}$ is referred to as *bidirectional* if $\Theta(\mathcal{C})$ is a completely positive and trace-preserving (CPTP) map where Θ denotes the *input-output inversion map*. As demanded in Ref. [40], this map Θ should have certain properties including "order reversing", "identity-preserving", $\Theta(\mathcal{A}) \neq \Theta(\mathcal{B})$ when channels $\mathcal{A}, \mathcal{B}$ are unequal, and $\Theta\big(q\mathcal{A} + (1-q)\mathcal{B}\big) = q\Theta(\mathcal{A}) + (1-q)\Theta(\mathcal{B})$ with $q \geq 0$. Moreover, the Kraus operators $\{C_i\}$ of $\mathcal{C}(*) = \sum_i C_i(*)C_i^\dagger$ satisfy bistochasticity conditions, i.e. $\sum_i C_i^\dagger C_i = \sum_i C_i C_i^\dagger = I$, where I is the identity matrix on the Hilbert space of the system. The only two possibilities of Θ are $\Theta(\mathcal{C})(*) = \mathcal{C}^\dagger(*) = \sum_i C_i^\dagger(*)C_i$ or $\Theta(\mathcal{C})(*) = \mathcal{C}^T(*) = \sum_i C_i^T(*)C_i^{T^\dagger}$, up to unitary equivalence. The operation of quantum time flip supermap $T_\mathcal{C}$ is described by $T_\mathcal{C}(\rho_c \otimes \rho) = \sum_i T_i(\rho_c \otimes \rho)T_i^\dagger$ where $T_i(\mathcal{C}) = |0\rangle\langle 0| \otimes C_i + |1\rangle\langle 1| \otimes \Theta(C_i)$ are the Kraus operators and the first register functions as the control for the time direction. We perform encoding in parameter estimation protocol with the aid of operations with indefinite time direction, defined as ITDM.

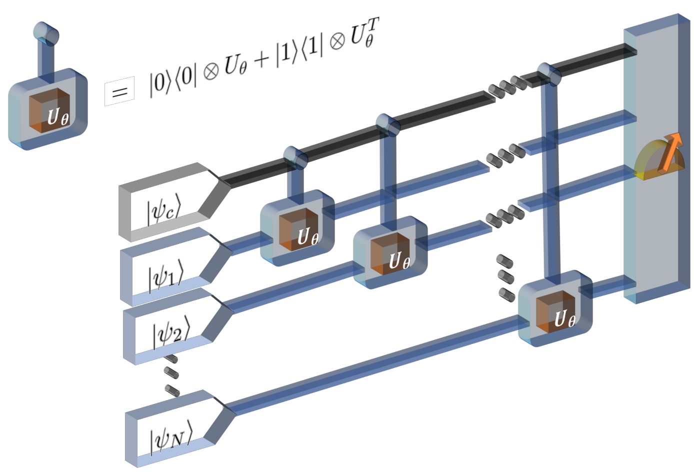

Figure 4.1: **ITDM scheme.** Taking N-qubit pure product probe states along with a control qubit we encode the parameter θ of U_θ on the probe state using bipartite time-flip supermap $T_{U_\theta} = |0\rangle\langle 0| \otimes U_\theta + |1\rangle\langle 1| \otimes U_\theta^T$ which is a controlled unitary itself. Therefore, the whole encoding procedure is done in a single time step with N queries of T_{U_θ}, given by $\mathbb{T}_{U_\theta} = \prod_{i=1}^N (T_{U_\theta}^i \otimes \mathbb{I}_{N-1}^{\neq i}) = \Big(|0\rangle\langle 0| \otimes U_\theta^{\otimes N} + |1\rangle\langle 1| \otimes U_\theta^{T\otimes N}\Big)$ with $\mathbb{I}_{N-1}^{\neq i} = \bigotimes_{\substack{j=1 \\ j\neq i}}^N I_j$. This encoded state is then measured either locally on the control qubit or globally on the basis of symmetric logarithmic derivative operator to obtain the information about θ.

4.2.1 Time-flipped encoding stratgey

In quantum estimation theory, given a unitary gate U which is a function of θ, i.e., $U \equiv U_\theta$, our task is to estimate θ. Instead of conventional unitary encoding schemes, we employ TF-encoding strategy comprising of N number of bipartite TF gates, $T_{U_\theta} = |0\rangle\langle 0| \otimes U_\theta + |1\rangle\langle 1| \otimes U_\theta^T$ on N-qubit input probe, $\left|\psi^N\right\rangle$ assisted by control qubit $|\psi_c\rangle = \sqrt{p_c}\,|0\rangle + e^{i\theta_c}\sqrt{1-p_c}\,|1\rangle$ with $0 \leq p_c \leq 1$ and $0 \leq \theta_c \leq 2\pi$ (see Fig. 4.1). Mathematically, the state after encoding operation can be written as $|\Phi\rangle = \mathbb{T}_{U_\theta}|\Psi\rangle$, where

$$\begin{aligned}
\mathbb{T}_{U_\theta} &= \prod_{i=1}^{N}(T^i_{U_\theta} \otimes \mathbb{I}^{\neq i}_{N-1}) = \prod_{i=1}^{N}\left(|0\rangle\langle 0| \otimes I^{\otimes i-1} \otimes U_\theta \otimes I^{\otimes N-i} + |1\rangle\langle 1| \otimes I^{\otimes i-1} \otimes U_\theta^T \otimes I^{\otimes N-i}\right) \\
&= |0\rangle\langle 0| \otimes U_\theta^{\otimes N} + |1\rangle\langle 1| \otimes U_\theta^{T\otimes N},
\end{aligned} \tag{4.1}$$

with $\mathbb{I}^{\neq i}_{N-1} = \bigotimes_{\substack{j=1\\ j\neq i}}^{N} I_j$ and $|\Psi\rangle = |\psi_c\rangle \otimes \left|\psi^N\right\rangle$. Specifically, for a product probe state, i.e., $|\Psi\rangle = |\psi_c\rangle \bigotimes_{i=1}^{N}|\psi_i\rangle$, the encoded state can be written as

$$|\Phi\rangle = \sqrt{p_c}\,|0\rangle \bigotimes_{i=1}^{N}|\chi_i\rangle + e^{i\theta_c}\sqrt{1-p_c}\,|1\rangle \bigotimes_{i=1}^{N}|\omega_i\rangle\,, \tag{4.2}$$

where $U_\theta|\psi_i\rangle = |\chi_i\rangle\,,\ U_\theta^T|\psi_i\rangle = |\omega_i\rangle$. Subsequently we analyze the performance of the estimation protocol with product probe states and compare its performance with the entangled one.

4.2.2 Quantum Fisher information in ITDM

The goal here is to estimate the parameter θ involved in U_θ with a high precision which can be fulfilled by performing measurements on the encoded state. Importantly for any kind of measurements, the precision in estimating θ with an unbiased estimator, quantified by the variance of θ, is bounded below by the Cramer-Rao bound via Fisher information (FI), $\mathcal{F}_\theta$ as $(\Delta\theta)^2 \geq (\lambda\mathcal{F}_\theta)^{-1}$, where λ denotes the number of measurements available [65, 90]. In particular when the decoding measurement is performed in the basis of symmetric logarithmic derivative (SLD), Cramer-Rao bound is saturated and FI is termed as quantum Fisher information (QFI). The QFI for a pure state $|\Xi\rangle$ can be written as

$$\mathcal{Q}_\theta = 4\left(\langle\dot{\Xi}|\dot{\Xi}\rangle - \left|\langle\dot{\Xi}|\Xi\rangle\right|^2\right), \tag{4.3}$$

where $|\dot{\Xi}\rangle = \frac{\mathrm{d}\,|\Xi\rangle}{\mathrm{d}\theta}$. For N number of uncorrelated particles $(\Delta\theta)^2$ is known to scale as $1/N$, referred to as the standard quantum limit (SQL). While with the help of quantum entanglement, it is possible to diminish the error, as $(\Delta\theta)^2 \sim 1/N^2$ [65–68], known as the Heisenberg Limit (HL). It will be interesting to find that when encoding is performed with TF operator, how quantum Fisher information scales with N. In our case of product probes in Eq. (4.2), QFI takes the form as (see appendix 7.1)

$$\begin{aligned}\mathcal{Q} \;=\; 4\Bigg[p_c\left(\sum_{k=1}^{N}|\dot{\chi}_k| + \sum_{\substack{j,k=1,\\ j\neq k}}^{N}\alpha_k\alpha_j^*\right) + (1-p_c)\left(\sum_{k=1}^{N}|\dot{\omega}_k| + \sum_{\substack{j,k=1,\\ j\neq k}}^{N}\beta_k\beta_j^*\right)\\ -\left|p_c\sum_{k=1}^{N}\alpha_k + (1-p_c)\sum_{k=1}^{N}\beta_k\right|^2\Bigg],\end{aligned} \tag{4.4}$$

where

$$\begin{aligned}\langle\dot{\chi}_k|\chi_k\rangle = \alpha_k, \quad \langle\dot{\chi}_k|\dot{\chi}_k\rangle = |\dot{\chi}_k|,\\ \langle\dot{\omega}_k|\omega_k\rangle = \beta_k, \quad \langle\dot{\omega}_k|\dot{\omega}_k\rangle = |\dot{\omega}_k|.\end{aligned} \tag{4.5}$$

To analyze the scaling of QFI, let us concentrate on the simplest scenario where all the qubit probe states are equal, i.e., $|\psi_i\rangle \equiv |\psi\rangle\ \forall i$. Therefore, the N-qubit symmetric product probe state along with control can be written as $\left|\Psi^S\right\rangle = |\psi_c\rangle\,|\psi\rangle^{\otimes N}$ with $\alpha_k = \alpha,\ \beta_k = \beta,\ \ |\dot{\chi}_k| = |\dot{\chi}|$, and $|\dot{\omega}_k| = |\dot{\omega}|$. When $|\psi_i\rangle \neq |\psi\rangle\ \ \forall i$, we call the N qubit state to be asymmetric one. In the symmetric scenario, the QFI reduces to

$$\begin{aligned}\mathcal{Q}^S &= 4N^2\Big[p_c|\alpha|^2 + (1-p_c)|\beta|^2 - |p_c\alpha + (1-p_c)\beta|^2\Big]\\ &\quad + 4N\Big[p_c\Big(|\dot{\chi}| - |\alpha|^2\Big) + (1-p_c)\Big(|\dot{\omega}| - |\beta|^2\Big)\Big],\\ &= 4N^2 p_c(1-p_c)|\alpha-\beta|^2\\ &\quad + 4N\Big[p_c\Big(|\dot{\chi}| - |\alpha|^2\Big) + (1-p_c)\Big(|\dot{\omega}| - |\beta|^2\Big)\Big].\end{aligned} \tag{4.6}$$

Since in the limit $N \to \infty$, QFI $\mathcal{Q}^S \sim N^2$, it implies that using symmetric product state $\left|\Psi^S\right\rangle$ and encoding θ by the time-flipped operation which comprises multiple two-qubit controlled gates (see Fig. 4.1), the precision limit of θ can go beyond SQL and reach HL.

It is now natural to ask – *Is the symmetric product probe state optimal for ITDM?* In other words, if we can exhibit that one cannot achieve higher scaling with asymmetric product probes than the one obtained with symmetric states, the query above is resolved. Indeed, we answer this question positively in the following Theorem, which is one of the main results of our work.

Theorem 1. *Among all pure product states, given an asymmetric state, there exists a symmetric state which provides a higher value of QFI in ITDM.*

Proof. Given an arbitrary product state $|\Psi\rangle = |\psi_c\rangle \bigotimes_{i=1}^{N} |\psi_i\rangle$, we denote the set of N symmetric product states as $\mathcal{S}_\Psi := \{\left|\Psi_l^S\right\rangle\}_{l=1}^{N}$. Here, the state $\left|\Psi_l^S\right\rangle = |\psi_c\rangle |\psi_l\rangle^{\otimes N}$ in this set have QFI $\mathcal{Q}_l^S$. We denote the QFI for the asymmetric probe state $|\Psi\rangle$ as $\mathcal{Q}^A$.

Without loss of generality, we assume that the optimal probe state among all symmetric product states in $\mathcal{S}_\Psi$ is $\left|\Psi_1^S\right\rangle$. Therefore, mathematically, we can write

$$\begin{aligned} & \mathcal{Q}_1^S \geq \mathcal{Q}_l^S \quad \forall l \in [N], \\ \implies & \mathcal{Q}_1^S - \mathcal{Q}_{avg} \geq 0, \end{aligned} \tag{4.7}$$

where $\mathcal{Q}_{avg} = \frac{1}{N}\sum_{l=1}^{N} \mathcal{Q}_l^S$. Note that, the equality sign holds when $l = 1$. Let us now consider the quantity, $\mathcal{Q}_{avg} - \mathcal{Q}^A$. In appendix 7.2 we show that

$$\begin{aligned} & \mathcal{Q}_{avg} - \mathcal{Q}^A \\ = \ & 4Np_c(1-p_c)\sum_{k=1}^{N} |\alpha_k - \beta_k|^2 - 4p_c(1-p_c)\left|\sum_{k=1}^{N} \alpha_k - \beta_k\right|^2 \\ \geq \ & 0. \end{aligned} \tag{4.8}$$

Therefore, we get $\mathcal{Q}_1^S \geq \mathcal{Q}^A$. It is easy to see that the equality sign holds when $|\Psi\rangle \to \left|\Psi_1^S\right\rangle$. Hence, the theorem is proved. □

From Theorem 1 we can conclude that:

Corollary 2. *Maximal QFI in the case of ITDM for product probe states is achieved by symmetric states of the form $\left|\Psi^S\right\rangle = |\psi_c\rangle |\psi\rangle^{\otimes N}$ where we have to optimize over only the doubly-parametrized set of states, $|\psi\rangle = \sqrt{p_s}\,|0\rangle + e^{i\theta_s}\sqrt{1-p_s}\,|1\rangle$ with $\theta_s \in [0, 2\pi]$ and $p_s \in [0,1]$ along with optimal control qubit and encoding axis.*

Remark on *No advantage condition.* ITDM can not surpass the standard quantum limit when $\alpha = \beta$. This condition, referred to as the "no advantage condition" (NAC), simplifies to $(\partial_\theta U_\theta)^\dagger U_\theta = (\partial_\theta U_\theta^T)^\dagger U_\theta^T$. If U_θ satisfies NAC, it implies that there do not exist any probe and control state for which the SQL can be beaten. Notably, the NAC is satisfied when $U^T = \pm U$. Although, additional solutions for U may also exist. We propose a measure of our advantage as the maximum achievable coefficient of N^2 in Eq. (4.6), which is $4p_c(1-p_c)\max_{|\psi\rangle}\left|\left\langle(\partial_\theta U_\theta)^\dagger U_\theta - (\partial_\theta U_\theta^T)^\dagger U_\theta^T\right\rangle\right|^2 = 4p_c(1-p_c)|\lambda_{max}|^2$ where λ_{max} is the eigenvalue of $(\partial_\theta U_\theta)^\dagger U_\theta - (\partial_\theta U_\theta^T)^\dagger U_\theta^T$ with the biggest modulus. There is no advantage exactly when either $p_c = 0, 1$ i.e., the time flip does not work or when NAC is satisfied where $|\lambda_{max}|^2 = 0$ and our measure gives zero. Whenever the measure is non-zero we can in principle set our probe to the eigenvalue corresponding to λ_{max} and gain QFI with an N^2 coefficient of $4p_c(1-p_c)|\lambda_{max}|^2$.

4.3 Estimating phases with ITDM

After establishing the advantage of TF operation in the context of quantum metrology, let us concentrate on an explicit phase estimation scheme to achieve Hiesenberg limit. In particular, given a unitary $U_\theta = e^{-i\frac{\theta}{2}\vec{\sigma}.\hat{n}}$ our goal is to estimate the value of the parameter θ, where $\hat{n} = \hat{x}n_1 + \hat{y}n_2 + \hat{z}n_3$ is referred as the encoding axis. According to Corollary 2, we initialize the input state as $\left|\Psi^S\right\rangle = |\psi_c\rangle\,|\psi\rangle^{\otimes N}$ where $|\psi_c\rangle = \sqrt{p_c}\,|0\rangle + e^{i\theta_c}\sqrt{1-p_c}\,|1\rangle$ with $\theta_c \in [0, 2\pi]$, and $p_c \in [0, 1]$. In this scenario, we find that

$$\begin{aligned}
\alpha &= in_3(p_s - 1/2) + i\sqrt{p_s(1-p_s)}(n_1\cos\theta_s + n_2\sin\theta_s), \\
\beta &= in_3(p_s - 1/2) + i\sqrt{p_s(1-p_s)}(n_1\cos\theta_s - n_2\sin\theta_s), \\
|\dot{\chi}| &= 1/4, \text{ and } |\dot{\omega}| = 1/4.
\end{aligned} \tag{4.9}$$

The QFI is calculated as $\mathcal{Q}_\theta(A, B) = AN^2 + BN$, where

$$A = 4p_c(1-p_c) * 4p_s(1-p_s)n_2^2\sin^2\theta_s, \tag{4.10}$$

and

$$\begin{aligned}
B &= 4p_c\left[\frac{1}{4} - \left\{n_3(p_s - 1/2) + \sqrt{p_s(1-p_s)}(n_1\cos\theta_s + n_2\sin\theta_s)\right\}^2\right] \\
&+ 4(1-p_c)\left[\frac{1}{4} - \left\{n_3(p_s - 1/2) + \sqrt{p_s(1-p_s)}(n_1\cos\theta_s - n_2\sin\theta_s)\right\}^2\right].
\end{aligned} \tag{4.11}$$

Notice that NAC in this case reduces to $(\vec{\sigma}.\hat{n})^T = \vec{\sigma}.\hat{n}$ which implies $\hat{n}_2 = 0$. Interestingly, QFI $\mathcal{Q}_\theta(A, B)$ is independent of the parameter θ itself which we want to estimate, and also on θ_c. However, to find the maximum value of QFI, $\bar{\mathcal{Q}}_\theta^{\hat{n}}$ for a given encoding direction

$\hat{n}$, we have to optimize over the control and the input state. To address the optimization let us group the parameters θ_s, p_s, p_c in a set $\boldsymbol{\mu}$, i.e., $\boldsymbol{\mu} = \{\theta_s, p_s, p_c\}$. Mathematically, the optimization can be cast into the form $\mathcal{Q}_\theta^{\hat{n}} = \max_{\boldsymbol{\mu}} \mathcal{Q}_\theta(A, B)$. Since optimization over multiple (three) parameters is not straightforward to address we maximize the coefficient A to obtain the Heisenberg scaling N^2. Now, one can trivially calculate that the maximal value of the coefficient, $A = n_2^2$ with $\boldsymbol{\mu}_A = \{\frac{\pi}{2}, \frac{1}{2}, \frac{1}{2}\}$ which leads to QFI $\mathcal{Q}_\theta|_{\boldsymbol{\mu}_A} = N^2 n_2^2 + N(1-n_2^2)$. Let us now prove in the following Theorem that this is indeed the maximum value of QFI.

Theorem 3. *The maximum value of QFI which can be achieved by a N-qubit product state in the ITDM protocol is given by $\bar{\mathcal{Q}}_\theta^{\hat{n}} = N^2 n_2^2 + N(1 - n_2^2)$.*

Proof. To demonstrate that $\mathcal{Q}_\theta|_{\boldsymbol{\mu}_A}$ represents the optimal value of the QFI, we have to prove $\mathcal{Q}_\theta|_{\boldsymbol{\mu}_A} - \mathcal{Q}_\theta(A, B) \geq 0$, i.e.,

$$\begin{aligned} & N^2 n_2^2 + N(1 - n_2^2) - (AN^2 + BN) \geq 0, \\ \implies & N(n_2^2 - A) \geq B + n_2^2 - 1. \end{aligned} \tag{4.12}$$

As n_2^2 is the optimal value of A, $n_2^2 - A \geq 0$. Therefore, if Eq. (4.12) is true for $N = 1$ then it will be valid for all values of $N > 1$. For $N = 1$ it simplifies to $A + B \leq 1$, which we prove in appendix 7.3. Hence, $\bar{\mathcal{Q}}_\theta^{\hat{n}} = N^2 n_2^2 + N(1 - n_2^2)$. □

Let us now determine the optimal encoding direction $\hat{n}$ for which the maximum of QFI is attained. To do so, we define

$$\bar{\mathcal{Q}}_\theta = \max_{\hat{n}} \bar{\mathcal{Q}}_\theta^{\hat{n}} = \max_{\hat{n}, \boldsymbol{\mu}} \mathcal{Q}_\theta(A, B), \tag{4.13}$$

which includes optimization over $\hat{n}$, input and control qubits. As a direct consequence of Theorem 3, the following corollary can be established:

Corollary 4. *By fixing the optimal encoding axis $\hat{n} = \hat{y}$ and $\boldsymbol{\mu}_A = \{\frac{\pi}{2}, \frac{1}{2}, \frac{1}{2}\}$, the maximum QFI turns out to be N^2.*

Note that, the maximum QFI for the estimation of the axis parameter of $U = \exp\left(-i\frac{\theta}{2}\vec{\sigma} \cdot \hat{n}\right)$, where either ϕ or ξ of the axis $\hat{n} = \hat{x}\sin\phi\cos\xi + \hat{y}\sin\phi\sin\xi + \hat{z}\cos\phi$ is to be estimated, is determined to be $4N^2$ following Eq. (4.6), as detailed in appendix 7.4. This demonstrates that our protocol is capable of achieving the Heisenberg limit for arbitrary unitary parameters, as expected from our derivations in Section 4.2.

We now show that the maximum QFI, $\mathcal{Q}_\theta = N^2$ for optimal encoding is, in fact, achievable with a local measurement scheme as a decoding strategy. The scheme consists of the following steps: (1) Prepare the control state as $|\psi_c\rangle = |+\rangle = (|0\rangle + |1\rangle)/\sqrt{2}$ and probe state as $|\psi\rangle = |+i\rangle = (|0\rangle + i\,|1\rangle)/\sqrt{2}$, i.e., the input state is $|\Psi^s\rangle = |+\rangle\,|+i\rangle^{\otimes N}$. (2) The encoded state after application of the gate $\mathbb{T}_{U_\theta}$ with $U_\theta = e^{-i\theta\sigma_y/2}$ (i.e., $\hat{n} = \hat{y}$) on $|\Psi_s\rangle$ is given by

$$|\Phi\rangle = \frac{1}{\sqrt{2}} e^{-iN\theta/2} \left(|0\rangle + e^{iN\theta}\,|1\rangle\right) \otimes |+i\rangle^{\otimes N}. \tag{4.14}$$

(3) Perform projective measurement on the control qubit in the basis of σ_x, i.e., $\{|+\rangle\,, |-\rangle\}$.
(4) Repeat the above procedure λ number of times and record the measurement outcome.

The probability statistics for the outcome $|\pm\rangle$ is given by $p(\pm|\theta) = \frac{1}{2}[1 \pm \cos{(N\theta)}]$. Therefore, the classical Fisher information (FI) [90] turns out to be

$$\mathcal{F}_\theta = \sum_{b\in\{+,-\}} p(b|\theta) \left[\frac{\partial \ln p(b|\theta)}{\partial\theta}\right]^2, \tag{4.15}$$

$$= N^2 = \bar{\mathcal{Q}}_\theta. \tag{4.16}$$

Notably in this scenario, the probe and control states (Eq. (4.14)) remain as a pure product state even after bidriectional encoding along y-axis, which is a global operation, while still providing HL. This demonstrates that entanglement is not necessary for surpassing SQL in ITDM protocol, while at the same time the protocol can be done parallelly, which is important for systems with low coherence times. However, in general, the two qubit unitaries generated by time flip may generate entanglement for arbitrary input product probe states.

The above-discussed protocol is optimal when $\hat{n} = \hat{y}$ and the RMSE scales as $1/N$. However, it is interesting to ask – *Given the direction of the encoding axis, how do FI, $\mathcal{F}_\theta$ scale when the decoding measurement basis is fixed in* $\{|+\rangle\,, |-\rangle\}$? We answer this question in the following subsection.

4.3.1 Classical Fisher Information by projective measurement on control qubit

By initializing the control and probe state in general product states (Eq. (4.2)) and encoding axis as $\hat{n}$, let us consider the decoding measurement only on the control qubit in $\{|+\rangle\,, |-\rangle\}$ basis. In this scenario, the outcome statistics is given by

$$
\begin{aligned}
p(\pm|\theta) \quad &= \mathrm{Tr}\left[\left(|\pm\rangle\langle\pm|_c \otimes I_p\right)|\Phi\rangle\langle\Phi|\right] \\
&= \frac{1}{2} \pm \frac{\sqrt{p_c(1-p_c)}}{2}\left(e^{i\theta_c}\prod_{i=1}^{N}\langle\chi_i|\omega_i\rangle + e^{-i\theta_c}\prod_{i=1}^{N}\langle\omega_i|\chi_i\rangle\right).
\end{aligned} \tag{4.17}
$$

Since, $\langle\chi_i|\omega_i\rangle$ is a complex number, we parametrize it as $\langle\chi_i|\omega_i\rangle = r_i(\boldsymbol{\nu})e^{if_i(\boldsymbol{\nu})}$ where $\boldsymbol{\nu} = \{\theta, \theta_s, p_s, \hat{n}\}$. According to this parametrization, we have

$$
p(\pm|\theta) = \frac{1}{2} \pm \sqrt{p_c(1-p_c)}\cos\left(\sum_{i=1}^{N} f_i(\boldsymbol{\nu}) + \theta_c\right)\prod_{i=1}^{N} r_i(\boldsymbol{\nu}). \tag{4.18}
$$

Finally, using Eq. (4.15), the FI can be calculated as

$$
\begin{aligned}
\mathcal{F}_\theta \;&=\; \frac{4}{p_c}(1-p_c)\left[\sum_{j=1}^{N}\left(\prod_{i\neq j}^{N} r_i(\boldsymbol{\nu})\right)\left\{\dot{r_j}(\boldsymbol{\nu})\cos\left(\sum_{i=1}^{N} f_i(\boldsymbol{\nu}) + \theta_c\right)\right.\right. \\
&\left.\left. - \left(\frac{r_j(\boldsymbol{\nu})}{N}\right)\sin\left(\sum_{i=1}^{N} f_i(\boldsymbol{\nu}) + \theta_c\right)\left(\sum_{i=1}^{N} \dot{f}_i(\boldsymbol{\nu})\right)\right\}\right]^2 \Big/ 1 - 4p_c(1-p_c) \\
&\times \left(\prod_{i=1}^{N} r_i(\boldsymbol{\nu})\right)^2 \cos^2\left(\sum_{i=1}^{N} f_i(\boldsymbol{\nu}) + \theta_c\right), \qquad (4.19)
\end{aligned} \tag{4.20}
$$

which is optimal at $p_c = 1/2$. We consider $|\psi_i\rangle = |\psi\rangle$ for all i, which is determined to be optimal based on rigorous numerical investigations. This implies $r_i(\boldsymbol{\nu}) = r(\boldsymbol{\nu})$, $f_i(\boldsymbol{\nu}) = f(\boldsymbol{\nu})$ $\forall i$ and along with $p_c = 1/2$, we have

$$
\mathcal{F}_\theta = \frac{N^2 r^{2N-2}(\boldsymbol{\nu})\left\{\dot{r}(\boldsymbol{\nu})\cos\left(Nf(\boldsymbol{\nu}) + \theta_c\right) - r(\boldsymbol{\nu})\dot{f}(\boldsymbol{\nu})\sin\left(Nf(\boldsymbol{\nu}) + \theta_c\right)\right\}^2}{1 - r^{2N}(\boldsymbol{\nu})\cos^2\left(Nf(\boldsymbol{\nu}) + \theta_c\right)}. \tag{4.21}
$$

To approach the question of the optimal probe state, similar to QFI, we define

$$
\bar{\mathcal{F}}_\theta = \max_{\hat{n}} \bar{\mathcal{F}}_\theta^{\hat{n}}, \tag{4.22}
$$

where $\bar{\mathcal{F}}_\theta^{\hat{n}}$ is the maximum FI for a given axis $\hat{n}$ by choosing optimal probe and performing decoding measurement in $\{|+\rangle, |-\rangle\}$ basis on optimal control qubit, i.e., $\bar{\mathcal{F}}_\theta^{\hat{n}} = \max_{\boldsymbol{\mu},\theta_c} \mathcal{F}_\theta$.

Note that, $U_\theta^\dagger U_\theta^T$ being unitary, we have $0 \leq r(\boldsymbol{\nu}) \leq 1$. Therefore, from Eq. (4.21) it is evident that if $r(\boldsymbol{\nu}) < 1$, $\mathcal{F}_\theta$ decreases exponentially with increasing value of N. This means it is desirable to set $r(\boldsymbol{\nu}) = 1$ by taking initial probe state $|\psi\rangle = |u(\hat{n},\theta)^{\pm}\rangle$ where $|u(\hat{n},\theta)^{\pm}\rangle = (\mathrm{g}^{\mp}(\hat{n},\theta)|0\rangle + |1\rangle)/\sqrt{1+|\mathrm{g}^{\mp}(\hat{n},\theta)|^2}$ is the eigenstate of $U_\theta^\dagger U_\theta^T$, i.e., $U_\theta^\dagger U_\theta^T |u(\hat{n},\theta)^{\pm}\rangle = \exp(\pm i\mathrm{f}(n_2,\theta))|u(\hat{n},\theta)^{\pm}\rangle$. In this scenario, $p_s = \mathrm{g}^{\mp}(\hat{n},\theta)^2/\sqrt{1+|\mathrm{g}^{\mp}(\hat{n},\theta)|^2}$ and $\theta_s = i\ln(1+|\mathrm{g}^{\mp}(\hat{n},\theta)|^2 - \mathrm{g}^{\mp}(\hat{n},\theta)^2)/2$. Moreover, we have

$$\mathrm{f}(n_2,\theta) = \tan^{-1}\left(\frac{\sqrt{4n_2^2\sin^2\frac{\theta}{2}\left(1-n_2^2\sin^2\frac{\theta}{2}\right)}}{1-2n_2^2\sin^2\frac{\theta}{2}}\right), \tag{4.23}$$

and the explicit forms of $g^{\mp}(\hat{n},\theta)$ are given in appendix 7.5 which shows that eigenvectors are dependent on the encoding axis and moreover the parameter θ itself. This implies $\dot{r}(\boldsymbol{\nu}) = 0$ and $f(\boldsymbol{\nu}) = \mathrm{f}(n_2,\theta)$. Therefore, preparing the probe $|\psi\rangle^{\otimes N}$ in either $|u(\hat{n},\theta)^{+}\rangle^{\otimes N}$ or $|u(\hat{n},\theta)^{-}\rangle^{\otimes N}$ and $|\psi_c\rangle = (|0\rangle + e^{i\theta_c}|1\rangle)/\sqrt{2}$ and measuring the control qubit on the $\{|+\rangle, |-\rangle\}$ basis lead to FI (following Eq. (4.21))

$$\bar{\mathcal{F}}_\theta^{\hat{n}} = N^2\dot{\mathrm{f}}(n_2,\theta)^2. \tag{4.24}$$

However, the complexity in attaining such outcome si that thethe input state parameters θ_s, p_s is θ dependent means that one requires a decent amount of prior knowledge of θ beforehand. Notice that, choosing $\hat{n} = \pm\hat{y}$ gets rid of such complexities and gives $\mathrm{f} = -\theta \pm \pi$ which achieves $\bar{\mathcal{F}}_\theta = N^2 = \bar{\mathcal{Q}}_\theta$ in consistent with Eq. (4.16). Next, we consider the scenario in the limit where the parameter θ has a small value where we show that the above-mentioned subtlety can be removed.

Optimal input probes for small θ

Let us write our input probe as $\rho = |\psi\rangle\langle\psi| = (I + \hat{s}.\vec{\sigma})/2$ where $\hat{s} = \hat{x}s_x + \hat{y}s_y + \hat{z}s_z$ and $s_x = 2\sqrt{p_s(1-p_s)}\cos\theta_s$, $s_y = 2\sqrt{p_s(1-p_s)}\sin\theta_s$, $s_z = (2p_s - 1)$. The overlap $\langle\chi|\omega\rangle$ can be written as

$$\begin{aligned}\langle\chi|\omega\rangle = \langle\psi|U_\theta^\dagger U_\theta^T|\psi\rangle = \mathrm{Tr}\Big(U_\theta^T\rho U_\theta^\dagger\Big) \;&=\; 1 - n_2^2(1-\cos\theta) + in_2n_3s_x(1-\cos\theta) \\ &\quad - in_1n_2s_z(1-\cos\theta) + in_2s_y\sin\theta.\end{aligned} \tag{4.25}$$

Therefore, the modulus and phase of the complex number in Eq. (4.25) is given by

$$r(\boldsymbol{\nu}) \;=\; \left[\left\{1-n_2^2(1-\cos\theta)\right\}^2 + \left\{n_2s_y\sin\theta + (n_2n_3s_x - n_1n_2s_z)(1-\cos\theta)\right\}^2\right]^{1/2}, \tag{4.26}$$

and

$$f(\boldsymbol{\nu}) = \tan^{-1} \frac{n_2 s_y \sin\theta + (n_2 n_3 s_x - n_1 n_2 s_z)(1-\cos\theta)}{1 - n_2^2(1-\cos\theta)}, \tag{4.27}$$

respectively. By considering up to 2nd order correction in θ ($\mathcal{O}(\theta^2)$), i.e., for small value of $\theta = \tilde{\theta}$ we show that (see details in appendix 7.6)

$$\begin{aligned} \mathcal{F}_{\tilde{\theta}} &= s_y^2 n_2^2 N^2 + (1-s_y^2) n_2^2 N \delta_{\theta_c,0}, \\ &= s_y^2 n_2^2 N(N - \delta_{\theta_c,0}) + n_2^2 N \delta_{\theta_c,0}. \end{aligned} \tag{4.28}$$

where $\delta_{\theta_c,0} = 1$ if $\theta_c = 0$ and 0 elsewhere. Interestingly, in the limit $N \to \infty$, classical Fisher information $\mathcal{F}_{\tilde{\theta}}\big|_{N\to\infty} = s_y^2 n_2^2 N^2$ is $\tilde{\theta}$-independent and reaches HL irrespective of any probe state. From Eq. (4.28) it immediately follows that the optimal probe for $\tilde{\theta}$ estimation is given by $s_y = \pm 1$, i.e., $\boldsymbol{\mu} = \boldsymbol{\mu}_A = \{\pi/2 + 2m\pi, 1/2, 1/2\} \forall m \in \mathbb{Z}$ which implies

$$\bar{\mathcal{F}}_{\tilde{\theta}}^{\hat{n}} = n_2^2 N^2 = \bar{\mathcal{Q}}_{\tilde{\theta}}^{\hat{n}}|_{N\to\infty}. \tag{4.29}$$

Hence, we arrive at the following result which shows that the two-fold complexity previously described vanishes under the given scenario –

Theorem 5. *In the limit $N \to \infty$, independent of the small value $\tilde{\theta}$ to be estimated, the classical FI, $\bar{\mathcal{F}}_{\tilde{\theta}}^{\hat{n}} = n_2^2 N^2$, saturates the QFI, $\bar{\mathcal{Q}}_{\tilde{\theta}}^{\hat{n}}\big|_{N\to\infty}$, using the control qubit $|\psi_c\rangle = (|0\rangle + e^{i\theta_c}|1\rangle)/\sqrt{2}$ along with the probe state as $|\pm i\rangle = (|0\rangle + |1\rangle)/\sqrt{2}$ and decoding measurement in the σ_x basis.*

4.4 Entanglement can not beat N^2-scaling

To this point, our analysis has focused on utilizing product states as the initial probe state. A natural progression of this inquiry involves examining whether the use of entangled probe states could facilitate scaling improvements surpassing the Heisenberg limit. To address the same we write the general N-qubit probe state as

$$|\Psi\rangle = \sum_{i=1}^{2^N} \Lambda_i |\lambda_i\rangle, \tag{4.30}$$

where $\sum_{i=1}^{2^N} |\lambda_i\rangle\langle\lambda_i| = I_{2^N}$ and $\langle\lambda_i|\lambda_j\rangle = \delta_{ij}$. Defining $|\lambda_i\rangle = \bigotimes_{j=1}^N |\psi_j^i\rangle$ we rewrite $|\Psi\rangle = \sum_{i=1}^{2^N} \Lambda_i \bigotimes_{j=1}^N |\psi_j^i\rangle$, where $|\psi_j^i\rangle$ is the ith basis state for jth qubit with $\langle\psi_j^i|\psi_j^k\rangle = \delta_{ik}$ and

$\sum_{i=1}^{2} |\psi_j^i\rangle\langle\psi_j^i| = I_2$. Extending beyond the use of product states as probes, our theorem below indicates that entanglement does not provide an advantage in achieving scaling of the QFI with the number of qubits beyond the HL.

Theorem 6. *In the ITDM protocol, the maximum QFI extractible from any probe state, including all entangled states, is upper bounded by $\gamma N^2 + \zeta N$, where γ and ζ are constants independent of N.*

Proof. Let us present a brief outline of our comprehensive proof, which is available in appendix 7.7. Using the general N-qubit probe state as defined above, we derive an upper bound on QFI as

$$\begin{aligned}\mathcal{Q}_\theta \;\leq\; \tilde{\mathcal{Q}}_\theta = 4\langle\dot{\Phi}|\dot{\Phi}\rangle, = 4\sum_{i=1}^{2^N}\sum_{k=1}^{2^N}\Lambda_i\Lambda_k^*\Bigg[p_c\sum_{m=1}^{N}\Bigg(\dot{\chi}_m^{ki}\prod_{j\neq m}a_j^{ki} \\ +\sum_{l\neq m}\alpha_m^{ki}\alpha_l^{ik*}\prod_{j\neq m,l}a_j^{ki}\Bigg)+(1-p_c)\sum_{m=1}^{N}\Bigg(\dot{\omega}_m^{ki}\prod_{j\neq m}b_j^{ki}+\sum_{l\neq m}\beta_m^{ki}\beta_l^{ik*}\prod_{j\neq m,l}b_j^{ki}\Bigg)\Bigg],\end{aligned} \tag{4.31}$$

where

$$\begin{aligned}\langle\dot{\chi}_m^k|\dot{\chi}_m^i\rangle &= \dot{\chi}_m^{ki}, \quad \langle\chi_j^k|\chi_j^i\rangle = a_j^{ki}, \\ \langle\dot{\omega}_m^k|\dot{\omega}_m^i\rangle &= \dot{\omega}_m^{ki}, \quad \langle\omega_j^k|\omega_j^i\rangle = b_j^{ki}, \\ \langle\dot{\chi}_m^k|\chi_m^i\rangle &= \alpha_m^{ki}, \quad \langle\dot{\omega}_j^k|\omega_j^i\rangle = \beta_j^{ki},\end{aligned} \tag{4.32}$$

and $|\chi_j^i\rangle = U_\theta\,|\psi_j^i\rangle$ and $|\omega_j^i\rangle = U_\theta^T\,|\psi_j^i\rangle$.

In Eq. (4.31) the terms $\prod_{j\neq m} a_j^{ki}$, and $\prod_{j\neq m} b_j^{ki}$ are the products of the inner products of $(N-1)$ of the qubits. Hence, if the qubits in $|\lambda_i\rangle$ and $\langle\lambda_k|$ differ in more than one position then, $\prod_{j\neq m} a_j^{ki} = \prod_{j\neq m} b_j^{ki} = 0$. Similarly, if the qubits in $|\lambda_i\rangle$ and $\langle\lambda_k|$ differ in more than two positions then the terms $\prod_{j\neq m,l} b_j^{ki} = \prod_{j\neq m,l} a_j^{ki} = 0$. Defining, $\tilde{\mathcal{Q}}_\theta^X$ as the term which involves contribution only from N-qubit basis states where qubits differ in X number of positions, we can write $\tilde{\mathcal{Q}}_\theta = \sum_{X=0}^{N}\tilde{\mathcal{Q}}_\theta^X = \sum_{X=0}^{2}\tilde{\mathcal{Q}}_\theta^X$ since, $\tilde{\mathcal{Q}}_\theta^X = 0\ \forall X \geq 3$. In appendix 7.7, we show that each of these three terms is bounded by an expression of the form $\gamma_i N^2 + \zeta_i N$. Hence, $\tilde{\mathcal{Q}}_\theta \leq \gamma N^2 + \zeta N$ where γ, ζ are constants independent of N. □

Although entangled states do not offer superior scaling compared to product-probe states, we investigate whether they can yield higher QFI. To this aim, given an encoding axis $\hat{n}$, we perform numerical maximization of QFI over the whole state space (see Eq. (4.30)) for

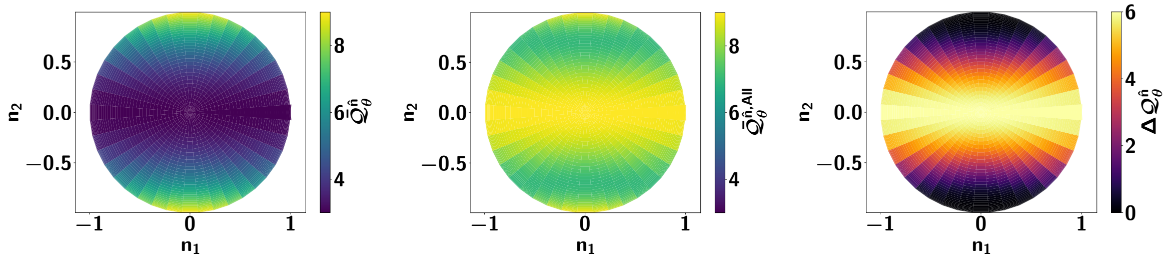

Figure 4.2: **QFI obtained by the optimal states using 3-qubit probe states for difference axis. (a) $\bar{\mathcal{Q}}_\theta^{\hat{n}}$, Optimized over all product states, (b) $\bar{\mathcal{Q}}_\theta^{\hat{n},All}$ optimized over all states, (c) Difference $\Delta\mathcal{Q}_\theta^{\hat{n}} = \bar{\mathcal{Q}}_\theta^{\hat{n},All} - \bar{\mathcal{Q}}_\theta^{\hat{n}}$.** We see that the difference goes to zero near $n_2 = \pm 1$ precisely where both (a) and (b) attain their maximal QFI of $N^2 = 9$. We conclude that product states can give as much QFI as entangled states when optimized over the axis for a 3-qubit probe system. All the axis are dimensionless.

$N = 3$ denoted as $\bar{\mathcal{Q}}_\theta^{\hat{n},All}$ (see Fig. 4.2(b)). Interestingly, for $n_2 = 1$, $\bar{\mathcal{Q}}_\theta^{\hat{y},All}$ is the same as that with QFI for optimal product probe state, i.e., $\bar{\mathcal{Q}}_\theta^{\hat{y},All} = \bar{\mathcal{Q}}_\theta^{\hat{y}} = 9 = \bar{\mathcal{Q}}_\theta$. Notice that, $\hat{n} = \hat{y}$ is indeed the universal optimal encoding axis which means maximal attainable value of QFI by optimizing over the whole state space and encoding axis is 9. However, as value of n_2 deviates from 1, the difference between the maximum value of QFI with optimal product probe and $\bar{\mathcal{Q}}_\theta^{\hat{n},All}$, i.e., $\Delta\mathcal{Q}_\theta^{\hat{n}} = \bar{\mathcal{Q}}_\theta^{\hat{n},All} - \bar{\mathcal{Q}}_\theta^{\hat{n}}$ increases significantly as demonstrated in Fig. 4.2(c). For $n_2 = 0$ we have QFI $\bar{\mathcal{Q}}_\theta^{\hat{n},All} = 9$ and $\bar{\mathcal{Q}}_\theta^{\hat{n}} = 3$ where the difference $\Delta\mathcal{Q}_\theta^{\hat{n}}$ reaches a maximum value of 6. This observation ensures the fact that the optimal probe states which give higher QFI than fully separable pure product probe states must be entangled in at least some bipartition. However, since we are concerned with scaling of QFI with N, in the rest of the paper we use symmetric product probe states in our protocol. Notice that $\Delta\mathcal{Q}_\theta^{\hat{n}} \approx \mathcal{O}(10^{-2})$ in the region $\pm 0.95 \lesssim n_2 \leq \pm 1$ irrespective of n_1 and n_3 which shows the robustness of optimal product probe states compared to entangled ones for nonoptimal encoding.

4.5 Advantage in noisy Unitary encoding

Considering the pervasiveness of noise in quantum metrology with both theoretical and practical standpoints, and the numerous advantages of ICO protocols in noisy metrology, it is instructive to analyze the ITDM protocol under noise. To evaluate the performance of ITDM in the noisy scenario, we consider a noisy input probe $\rho = (I + \vec{s}.\vec{\sigma})/2$ with $|\vec{s}| \leq 1$ and depolarizing noise $\mathcal{N}(\rho) = q\rho + (1-q)I/2$ [96] is acted after unitary encoding U_θ. Consequently the effective channel $\mathcal{N}_\theta(\rho) = qU_\theta\rho U_\theta^\dagger + (1-q)I/2$ is termed as noisy unitary channel with Kraus operators $\{K_0 = \sqrt{1-p}U_\theta, K_1 = \sqrt{p/3}\sigma_x U_\theta, K_2 = \sqrt{p/3}\sigma_y U_\theta, K_3 = \sqrt{p/3}\sigma_z U_\theta\}$

where $q = 1 - 4p/3 \in [0,1]$. Application of time-flip to such a bistochastic channel [40] leads to a quantum operation $T_{\mathcal{N}_\theta}(\rho_c \otimes \rho) = \sum_{j=0}^{3} F_j(\rho_c \otimes \rho)F_j^\dagger$ with Kraus operators $F_j = |0\rangle\langle 0| \otimes K_j + |1\rangle\langle 1| \otimes K_j^T$ where $\rho_c = |\psi_c\rangle\langle\psi_c|$. Therefore, after the encoding procedure in ITDM scheme with noisy encoding operation (NITDM), the output state is given by $\Theta = \mathbb{T}_{\mathcal{N}_\theta}(\rho_c \bigotimes_{i=1}^N \rho_i) = \sum_{j\in\Pi} \mathbb{F}_j(\rho_c \bigotimes_{i=1}^N \rho_i)\mathbb{F}_j^\dagger$ with $\mathbb{F}_j = |0\rangle\langle 0| \bigotimes_{i=1}^N K_{j[i]} + |1\rangle\langle 1| \bigotimes_{i=1}^N K_{j[i]}^T$, where Π is the set of 4^N integer strings j, with each string specifying which Kraus operator $K_{j[i]}$ acts on the ith qubit. We have normalization conditions $\sum_{j\in\Pi} \mathbb{F}_j^\dagger \mathbb{F}_j = I$ and $\sum_{j\in\Pi} \left(\bigotimes_{i=1}^N K_{j[i]}\right)^\dagger \left(\bigotimes_{i=1}^N K_{j[i]}\right) = I$. This can further be simplified as

$$\begin{aligned}\Theta = p_c|0\rangle\langle 0| \bigotimes_{i=1}^{N}\left(\sum_{j=0}^{3} K_j\rho_i K_j^\dagger\right) + \sqrt{p_c(1-p_c)}e^{-i\theta_c}|0\rangle\langle 1| \bigotimes_{i=1}^{N}\left(\sum_{j=0}^{3} K_j\rho_i K_j^{T\dagger}\right)\\ + \sqrt{p_c(1-p_c)}e^{i\theta_c}|1\rangle\langle 0| \bigotimes_{i=1}^{N}\left(\sum_{j=0}^{3} K_j^T\rho_i K_j^\dagger\right) + (1-p_c)|1\rangle\langle 1| \bigotimes_{i=1}^{N}\left(\sum_{j=0}^{3} K_j^T\rho_i K_j^{T\dagger}\right).\end{aligned} \tag{4.33}$$

Defining $\mathrm{Tr}\left(\sum_j K_j^T\rho_i K_j^\dagger\right) = r_i(\boldsymbol{\nu})e^{if_i(\boldsymbol{\nu})}$ with $\boldsymbol{\nu} = \{\theta, \vec{s}, \hat{n}, q\}$ as the updated set $\boldsymbol{\nu}$, outcome probabilities of measurement in σ_x basis on the control qubit can be written as

$$p(\pm|\theta) = \frac{1}{2} \pm \sqrt{p_c(1-p_c)}\cos\left(\sum_{i=1}^{N} f_i(\boldsymbol{\nu}) + \theta_c\right)\prod_{i=1}^{N} r_i(\boldsymbol{\nu}). \tag{4.34}$$

Following Eq. (4.15), we calculate FI, $\mathcal{F}_\theta^q$ in NITDM which have exactly same mathematical form as Eq. (4.21), i.e., $\mathcal{F}_\theta^q \equiv \mathcal{F}_\theta$ with updated $r_i(\boldsymbol{\nu}) = \left|\mathrm{Tr}\left(\sum_j K_j^T\rho_i K_j^\dagger\right)\right|$ and $f_i(\boldsymbol{\nu}) = \arg\left[\mathrm{Tr}\left(\sum_j K_j^T\rho_i K_j^\dagger\right)\right]$. With the tools in hand, we are now ready to analyze the effect of noisy encoding.

4.5.1 Comparison of NITDM with "switched" and regular strategy in single qubit

In the case of $N = 1$, the value of FI corresponding to NITDM is given by (see appendix 7.8)

$$\mathcal{F}_\theta^q = \frac{n_2^4 q^2 \sin^2\theta}{1 - \left\{\frac{1+q}{2} - n_2^2 q(1-\cos\theta)\right\}^2}, \tag{4.35}$$

which is independent of the input probe configuration. Being periodic in θ we can safely choose $\theta \in [0, 2\pi)$ for our analysis. We compare NITDM with two other metrological schemes – (1) "switched" strategy where encoding is done using the quantum switch as described in [23], (2) regular strategy [23] where conventional unitary encoding is used. The "switched" FI, $\mathcal{F}_\theta^{q,S}$ and QFI, $\mathcal{Q}_\theta^{q,R}$ in regular strategy is given by

$$\mathcal{F}_\theta^{q,S} = q^2(1-q)^2 \sin^4\theta \left[1 - \left\{q(1-q)\cos\theta + \frac{1}{4}(1+q)^2\right\}^2\right]^{-1},$$

and $\mathcal{Q}_\theta^{q,R} = q^2(\vec{n} \times \vec{s})^2$ respectively. Let us now compare these three strategies in terms of metrological power.

Fixing Optimally encoded direction

Notice that, $\mathcal{F}_\theta^q$ is optimal for encoding axis $\hat{n} = \hat{y}$ (see appendix 7.8) where optimal QFI for regular probe $\mathcal{Q}_\theta^{q,R} = q^2$ is attained by choosing $\hat{s} \perp \hat{n}$. Due to the θ-dependency of the FI in the NITDM, there exist specific regions of θ where our protocol demonstrates superior performance compared to the regular protocol, as well as regions where it lags behind. Specifically, $\mathcal{F}_\theta^q|_{\hat{n}=\hat{y}}$ gives TF advantage compared to $\mathcal{Q}_\theta^{q,R}|_{\hat{s}\perp\hat{n}} = q^2$ in the parameter region $\pi/3 < \theta < 4\tan^{-1}\left(\sqrt{q_1 - 4\sqrt{q_2}}\right)$ and $4\tan^{-1}\left(\sqrt{q_1 + 4\sqrt{q_2}}\right) < \theta < 5\pi/3$ where $q_1 = (5+7q)/(3+q)$ and $q_2 = (1+4q+3q^2)/(3+q)^2$. Contrastingly, in the regime $\cos^{-1}\left[\frac{-1+q}{2(1+q)}\right] < \theta < 2\pi - \cos^{-1}\left[\frac{-1+q}{2(1+q)}\right]$; $0 \leq \theta < \pi/3$ and $5\pi/3 < \theta < 2\pi/3$, we have $\mathcal{F}_\theta^q|_{\hat{n}=\hat{y}} < \mathcal{Q}_\theta^{q,R}|_{\hat{s}\perp\hat{n}}$, i.e., regular strategy outperforms NITDM.

Note that, these ranges of θ are reliant on the strength of noise q. Interestingly, there exist smaller intervals of θ where NITDM surpasses regular strategy irrespective of the strength of the noise. Our analysis reveals that, $\mathcal{F}_\theta^q|_{\hat{n}=\hat{y}} > \mathcal{Q}_\theta^{q,R}|_{\hat{s}\perp\hat{n}}\,\forall q$ when $\{\pi/3 < \theta < \pi/2; 3\pi/2 < \theta < 5\pi/3\}$. On the other hand, $\mathcal{F}_\theta^q|_{\hat{n}=\hat{y}} < \mathcal{Q}_\theta^{q,R}|_{\hat{s}\perp\hat{n}}\,\forall q$ for $\{2\pi/3 < \theta < 4\pi/3; 0 \leq \theta < \pi/3; 5\pi/3 < \theta < 2\pi/3\}$.

Moreover, setting $\hat{n} = \hat{y}$ as the encoding axis, we always get advantage over "switched" scheme, i.e., $\mathcal{F}_\theta^q|_{\hat{n}=\hat{y}} \geq \mathcal{F}_\theta^{q,S}$ (appendix 7.8) for any value of θ and arbitrary noise strength q.

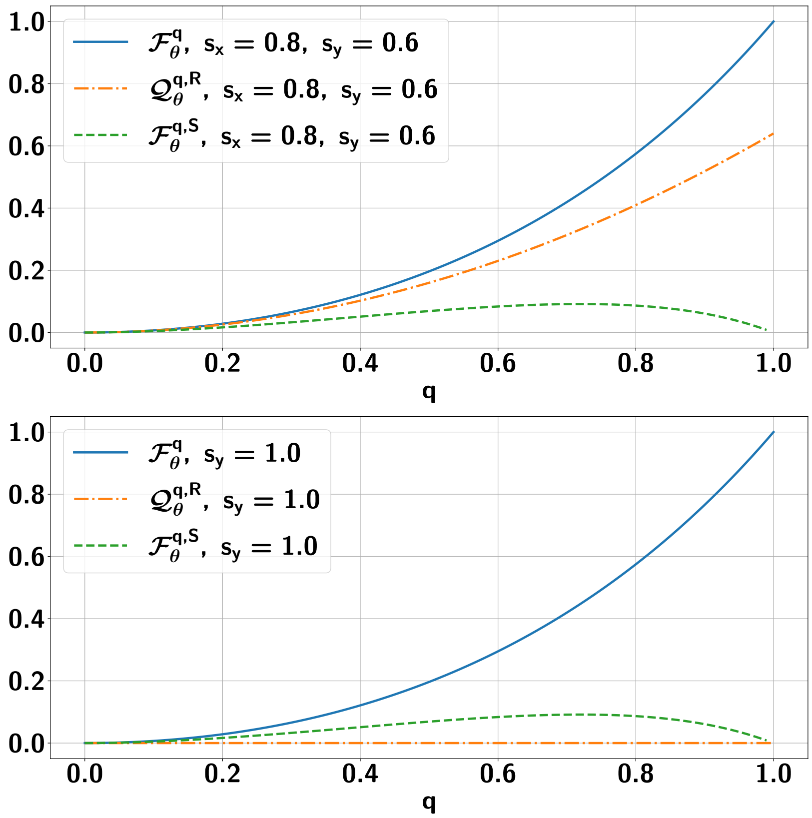

Figure 4.3: **Fisher information (vertical axis) with respect to noise parameter q (horizontla axis). Comparison between time-flipped, "switched" and regular strategies.** Choosing $\hat{n} = \hat{y}$ with $\theta = \pi/4$, FI for NITDM, $\mathcal{F}_\theta^q$ (blue lines) always outperforms switched FI, $\mathcal{F}_\theta^{q,S}$ (green lines) which are independent of probe state. $\mathcal{F}_\theta^q$ is higher than $\mathcal{Q}_\theta^{q,R}$ (orange lines) with both $\hat{s} = [0.8, 0.6, 0]$ and $\hat{s} = \hat{y}$ probe state which are not optimal for regular strategy. All axes are dimensionless.

Arbitrary probe state. Since $\mathcal{Q}_\theta^{q,R}$ is dependent on probe states choosing nonoptimal probe states can reduce the performance of regular strategy whereas NITDM bypasses the probe dependency and illustrates supremacy as shown in Fig. 4.3. We choose $\theta = \pi/4$ and illustrate the advantage of time-flip choosing probe state ρ with $s_x = 0.8, s_y = 0.6$ where $\mathcal{F}_\theta^q$ outperforms both $\mathcal{F}_\theta^{q,S}$ and $\mathcal{Q}_\theta^{q,R}$. Interestingly, even when the probe is in a maximally mixed state or orthogonal to $\hat{n}$, $\mathcal{F}_\theta^q$ is always positive (except for $q = 0$ and $\theta \neq 2m\pi \forall \pi \in \mathbb{Z}$) where regular QFI is $\mathcal{Q}_\theta^{q,R} = 0$. Moreover, the dominance of NITDM over "switched" and regular strategy exists in the low noise region for nonoptimal encoding as illustrated in appendix 7.8.

θ-averaged performance.

Since both $\mathcal{F}_\theta^q$ and $\mathcal{F}_\theta^{q,S}$ depends on the θ itself, let us analyze the average performance of NITDM ($\langle\mathcal{F}_\theta^q\rangle$), "swtiched" ($\langle\mathcal{F}_\theta^{q,S}\rangle$) strategy where $\langle\mathcal{F}_\theta\rangle = \int_0^{2\pi}\mathcal{F}_\theta d\theta\,/(2\pi)$ and regular strategy ($\mathcal{Q}_\theta^{q,R}$, θ-independent). Now, after performing integration, for the NITDM and "switched" strategy, we have

$$\langle\mathcal{F}_\theta^q\rangle = 1 \;-\; \frac{1}{4}\sqrt{(3+q)(3+q-4qn_2^2)} - \frac{1}{4}\sqrt{(1-q)(1-q+4qn_2^2)}, \tag{4.36}$$

and $\langle\mathcal{F}_\theta^{q,S}\rangle = 1 - \frac{\sqrt{3}}{8}(1-q)\sqrt{(1-q)(3+5q)} - \frac{1}{8}\sqrt{(5+6q-3q^2)(5-2q+5q^2)}$ [23] respectively. Given the noise strength q, although $\langle\mathcal{F}_\theta^q\rangle$ and $\langle\mathcal{F}_\theta^{q,S}\rangle$ are both less than the optimal regular QFI, $\mathcal{Q}_\theta^{q,R}|_{\hat{n}=\hat{y}} = q^2 = \langle\mathcal{Q}_\theta^{q,R}|_{\hat{n}=\hat{y}}\rangle$, in the range $\pm n_2^{\min} \leq n_2 \leq \pm 1$ "flipped" strategy is better than the "switched" one on an average, i.e., $\langle\mathcal{F}_\theta^q\rangle > \langle\mathcal{F}_\theta^{q,S}\rangle$. Here, $n_2^{\min} = n_2^0[1-q^g]^{h^{-1}}$ represents the χ^2-fitted curve, where $g = 1.14147 \pm (0.48\%)$ and $h = 2.38455 \pm (0.25\%)$ are fitting parameters (see appendix 7.9), and $n_2^0 = 0.945742$ denotes the value of $n_2^{\min}$ in the complete depolarizing scenario. This signifies another distinct advantage of the quantum time flip strategy over the "switched" strategy. While, in very high noises, flip always outperforms switch when $\pm 0.945742 \leq n_2 \leq \pm 1$, as noise starts to decrease this range increases with the noise parameter, making flip highly favorable in low noise scenarios. Moreover, since the FI with switch method does not depend on n_2, for $\pm n_2^{\min}(q) \leq n_2 \leq \pm 1$ the FI obtained with flip is strictly higher than the highest possible FI obtainable through the switch at various levels of noise q. Because n_2 can be controlled, we can always obtain higher average FI values with time-flip for any value of q.

4.5.2 Advantage in multiqubit strategy

Going beyond the single qubit scenario, we analyze the superiority in the case of multiqubit NITDM. While the optimal strategy for multiqubit NITDM falls outside the scope of this study, we provide a brief overview of its key aspects. Note that while $\mathcal{F}_\theta^q$ is independent of the input probe for $N = 1$, this dependence emerges when $N \geq 2$. By assuming $\theta = \pi/4, n_2 = 1$, we initialize the probe state to be $|+i\rangle^{\otimes N}$ and evaluate $\mathcal{F}_\theta^q$ (given by Eq. (4.21)) for different values of noise content q. In Fig. 4.4, we compare NITDM (by fixing $\theta = \pi/4$) with the regular strategy with optimal product-probe states, i.e, all the N-qubit state is initialized along $\hat{s} = \hat{y}$, which gives QFI, $\mathcal{Q}_\theta^{q,R} = Nq^2$.

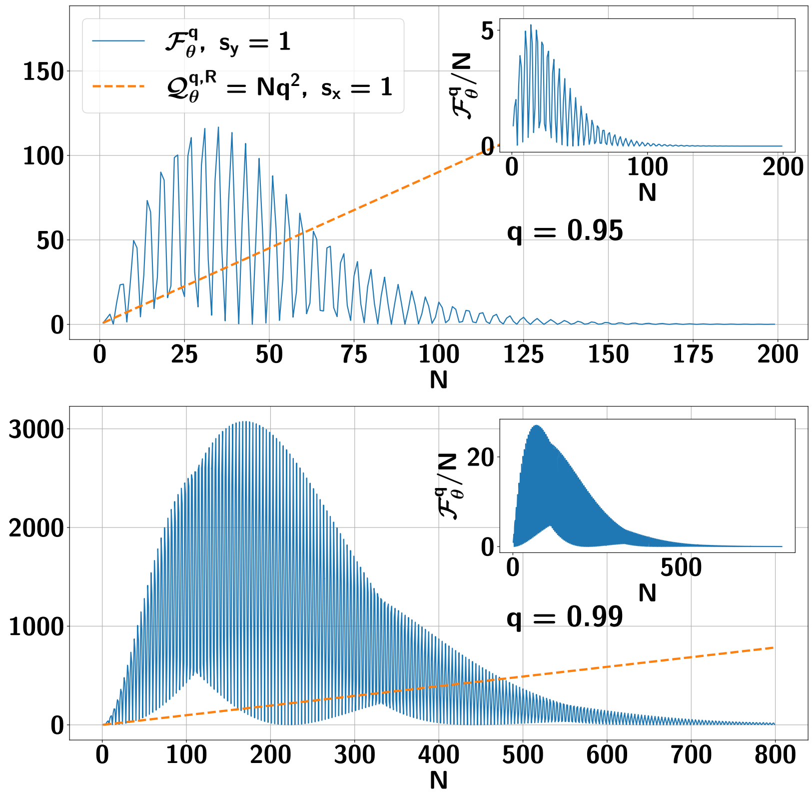

Figure 4.4: **Fisher information (ordinate) with respect to number or qubits N (abscissa) for different values of noise parameter q. Competition between Flip and regular strategy.** Classical Fisher information for time-flip, $\mathcal{F}_\theta^q$ (blue lines) shows oscillatory behavior and after reaching the maximum it decays. Here, we fix the parameter values $\theta = \pi/4$ and $\hat{n}_2 = 1$. Contrastingly, QFI for regular case, $\mathcal{Q}_\theta^{(q,R)}$ (orange dotted lines) increases linearly. **Inset: Fisher information per qubit $\mathcal{F}_\theta^q/N$ (ordinate, blue lines) against number or qubits N (abscissa).** All axes are dimensionless.

Due to N^2 term in Eq. (4.21), $\mathcal{F}_\theta$ increases, along with other terms exponential term in it causes loss of Fisher information with N which is shown in Fig. 4.4 where depending on the system configuration and noise content, $\mathcal{F}_\theta^q$ reaches maximum at a certain value of N. However, FI per qubit, $\mathcal{F}_\theta^q/N$, is maximized, where the first slope change of the envelope of $\mathcal{F}_\theta^q$ occurs. According to this, for a given $\theta, \vec{s}, \hat{n}$, we define the set $\{\tilde{\mathcal{F}}_\theta^q, \tilde{N}\}$ where $\tilde{\mathcal{F}}_\theta^q$ is the value of FI of $\tilde{N}$-qubit NITDM protocol corresponding to maximized value of $\mathcal{F}_\theta^q/N$ at $\tilde{N}$. Now given a high value of $N \gg \tilde{N}$ we perform $\tilde{N}$-qubit NITDM and repeat the procedure for $\lfloor N/\tilde{N} \rfloor$ times to get an advantage over regular additive strategy with N-qubit product probe states. Note that, if $N < \tilde{N}$ then we have to perform N-qubit NITDM to get higher value of FI over the regular stratgey.

To demonstrate, for $q = 0.99$ and $q = 0.95$, the maximum values of FI, $\mathcal{F}_\theta^q$ are 3074.72 and 116.77, respectively, achieved at $N = 170$ and $N = 34$ in the NITDM scheme, while the maximum values of per qubit FI, $\mathcal{F}_\theta^q/N$ are 27.46 and 5.51, achieved at $\{\tilde{\mathcal{F}}_\theta^q, \tilde{N}\} = \{1894.5, 69\}$ and $\{49.68, 9\}$ respectively. For a fixed number of qubits $N = 1000$ qubits and noise level $q = 0.95$, employing the NITDM with $\tilde{N} = 9$ qubits for 111 repetitions yields an effective Fisher information of $111\tilde{\mathcal{Q}}_\theta^{q=0.95} = 111 \times 49.68 = 5514.48$, surpassing the QFI achievable with a standard 1000-qubit system under the same noise conditions, $\mathcal{Q}_\theta^{(q=0.95,R)} = Nq^2 = 1000 \times 0.95^2 = 902.5$. Similarly, for $q = 0.99$, we can perform NITDM strategy with $\tilde{N} = 69$ repeatedly for 14 times to get the best possible result $14\mathcal{F}_\theta^{q=0.99} = 26523 \gg \mathcal{Q}_\theta^{(q=0.99,R)} = 980.1$. This demonstrates a notable performance gain compared to the regular strategy in low-noise regimes. While the superiority of NITDM is demonstrated for a specific parameter θ in low noise regions, appendix 7.10 provides evidence that this advantage holds true when averaged over the parameter space of θ as previously defined.

Chapter 5

Capacity Enhancement with Supermaps

5.1 Quantifying Quantum Communication

Quantum information theory has its roots in Shannon's ideas. The theory's core is the use of quantum physics for information storage, transmission, decoding and encoding purposes [97, 98]. The discipline has shown a wide array of promises in this regard with the availability of protocols such as quantum teleportation, which allows the sharing of quantum states by classical bits of information and a pre-shared entanglement, as well as super-dense coding, which allows sharing significant amount of classical bits (upto two bits) with one qubit transmission and a pre-shared entanglement. In particular, one of the major principles in communication theory is that of capacity, which quantifies the amount of information that can be transmitted using quantum/classical states and channels. Here, we give a brief overview of the literature on quantum capacity.

Consider a simplistic scenario where Alice wants to send some information to Bob, and she has access to a single qubit. She can prepare the qubit in state $|0\rangle$ for message a_1, or she can prepare it in state $|1\rangle$ for message a_2. Bob can then measure the qubits in the basis $\{|0\rangle, |1\rangle\}$ to which they agreed prior to establishing the communication, from which he can infer the message. Notice that Bob's ability to distinguish the states from an ensemble allows communication. Now, this protocol can be modified in several ways. While this protocol serves to share classical information and will thus be quantified by the classical capacity, one could wish to share qubit states, which is quantified by quantum capacity. Similarly, the amount of information that can be sent privately is estimated by private capacities. Lastly, one can wonder about scenarios like dense coding where the parties in question possess pre-shared entanglement, which is quantified by entanglement-assisted or dense coding capacity. Ref. [99, 100] provides a brief overview of these scenarios and the involved capacities.

Coming back to our original example. If Alice is encoding message i with probability p_i by preparing density matrix ρ_i, and the states are perfectly transmitted to Bob. Then, the density matrix of the ensemble with no information of Alice's choice is $\rho = \sum_i p_i \rho_i$, while the density matrix of Bob's ensemble with information of Alice's choice i is ρ_i. The information content of a message encoded in quantum systems is quantified by Von Neumann entropy S, with $S(\rho) = -\operatorname{Tr}(\rho \log_2 \rho)$. For the example above, when Bob receives states $|0\rangle$ or $|1\rangle$ with probabilities $p_{0,1} - 1/2$ and thus the ensemble $I/2$ its entropy is $-\operatorname{Tr}(I/2 \log_2 I/2) = 1$. That is, one bit of information was transmitted. The quantifier of the classical communication between two parties is that of mutual information, which would depend on Bob's choice of measurement; when optimised over all possible measurements, this gives accessible information. It can be shown that accessible information is upper bounded by the Holevo quantity $\chi(\mu) = S(\rho) - \sum_i p_i S(\rho_i)$ for ensemble $\mu = \{p_i, \rho_i\}$. Thus, the Holevo quantity gives a measure or upper bound on the amount of information that can be transmitted through an ensemble.

Typically, however, these communication channels $\mathcal{N}$ are not perfect and may impart some noise to the ensemble. To counter such possibilities, the notion of classical and quantum capacities of noisy channels was formulated. The classical (quantum) capacity of a noisy channel $\mathcal{N}$ is defined as the maximum number of bits (qubits) one can reliably transmit per usage of channel $\mathcal{N}$ in the asymptotic limit of many parallel uses. For this, Holevo information of the channel is defined as

$$\chi(\mathcal{N}) = \max_{\mu} \left[S(\mathcal{N}(\rho)) - \sum_i p_i S(\mathcal{N}(\rho_i)) \right], \tag{5.1}$$

where $\rho = \sum_i p_i \rho_i$ and optimisation is done over all possible ensembles.

From the HSW theorem [101, 102], the classical capacity of the channel is given by

$$\mathcal{C}(\mathcal{N}) = \lim_{n\to\infty} \chi(\mathcal{N}^{\otimes n})/n \tag{5.2}$$

with the Holevo quantity being super-additive, this gives a lower bound $\mathcal{C}(\mathcal{N}) \geq \chi(\mathcal{N})$.

Similarly, for quantum capacity, coherent information of the channel is defined as

$$\mathcal{I}_{co}(\mathcal{N}) \;\; = \;\; \max_{\rho} \mathcal{V}(\mathcal{N}, \rho), \text{ with } \; \mathcal{V}(\mathcal{N}, \rho) = S(\mathcal{N}(\rho)) - S(\mathcal{N} \otimes \mathcal{I}(|\Psi_\rho\rangle \langle\Psi_\rho|)), \tag{5.3}$$

where $|\Psi_\rho\rangle$ is the purification of ρ. From the LSD theorem [103], the quantum capacity of a channel is given by

$$\mathcal{Q}(\mathcal{N}) = \lim_{n\to\infty} \mathcal{I}_{co}(\mathcal{N}^{\otimes n})/n. \tag{5.4}$$

Like Holevo quantity, coherent information is also super-additive in tensor product. Hence, one has lower bound $\mathcal{Q}(\mathcal{N}) \geq \mathcal{I}_{co}(\mathcal{N})$.

One can now begin to quantify the limits of communication of various quantum channels. In general quantifying the capacities is hard because of the asymptotic limit consideration. However, numerical methods exist for calculating Holevo bounds and coherent information. Since capacity is vital for communication tasks, enhancing capacity with the help of supermaps is a valuable goal in quantum communication. One can imagine the following situation: Alice wants to communicate with Bob by sending quantum systems via quantum channels. A third party, Charlie, manages the communication network and has to resolve the communication issues. There may arise a network breakdown where the channels from Alice to Bob become particularly noisy, reducing the communication capacity. Can Charlie employ supermaps over those noisy communication channels to improve communication capacity? This is possible, as we elaborate in the next section.

5.1.1 Capacity Enhancement with Quantum Switch

Let us suppose that in the communication network proposed earlier, the network breakdown is so severe that a completely depolarising channel (CDPC) [97] is acting between Alice and

Bob $\mathcal{N}(\rho) = I/2$. While it can be easily inferred that combining such channels in definite causal order would still give a zero capacity channel, In Ref. [10] the authors demonstrate that the quantum switch supermap can be employed over a pair of such CDPCs and the resulting channel has a finite non-zero capacity.

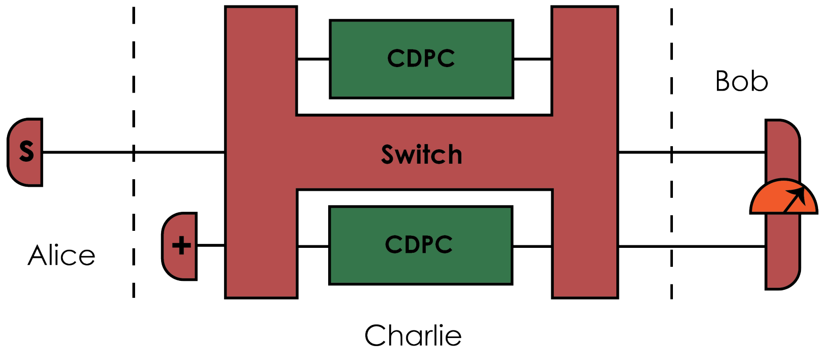

Figure 5.1: **Employing quantum switch for capacity enhancement.** Charlie uses the quantum switch supermap on a pair of CDPCs. The resulting channel has a finite capacity of 0.0488.

Therefore, CDPCs in an indefinite causal order can provide capacity enhancement, a phenomenon termed 'causal activation'. When the control qubit is fixed in $|+\rangle\langle+|$ state and the noisy channel is relaxed to a depolarising channel $\mathcal{N}(\rho) = (1-p)\rho + pI/2$ then the output state is evaluated as

$$\rho^{out} = |+\rangle\langle+| \otimes \left[(1-p)^2\rho + \frac{p^2}{2d^2}\rho + \frac{p^2}{2d}I + \frac{2p(1-p)}{d}I\right] + |-\rangle\langle-| \otimes \left[\frac{p^2}{2d}I - \frac{p^2}{2d^2}\rho\right] \quad (5.5)$$

Now, we state the labelled random channel theorem from Ref. [42]. "If there exists a fixed ensemble which achieves the Holevo quantity of all the channels $\mathcal{N}_k$, the Holevo quantity for the channel with output state $\sum_k |k\rangle\langle k| \otimes p_k\mathcal{N}_k(\rho)$ is equal to $\sum_k p_k\chi(\mathcal{N}_k)$. Moreover, if the individual channels $\mathcal{N}_k$ are Holevo additive, then the obtained Holevo quantity is also the classical capacity of the channel."

Note that the above theorem is valid for all qubit $d = 2$ channels with output state $\sum_k |k\rangle\langle k| \otimes p_k\mathcal{N}_k(\rho)$, where $\mathcal{N}_k(\rho) = \alpha_k\rho + \beta_k\rho^T + \gamma_k I$ where $sgn(\alpha_k * \beta_k)$ is same for all k. When $sgn(\alpha_k * \beta_k) = +1$ the common optimal ensemble is $\{(|0\rangle, |1\rangle), (1/2, 1/2)\}$ while for $sgn(\alpha_k * \beta_k) = -1$ it is $\{(|+i\rangle, |-i\rangle), (1/2, 1/2)\}$ where $|\pm i\rangle = (|0\rangle \pm i\,|1\rangle)$, moreover these $\mathcal{N}_k$ are unital and qubit unital channels are Holevo additive. Employing this theorem for the output of the switch above, we see that the Holevo quantity is achieved for ensemble $\{(|0\rangle, |1\rangle), (1/2, 1/2)\}$ which also gives the classical capacity. We plot the capacities in Fig. 5.2.

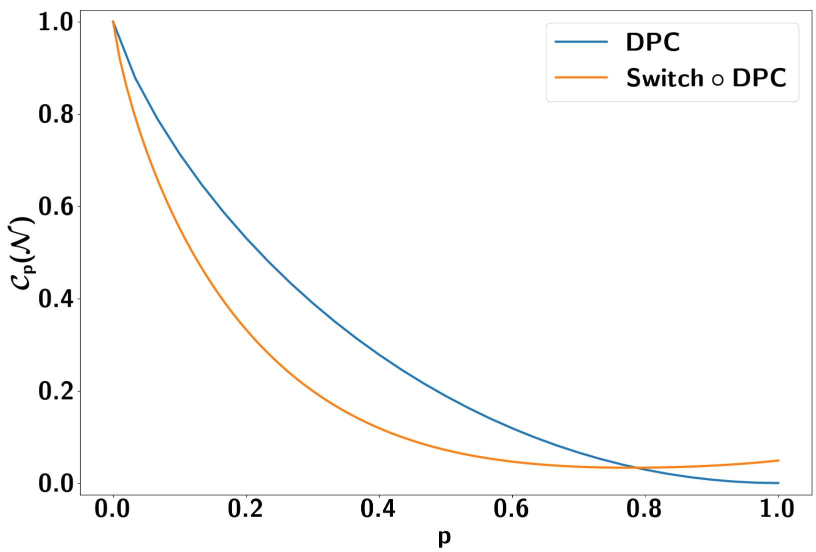

Figure 5.2: **Capacity of regular depolarising channel and causally activated depolarising channel.** While in the low noise regime, switch is doing worse, in the high noise regime, especially at CDPC quantum switch is providing a higher non-zero capacity.

In some sense, the convexity in the graph of Switch $\circ$ CDPC also points out competition between capacity enhancement due to switch, which seems to be increasing with p, and the decay in capacity due to Depolarising noise. Indeed, in Ref. [12, 16], the non-commutativity of the associated Kraus operators of the channels is proposed as the reason for the advantage and the probability of measuring control in $|-\rangle\langle-|$ state, caused by the non-commutativity is given as the advantage measure. The non-commutativity and the advantage measure increases with p while the capacity decreases with p. Another method to infer the same is to employ the labelled random channel theorem. The total capacity is the sum of capacities attained from the $|+\rangle\langle+|$ and $|-\rangle\langle-|$ branches. While the value associated to $|+\rangle\langle+|$ decays with p, the value associated to $|-\rangle\langle-|$ increases and provides a non zero value at $p = 1$. From the theorem, this capacity enhancement is directly proportional to the probability of getting the $|-\rangle\langle-|$ state; hence, one can quantify the enhancement with this quantity.

Along with these results, quantum switch has also shown applications in quantum capacity enhancement [11, 15]. Moreover, quantum N-switch, which coherently controls over N operations with a control qubit of dimensions $N!$, has also shown similar advantages [15, 17]. Particularly illustrative is the application of the categorical quantum mechanics / diagrammatic approach to this problem [14], which demonstrated the optimality of cyclic permutations in the N-switch case.

5.1.2 Capacity Enhancement with SDPPs

While processes with indefinite causal order, such as quantum switch, can provide capacity enhancement, are these the only supermaps that can do so? In particular, is ICO necessary or sufficient for such enhancement? In Ref. [62], the authors define a class of supermaps called superposition of direct pure processes (SDPPs), and demonstrate that such supermaps can also provide capacity enhancement while being definite casual ordered.

In particular, they define direct pure processes as those pure processes, e.g., where process matrix W is a rank one projector, which takes input maps $\mathcal{M}_A$ and $\mathcal{M}_B$ and outputs a quantum channel of the form $\mathcal{X} \circ \mathcal{M}_A \circ \mathcal{Y} \circ \mathcal{M}_B \circ \mathcal{Z}$ where all the input and output dimensions are the same d. If $|w_i\rangle$ are the Choi vectors of direct pure processes then SDPPs are defined as those process matrix with Choi vector $\frac{1}{\sqrt{k}} \sum_i^k |i\rangle\, |w_i\rangle$ where $|i\rangle$ is the control qubit. Transformations with coherent control on causal order are SDPPs, for example quantum switch is an SDPP with expression $\frac{1}{\sqrt{2}}(|0\rangle\, |\mathbb{1}^{C_1A_1}\rangle\rangle|\mathbb{1}^{A_2B_1}\rangle\rangle|\mathbb{1}^{B_2C_2}\rangle\rangle) + \frac{1}{\sqrt{2}}(|1\rangle\, |\mathbb{1}^{C_1B_1}\rangle\rangle|\mathbb{1}^{B_2A_1}\rangle\rangle|\mathbb{1}^{A_2C_2}\rangle\rangle)$.

Can SDPPs with definite causal order provide capacity enhancement? Yes. Specifically the SDPP $\frac{1}{\sqrt{2}}(|0\rangle\, |\mathbb{1}^{C_1A_1}\rangle\rangle|\mathbb{1}^{A_2B_1}\rangle\rangle|\mathbb{1}^{B_2C_2}\rangle\rangle) + \frac{1}{\sqrt{2}}(|1\rangle\, |\mathbf{X}^{C_1A_1}\rangle\rangle|\mathbb{1}^{A_2B_1}\rangle\rangle|\mathbb{1}^{B_2C_2}\rangle\rangle)$, which has a definite causal order, can provide a capacity of 1. When the target qubit is initialized to $|\pm\rangle$, the final control becomes $|\pm\rangle$ due to phase kickback from the target.

5.1.3 Capacity Enhancement by Coherent Control

In Ref. [104], the authors provide another method with coherent control over a channel that enhances capacity without employing ICO. They propose a photonic setup called "Half-Switch", as in Fig. 5.3, which coherently controls the usage of channels $\mathcal{M}_A$ and $\mathcal{M}_B$ using polarisation beam splitters.

The outcomes do not violate the impossibility of arbitrary coherent control [105] because, in reality, the transformation is being applied to a subspace, and the calculations do not consider the vacuum state that passes through one channel while the photon passes through the other. It is argued that such passing of vacuum state provides information on the specifics of channels undergoing coherent control; hence, they are no longer arbitrary. Further considerations on the issue of coherent control were discussed in [106].

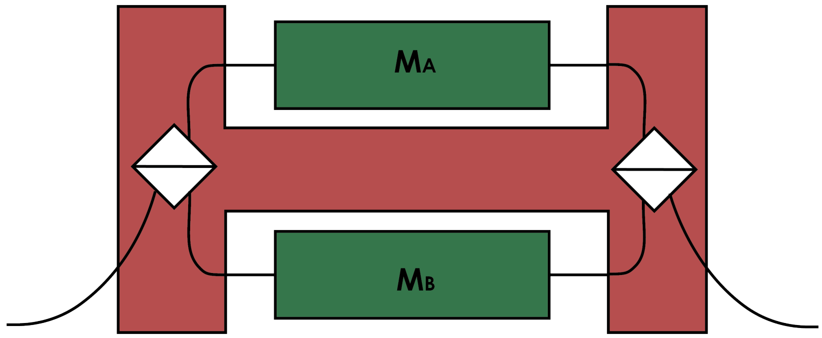

Figure 5.3: **Half Switch Circuit.** A photon with state $\rho \otimes |+\rangle \langle +|_{Pol}$ enters the circuit through left. The polarization beam splitters (white diamonds) coherently control the passage of photons according to the polarization state. Since the polarization is in superposition, the photon passes through the channels $\mathcal{M}_A$ and $\mathcal{M}_B$ in superposition.

The output of the resulting channel can be found by dilating the channels $\mathcal{M}_A$ and $\mathcal{M}_B$ on their respective environments. Surprisingly, the output state depends on the Kraus implementation and environment states. If the input state is $|+\rangle_c \otimes |\psi\rangle \otimes |E_A\rangle \otimes |E_B\rangle$ with $|\psi\rangle$ being the system and $|E_A\rangle$ and $|E_B\rangle$ being the environment, then the output system state reads $\Big[|0\rangle \langle 0|_c \otimes \mathcal{M}_A |\psi\rangle \langle\psi| + |1\rangle \langle 1|_c \otimes \mathcal{M}_B |\psi\rangle \langle\psi| \Big]/2 + \Big[|0\rangle \langle 1|_c \otimes \mathcal{T}_A |\psi\rangle \langle\psi| \mathcal{T}_B^\dagger + |1\rangle \langle 0|_c \otimes \mathcal{T}_B |\psi\rangle \langle\psi| \mathcal{T}_A^\dagger \Big]/2$, where $\mathcal{T}_A = \sum_i \langle E_A|i\rangle M_{A,i}$ and $\mathcal{T}_B = \sum_i \langle E_B|i\rangle M_{B,i}$ are termed as transformation matrices.

Plugging completely depolarising channel here gives $\mathbb{1}_c/2 \otimes \mathbb{1}/2 + \frac{|0\rangle\langle 1|_c + |1\rangle\langle 0|_c}{2} \otimes \mathcal{T}\rho\mathcal{T}^\dagger$ with $\mathcal{T} = \sum_i \sigma_i/4$ with $\sigma_0 = I/2$ and $\sigma_{1,2,3}$ being Pauli matrices. This clearly depends on the input state and provides a finite capacity of 0.16, higher than switch capacity enhancement.

5.2 Communication as a Resource Theory

The above results have shown that resources other than the quantum switch could also aid in the capacity enhancement of a CDPC. However, so far, there has been no uniform and systematic manner to discuss these resources. This problem was resolved in Ref. [13], which defines communication as a resource theory with supermaps as the available resources. The formalisation is done as follows:

- Two sets of channels are defined, those which can be made available to communicating parties by the communication provider, termed as unplaced channels $\mathcal{C}_{unpl}$ and those which are available to the communicating parties, termed as placed channels $\mathcal{C}_{pl}$.

- A resource theory of communication is defined in line of Ref. [107], by the set of free supermaps $\mathcal{S}_{free} \subset \mathcal{S}$, which is closed under the composition of channels and their tensor products. These contain (i) supermaps from unplaced channels to unplaced channels $\mathcal{S}_{u\to u}$, (ii) supermaps from unplaced channels to placed channels $\mathcal{S}_{u\to p}$, and (iii) supermaps from placed channels to placed channels $\mathcal{S}_{p\to p}$.

- Moreover, there is an additional constraint of No-side channel generation, otherwise one can always swap the noisy channel with one which provide an identity channel between communicating parties, making the theory trivial. The side channel generating operation is defined as a supermap $\mathcal{S}$ such that there exist two free supermaps $\mathcal{S}_1$ and $\mathcal{S}_2$ such that for all input channels $\mathcal{S}_2 \circ \mathcal{S} \circ \mathcal{S}_1(\mathcal{N}_1, \cdots, \mathcal{N}_k) = \mathcal{C}$ where $\mathcal{C}$ has some finite non-zero capacity.

- Now, standard quantum Shannon theory is one such instance of such a resource theory, where free operations are generated from compositions of basic placement: $\mathcal{S}_{place}(\mathcal{N}) = \mathcal{U} \circ \mathcal{N} \circ \mathcal{V}$ where $\mathcal{U}$ and $\mathcal{V}$ are unitaries from placed (unplaced) to unplaced (placed) systems, encoding supermap $\mathcal{S}_{enc(\mathcal{E})}(\mathcal{C}_1 \otimes \cdots \otimes \mathcal{C}_k) = (\mathcal{C}_1 \circ \mathcal{E}) \otimes \mathcal{C}_2 \otimes, \cdots, \otimes \mathcal{C}_k$, repeater supermap $\mathcal{S}_{rep(\mathcal{R}_t)}(\mathcal{C}_1 \otimes \cdots \otimes \mathcal{C}_k) = \mathcal{C}_1 \otimes, \cdots, \otimes \mathcal{C}_{m-1} \otimes (\mathcal{C}_{m+1} \circ \mathcal{R} \circ \mathcal{C}_m) \otimes \mathcal{C}_{m+2} \otimes, \cdots, \otimes \mathcal{C}_k$, and the decoding supermaps $\mathcal{S}_{dec(\mathcal{D})}(\mathcal{C}_1 \otimes \cdots \otimes \mathcal{C}_k) = \mathcal{C}_1 \otimes \mathcal{C}_2 \otimes, \cdots, \otimes (\mathcal{D} \circ \mathcal{C}_k)$.

- Generalised capacity of the channel $\mathcal{N}$ can now be defined as the maximum number of bits one can reliably transmit per usage of channel $\mathcal{N}$ by performing free operations from $\mathcal{S}_{free}$.

With such formalisation at hand it was shown that theories with coherent control or quantum switch included in the set of free supermaps form a valid resource theory of communication as the no-side channel generation condition is satisfied. While the theory involving SDPPs is invalid since it allows for side channel generation. Furthermore, resource theory with coherent control of operations requires vacuum extended channels [13], which are costlier resources than genuine ICO.

5.3 Capacity Enhancement with Quantum Time Flip

In Ref. [42], Liu et al. presented the applications of quantum time flip supermap towards capacity enhancement, consistent with the resource theory of communication. They consider a protocol involving Alice, Bob and communication provider Charlie as given in Fig. 5.4.

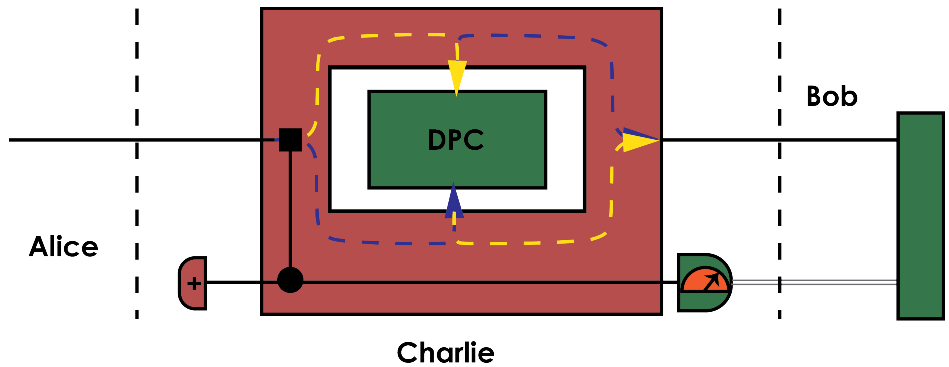

Figure 5.4: **Flip capacity enhancement protocol.** Alice encodes her ensemble $\{p_i, \rho_i\}$ which is passed to Bob through a Depolarising channel DPC $\rho \mapsto (1-p)\rho + pI/d$ under quantum time flip. The communication provider, Charlie, prepares the control in $|+\rangle$ state and measures it after the action of time flip. The output target state and the classical result of the control measurement are then sent to Bob, who can reconstruct the outcome of quantum Time flip for transposition invariant channels.

The output state with Charlie, after the application of quantum time flip, is

$$|+\rangle\langle+| \otimes \left[(1-p)\rho + \frac{p}{2d}\rho^T + \frac{p}{2d}I\right] + |-\rangle\langle-| \otimes \left[\frac{p}{2d}I - \frac{p}{2d}\rho^T\right] \tag{5.6}$$

Although Bob measures the control qubit, it is shown that for transposition invariant channels $\mathcal{C}$, e.g., those for which there exists a Kraus decomposition with $C_i^T = \pm C_i$, the state can be effectively reconstructed so that Bob can have the state of Eq. (5.8). Using the labelled random channel theorem which was introduced in the same work [42], the capacity is obtained by $\sum_k p_k \chi(\mathcal{N}_k)$ where $\chi(\mathcal{N}_k)$ is obtained for ensemble $\{(1/2, 1/2), (|0\rangle, |1\rangle)\}$. The attained capacity values and their comparison with switched and regular DPC capacity are plotted in Fig. 5.5. For a completely depolarising channel, the attained capacity is ~ 0.3113

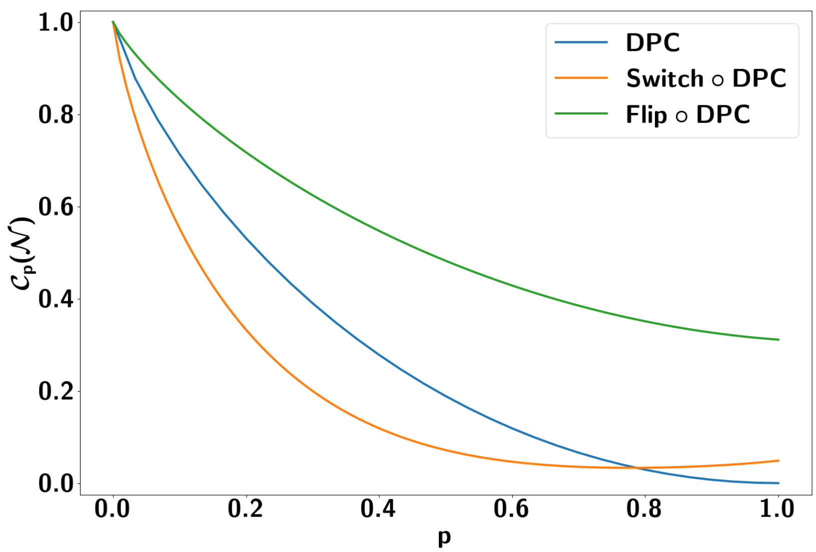

Figure 5.5: **Capacity of regular depolarising channel DPC, DPC under quantum switch and DPC under quantum time flip.** Quantum time flip provides the highest capacity enhancement in all regions. While switch had an adverse effect in low noise regions, no such effect is seen for a flip. The quantum switch takes two DPCs, and the quantum time flip only takes one.

Similar enhancements are also seen in quantum capacity as well. The work also presents classical capacity enhancement for dephasing channels by distilling them.

5.4 Capacity Enhancement with the Combination of Flip and Switch

In their closing remarks, Ref. [42] seeks the potential communication advantages in scenarios where both the input-output / time direction and causal order are subject to indefiniteness among multiple parties. The first step towards treating the most general scenario would be to identify the potential capacity enhancement in the presence of both quantum switch and quantum time flip and carry on from there. In this section, we present our numerical work on identifying such advantages.

In particular, we numerically calculate Holevo bounds for cases with compositions of quantum time flips and quantum switches. The optimization is done by generating four Haar uniform qubit states and 4 random probabilities to create an ensemble and optimize the quantity

$$\chi(\mathcal{N}) = \max_{\mu} \left[S(\mathcal{N}(\rho)) - \sum_i p_i S(\mathcal{N}(\rho_i)) \right]. \tag{5.7}$$

The qubit states are generated by randomly generating two qubit pure states and tracing them out with respect to one subsystem. Then, the sequential least square programming (SLSQP) method is used from Python's scipy optimize package. The validity of the method is confirmed by retrieving the known curves for Switch and Flip capacity enhancement. For the composition of Flip and Switch (see Fig. 5.6), the controls of both the supermaps are fixed to be in $|+\rangle\langle+|$ with the communication provider akin to the quantum time Flip case, and the resulting channel from one supermap is fed to the other supermap.

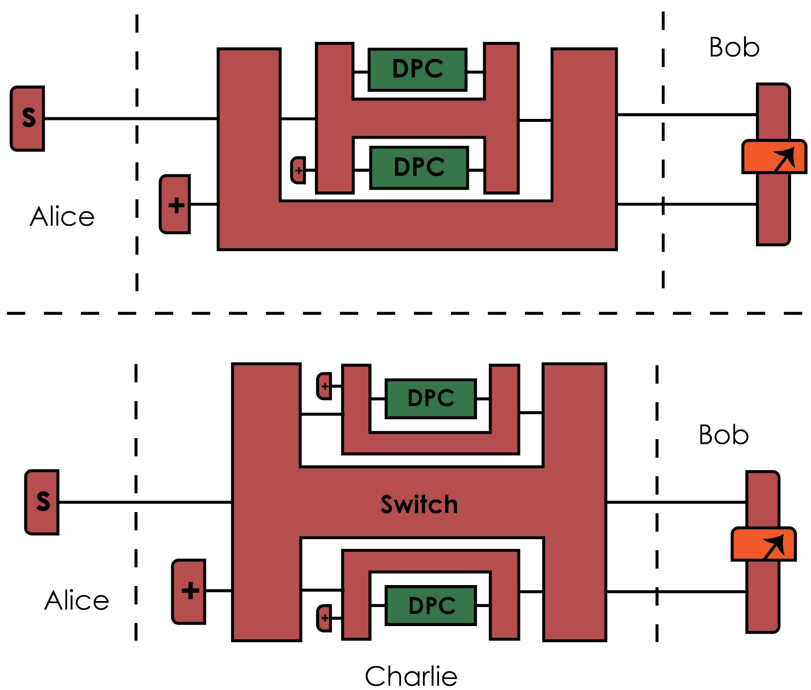

Figure 5.6: **Switch ∘ Flip and Flip ∘ Switch strategies for capacity enhancement.** The quantum time flip and quantum switch are composed keepeing the controls in a fixed state. The capacity enhancement for these circuits is evaluated numerically.

In Fig. 5.7, we observe capacity as a convex function of p, which is justifiable because of the argument given for the Switch composition case. At $p = 1$, at CDPC input, the enhancement acquired by the composition of quantum time flip and quantum switch is 0.5 for Flip ∘ Switch and ~ 0.569 for Switch $\circ$ Flip.

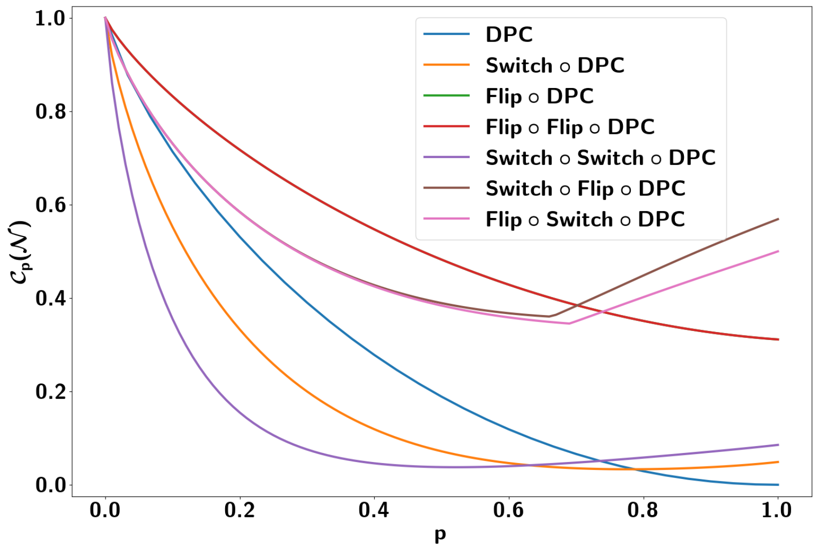

Figure 5.7: **Capacities enhancement due to different quantum supermaps.** At $p = 1$, e.g., at CDPC, the highest capacity enhancement is achieved by conjuction of Flip and Switch, e.g., by Flip $\circ$ Switch and Switch $\circ$ Flip supermaps.

The obtained advantage is higher than any composition of quantum time flips, and quantum switches can provide alone. For quantum time Flip, more than one composition simply results in one more qubit controlling the time direction. For instance, for two time flips, the output state reads

$$|+\rangle\langle+|\otimes|+\rangle\langle+|\otimes\left[(1-p)\rho+\frac{p}{2d}\rho^T+\frac{p}{2d}I\right]+|-\rangle\langle-|\otimes|-\rangle\langle-|\otimes\left[\frac{p}{2d}I-\frac{p}{2d}\rho^T\right], \quad (5.8)$$

which has the same capacity enhancement as is also visible from the plot above. Hence, the highest capacity enhancement for CDPC with the composition of N quantum time flips is 0.3113. For the composition of N quantum switch, note that the composition of N number of switches gives a channel which is a subcase of $2^N!-$ switch, e.g., one which controls the order of 2^N CDPCs. After all, the composition of N switches in the manner above would only give a particular set of permutations on the order of 2^N CDPCs. In Ref. [15], the authors provide the capacity for N switch at large N. Which is

$$\mathcal{C}(\mathcal{N}) = \frac{\log(d+1)}{d^2} - \left(1 - \frac{1}{d}\right)\log\left(1 - \frac{1}{d^2}\right) - \frac{1}{d}\log\left(1 + \frac{1}{d}\right) - \mathcal{O}\left(\left(1 - \frac{1}{d}\right)\frac{\log N}{N}\right). \tag{5.9}$$

The maximum is obtained at $N \to \infty$ and $d = 2$, which comes out to be 0.3113. Interestingly, both flip and switch compositions saturate to the same value. Moreover, that value is still lower than possible with the compositions of a single quantum time flip and switch. Retrieving the optimal ensembles for the conjunction case, we obtain that after the kinks ensemble $\{(1/2, 1/2), (|+i\rangle, |-i\rangle)\}$ and before the kinks ensemble $\{(1/2, 1/2), (|0\rangle, |1\rangle)\}$ are optimal. This is unlike other cases where a single ensemble is optimal for all values of p.

Working out the output states and Holevo bounds for the conjunction of quantum time flip and quantum switch becomes particularly cumbersome with linear algebraic methods with the growing number of operations. Instead, diagrammatic methods similar to Ref. [14] can be employed to calculate these states. With diagrammatics, a thorough analysis can be done on what compositions are optimal and the analytical reasons for the higher capacity enhancement when a conjunction of flip and switch is employed. This is a task for a future work.

Chapter 6

Conclusion

We have surveyed higher-order quantum operations, specifically those with two idiosyncratic properties, indefinite causal order and indefinite time directions. In particular, we studied the properties and interpretations of the quantum switch supermap and the quantum time flip supermap. We reviewed quantum metrology and ICO-assisted metrology and considered optimizations of metrological protocols, where we reproduced existing results in the literature.

In chapter four, we incorporated the concept of an indefinite time directed encoding process in the framework of quantum metrology to enhance the precision limit of parameter estimation beyond the standard quantum limit (SQL). To accomplish a higher precision than the SQL, referred to as the Heisenberg limit (HL), the conventional parameter estimation strategy relies on an entangled input probe, along with unitary encoding and multi-qubit measurement on the encoded state for decoding. In contrast, we demonstrated that achieving the HL is possible by employing unentangled input probes with discrete energy levels provided indefinite time directed encoding (ITDM) is performed. Specifically, we proved analytically that the symmetric product probe state is sufficient to reach Heisenberg scaling among all possible multiparty input states, although entangled input probe states can increase the precision of parameter estimation compared to the separable probe ones. Further, in some instances involving product probes, the bidirectionally encoded state remains a product state, indicating that entanglement is not generated throughout the protocol even after the global time-flip operation and, therefore, is unnecessary. Fixing the measurement on the control qubit, we illustrated that in the limit of small parameter values, both the input probe and quantum Fisher information (QFI), which provides a lower bound on the precision, are independent of the parameters involved. We also examined the impact of noise on a single-qubit scenario and assessed its advantages in certain cases over the "switched" (based on indefinite causal order) and conventional metrology protocols. Additionally, we discussed strategies for achieving higher Fisher information in noisy multi-qubit scenarios, in comparison to the regular scheme. A coherent superposition of arbitrary unitary transformations and their time-reversed counterparts can be experimentally simulated using an optical interferometer, as described in Refs. [43, 46]. Therefore, we believe that our proposed protocol is experimentally feasible and can be used to validate the Heisenberg limit of root mean square error utilizing a bidirectional encoding process without entangled probes, which are fragile to produce in laboratories.

Our results pave the way for the metrological utilization of quantum time flips in the discrete-variable regime. Going forward, it will be fascinating to explore the behaviour of QFI in the presence of noise using other estimation procedures such as parallel, adaptive, and indefinite-causal-order approaches [22, 26, 29] in conjunction with indefinite time direction. To determine whether time flip or more generic indefinite time directed [40] techniques outperform typical quantum comb or indefinite-causal-order systems, their hierarchies must be rigorously classified and evaluated, possibly using semi-definite optimization techniques [22, 26, 29, 71, 72].

We surveyed the existing literature on capacity enhancement with supermaps. After providing a brief introduction to quantum capacity, a study of capacity enhancement using a quantum switch is provided. We also reproduced the major results using recently introduced labelled random channel theorem and analyzed the qualitative behaviour of the graphs. We reviewed capacity enhancement with SDPPs, coherent control, quantum time flip, and the resource theory of quantum communication, putting all the enhancement literature in a general framework.

Finally, we numerically estimate the possible capacity enhancements with the conjunction of quantum time flip and quantum switch, showing that the available enhancement is strictly higher than any number of compositions of switch and flip alone. We comment on the newly observed behaviour of capacity vs noise parameter graphs. The results we derive provide the first steps in analyzing possible capacity enhancements using the broadest possible set of supermaps, namely those involving ITD and ICO. The possible future steps in this direction involve utilizing diagrammatic methods in line with [14] to determine the optimal usage and conjunction of the two supermaps. Moreover, it may also help determine the analytical reasons for the observed higher capacity enhancement. We also suspect that the analytical expressions for the obtainable capacities can be obtained via generalizations to the labelled random channel theorem.

Chapter 7

Appendix

7.1 Calculation of QFI for a general Product state

In the case of the product probe state, from Eq. (4.2) in the main text, we have

$$|\dot{\Phi}\rangle = \frac{\mathrm{d}\,|\Phi\rangle}{\mathrm{d}\theta} \;=\; \sqrt{p_c}\,|0\rangle \otimes \sum_{i=1}^{N}\left(|\dot{\chi_i}\rangle \bigotimes_{\substack{j=1\\ j\neq i}}^{N} |\chi_j\rangle\right) + e^{i\theta_c}\sqrt{1-p_c}\,|1\rangle \otimes \sum_{i=1}^{N}\left(|\dot{\omega_i}\rangle \bigotimes_{\substack{j=1\\ j\neq i}}^{N} |\omega_j\rangle\right).$$

Therefore, we can write the inner product of $|\dot{\Phi}\rangle$ with itself as

$$\langle\dot{\Phi}|\dot{\Phi}\rangle \;=\; p_c\left(\sum_{k=1}^{N}\langle\dot{\chi}_k|\dot{\chi}_k\rangle + \sum_{\substack{j,k=1\\ j\neq k}}^{N}\langle\dot{\chi}_k|\chi_k\rangle\langle\chi_j|\dot{\chi}_j\rangle\right) + (1-p_c)\left(\sum_{k=1}^{N}\langle\dot{\omega}_k|\dot{\omega}_k\rangle + \sum_{\substack{j,k=1\\ j\neq k}}^{N}\langle\dot{\omega}_k|\omega_k\rangle\langle\omega_j|\dot{\omega}_j\rangle\right). \tag{7.1}$$

On the other hand, we have

$$\langle\dot{\Phi}|\Phi\rangle = p_c\sum_{k=1}^{N}\langle\dot{\chi}_k|\chi_k\rangle + (1-p_c)\sum_{k=1}^{N}\langle\dot{\omega}_k|\omega_k\rangle. \tag{7.2}$$

Defining

$$\langle\dot{\chi}_k|\chi_k\rangle = \alpha_k, \quad \langle\dot{\chi}_k|\dot{\chi}_k\rangle = |\dot{\chi}_k|,$$
$$\langle\dot{\omega}_k|\omega_k\rangle = \beta_k, \quad \langle\dot{\omega}_k|\dot{\omega}_k\rangle = |\dot{\omega}_k|, \tag{7.3}$$

we can rewrite Eqs. (7.1) and (7.2) as

$$\langle\dot{\Phi}|\dot{\Phi}\rangle = p_c\left(\sum_{k=1}^{N}|\dot{\chi}_k| + \sum_{\substack{j,k=1\\ j\neq k}}^{N}\alpha_k\alpha_j^*\right) + (1-p_c)\left(\sum_{k=1}^{N}|\dot{\omega}_k| + \sum_{\substack{j,k=1\\ j\neq k}}^{N}\beta_k\beta_j^*\right),$$

and

$$\langle\dot{\Phi}|\Phi\rangle = p_c\sum_{k=1}^{N}\alpha_k + (1-p_c)\sum_{k=1}^{N}\beta_k, \tag{7.4}$$

respectively. Finally, we calculate the QFI corresponding to an arbitrary product probe state as shown in Eq. (4.4) of main text.

7.2 Proof of Theorem 1

$$\begin{aligned}
\mathcal{Q}_{\text{avg}} - \mathcal{Q}^A = {} & 4\Bigg[p_c\left(\sum_{k=1}^{N}|\dot{\chi}_k| + (N-1)\sum_{k=1}^{N}\alpha_k\alpha_k^*\right) + (1-p_c)\left(\sum_{k=1}^{N}|\dot{\omega}_k| + (N-1)\sum_{k}\beta_k\beta_k^*\right)\\
& \qquad -N\sum_{k=1}^{N}\Big|p_c\alpha_k + (1-p_c)\beta_k\Big|^2\Bigg]\\
& -4\Bigg[p_c\left(\sum_{k=1}^{N}|\dot{\chi}_k| + \sum_{k=1}^{N}\sum_{j\neq k}^{N}\alpha_k\alpha_j^*\right) + (1-p_c)\left(\sum_{k=1}^{N}|\dot{\omega}_k| + \sum_{k=1}^{N}\sum_{j\neq k}^{N}\beta_k\beta_j^*\right)\\
& \qquad -\Big|p_c\sum_{k=1}^{N}\alpha_k + (1-p_c)\sum_{k=1}^{N}\beta_k\Big|^2\Bigg]\\
= {} & 4\Bigg[p_c\left((N-1)\sum_{k=1}^{N}\alpha_k\alpha_k^* - \sum_{k=1}^{N}\sum_{j\neq k}^{N}\alpha_k\alpha_j^*\right) + (1-p_c)\left((N-1)\sum_{k=1}^{N}\beta_k\beta_k^* - \sum_{k=1}^{N}\sum_{j\neq k}^{N}\beta_k\beta_j^*\right)\\
& +\Big|p_c\sum_{k=1}^{N}\alpha_k + (1-p_c)\sum_{k=1}^{N}\beta_k\Big|^2 - N\sum_{k=1}^{N}\Big|p_c\alpha_k + (1-p_c)\beta_k\Big|^2\Bigg]
\end{aligned} \tag{7.5}$$

$$
\begin{aligned}
= \;& 2p_c \sum_{k=1}^{N}\sum_{j=1}^{N}\left(\alpha_k\alpha_k^* + \alpha_j\alpha_j^* - \alpha_k\alpha_j^* - \alpha_j\alpha_k^*\right) + 2(1-p_c)\sum_{k=1}^{N}\sum_{j=1}^{N}\left(\beta_k\beta_k^* + \beta_j\beta_j^* - \beta_k\beta_j^* - \beta_j\beta_k^*\right)\\
&+4\sum_{k=1}^{N}\sum_{j=1}^{N}\left(p_c^2\alpha_k\alpha_j^* + (1-p_c)^2\beta_k\beta_j^* + p_c(1-p_c)\beta_k\alpha_j^* + p_c(1-p_c)\alpha_k\beta_j^*\right)\\
&-4N\sum_{k=1}^{N}\left(p_c^2\alpha_k\alpha_k^* + (1-p_c)^2\beta_k\beta_k^* + p_c(1-p_c)\alpha_k\beta_k^* + p_c(1-p_c)\beta_k\alpha_k^*\right) \qquad (7.6)
\end{aligned}
$$

$$
\begin{aligned}
= \;& 4Np_c(1-p_c)\sum_{k=1}^{N}\alpha_k\alpha_k^* + 4Np_c(1-p_c)\sum_{k=1}^{N}\beta_k\beta_k^* - 4p_c(1-p_c)\sum_{k=1}^{N}\sum_{j=1}^{N}\alpha_k\alpha_j^*\\
&\qquad -4p_c(1-p_c)\sum_{k=1}^{N}\sum_{j=1}^{N}\beta_k\beta_j^*\\
&+4p_c(1-p_c)\sum_{k=1}^{N}\sum_{j=1}^{N}\alpha_k\beta_j^* + 4p_c(1-p_c)\sum_{k=1}^{N}\sum_{j=1}^{N}\beta_k\alpha_j^* - 4Np_c(1-p_c)\sum_{k=1}^{N}\alpha_k\beta_k^*\\
&\qquad -4Np_c(1-p_c)\sum_{k=1}^{N}\beta_k\alpha_k^* \qquad (7.7)\\
= \;& 4Np_c(1-p_c)\left(\sum_{k=1}^{N}\alpha_k\alpha_k^* + \sum_{k=1}^{N}\beta_k\beta_k^* - \sum_{k=1}^{N}\alpha_k\beta_k^* - \sum_{k=1}^{N}\beta_k\alpha_k^*\right)\\
&+4p_c(1-p_c)\left(\sum_{k=1}^{N}\sum_{j=1}^{N}\alpha_k\beta_j^* + \sum_{k=1}^{N}\sum_{j=1}^{N}\beta_k\beta_j^* - \sum_{k=1}^{N}\sum_{j=1}^{N}\alpha_k\alpha_j^* - \sum_{k=1}^{N}\sum_{j=1}^{N}\beta_k\beta_j^*\right)\\
= \;& 4Np_c(1-p_c)\sum_{k=1}^{N}|\alpha_k-\beta_k|^2 - 4p_c(1-p_c)\left|\sum_{k=1}^{N}\alpha_k-\beta_k\right|^2 \geq 0 \qquad (7.8)
\end{aligned}
$$

where the last inequality is due to Cauchy–Schwarz inequality.

7.3 Proof of $A + B \leq 1$ in Theorem 3

The sum of coefficients A and B is calculated as

$$
\begin{aligned}
A + B \;=\;& 1 - n_3^2(1-2p_s)^2 + 4\{n_1\cos\theta_s + n_2(2p_c-1)\sin\theta_s\}\\
&\times\left[n_3(1-2p_s)\sqrt{p_s(p_s-1)}\{n_1\cos\theta_s + n_2(2p_c-1)\sin\theta_s\}\right]. \qquad (7.9)
\end{aligned}
$$

To maximize $A + B$ with respect to the parameter p_c we calculate

$$\frac{\partial(A+B)}{\partial p_c} = 8n_2 \sin\theta_s \Big[n_3(1-2p_s)\sqrt{p_s(1-p_s)} - 2p_s(1-p_s)\big\{ n_1 \cos\theta_s + n_2(-1+2p_c)\sin\theta_s \big\} \Big] \quad (7.10)$$

Solving $\dfrac{\partial(A+B)}{\partial p_c} = 0$ we get

$$p_c = \frac{1}{2} - \frac{1}{4n_2}\left\{ 2n_1 \cot\theta_s + \frac{n_3(-1+2p_s)\csc\theta_s}{\sqrt{p_s(1-p_s)}} \right\} = p_c^o. \quad (7.11)$$

Now, the 2nd order derivative is given by

$$\frac{\partial^2(A+B)}{\partial {p_c}^2} = -32n_2^2 p_s(1-p_s)\sin^2\theta_s < 0, \quad (7.12)$$

for $-1 \leq n_2 \leq 1$, $0 < p_s < 1$ and $\theta_s \neq 2m\pi$ where m is any integer. Finally, the maximum value of $A+B$ is given by $A+B|_{p_c=p_c^o} = 1$.

7.4 Axis Estimation with ITDM

The 2×2 unitary matrix is given by

$$\begin{aligned} U &= \exp\left\{ -i\frac{\theta}{2}\big(\sin\phi\cos\xi\ \sigma_x + \sin\phi\sin\xi\ \sigma_y + \cos\phi\ \sigma_z \big) \right\}, \\ &= \begin{bmatrix} \cos\left(\frac{\theta}{2}\right) - i\cos\phi\sin\left(\frac{\theta}{2}\right) & -i\cos\xi\sin\phi\sin\left(\frac{\theta}{2}\right) - \sin\phi\sin\xi\sin\left(\frac{\theta}{2}\right) \\ -i\cos\xi\sin\phi\sin\left(\frac{\theta}{2}\right) + \sin\phi\sin\xi\sin\left(\frac{\theta}{2}\right) & \cos\left(\frac{\theta}{2}\right) + i\cos\phi\sin\left(\frac{\theta}{2}\right) \end{bmatrix} \end{aligned} \quad (7.13)$$

where θ is the phase and ϕ, ξ are the parameters of the axis of rotation of the unitary matrix. We aim to estimate ϕ. According to corollary 2, we initialize the input state as $\left|\Psi^S\right\rangle = |\psi_c\rangle\, |\psi\rangle^{\otimes N}$ where $|\psi\rangle = \sqrt{p_s}\,|0\rangle + e^{i\theta_s}\sqrt{1-p_s}\,|1\rangle$ with $\theta_s \in [0, 2\pi]$ and $p_s \in [0,1]$ and $|\psi_c\rangle = \sqrt{p_c}\,|0\rangle + e^{i\theta_c}\sqrt{1-p_c}\,|1\rangle$. In this scenario, we find that

$$\begin{aligned} \alpha = \langle\dot{\chi}|\chi\rangle &= i\Bigg[(1/2-p_s)\sin\phi\sin\theta\sqrt{p_s(1-p_s)}\cos\theta_s\Big(\sin\xi - \cos\theta\sin\xi\ + \cos\phi\cos\xi\sin\theta \Big) \\ &\qquad + \sqrt{p_s(1-p_s)}\sin\theta_s\Big(-\cos\xi + \cos\theta\cos\xi + \cos\phi\sin\xi\sin\theta \Big) \Bigg], \\ \beta = \langle\dot{\omega}|\omega\rangle &= i\Bigg[(1/2-p_s)\sin\phi\sin\theta + \sqrt{ps(1-ps)}\cos\theta_s\Big(\cos\theta\sin\phi - \sin\xi + \cos\phi\cos\xi\sin\theta \Big) \end{aligned}$$

$$+\sqrt{ps(1-ps)}\sin\theta_s\Big(-\cos\xi+\cos\theta\cos\xi-\cos\phi\sin\xi\sin\theta\Big)\Bigg],$$

$$|\dot{\chi}| = \langle\dot{\chi}|\dot{\chi}\rangle = \sin^2\frac{\theta}{2}, \quad |\dot{\omega}| = \langle\dot{\omega}|\dot{\omega}\rangle = \sin^2\frac{\theta}{2},$$

where the dot represents the derivative with respect to ϕ. This gives a QFI of $\mathcal{Q}_\phi = AN^2 + BN$, where

$$A = 4p_c(1-p_c)|\alpha-\beta|^2, \quad B = 4\Big[p_c\Big(|\dot{\chi}|-|\alpha|^2\Big)+(1-p_c)\Big(|\dot{\omega}|-|\beta|^2\Big)\Big]. \tag{7.14}$$

By optimizing A with respect to the state and unitary parameters we get $\max\limits_{p_c,p_s,\theta_s,\xi,\theta} A = 4$ at $p_c = 1/2,\ p_s = 1/2,\ \theta_s = \pi,\ \xi = \pi/2,\ \theta = \pi$ which in turn gives $B = 0$. Thus, we get a quantum Fisher information of $\mathcal{Q}_\phi = 4N^2$. It is easy to see that for any $AN^2 + BN$ and $CN^2 + DN$ with $A \geq C$ implies $AN^2 + BN \geq CN^2 + DN$ for all positive integer value of N iff $A + B \geq C + D$. Numerically optimizing $A + B$ indeed gives us a value of 4. Therefore the particular parameters employed provide us with the maximum value of QFI, $\mathcal{Q}_\phi = 4N^2$ with optimal pure product states and optimal unitary parameters. In a similar manner, we can also calculate that optimal $\mathcal{Q}_\xi$ scales as N^2.

7.5 Spectrum of $U_\theta^\dagger U_\theta^T$

$U_\theta^\dagger U_\theta^T$ is a unitary matrix, satisfying $U_\theta^\dagger U_\theta^T |u(\hat{n},\theta)^\pm\rangle = \exp(\pm i\mathrm{f}(n_2,\theta))\,|u(\hat{n},\theta)^\pm\rangle$. Here, $\mathrm{f}(n_2,\theta)$ is given by

$$\mathrm{f}(n_2,\theta) = \tan^{-1}\left(\frac{\sqrt{4n_2^2\sin^2\frac{\theta}{2}\left(1-n_2^2\sin^2\frac{\theta}{2}\right)}}{1-2n_2^2\sin^2\frac{\theta}{2}}\right). \tag{7.15}$$

The eigenvectors can be expressed as

$$\left|u(\hat{n},\theta)^\pm\right\rangle = \frac{\mathrm{g}^\mp(\hat{n},\theta)\,|0\rangle + |1\rangle}{\sqrt{1+|\mathrm{g}^\mp(\hat{n},\theta)|^2}}, \tag{7.16}$$

where

$$\mathrm{g}^\mp(\hat{n},\theta) = \frac{2n_1n_2\sin^2\frac{\theta}{2} \mp \sqrt{4n_2^2\sin^2\frac{\theta}{2}\left(1-n_2^2\sin^2\frac{\theta}{2}\right)}}{-2n_2n_3\sin^2\frac{\theta}{2} - in_2\sin\theta}. \tag{7.17}$$

7.6 FI for small values of θ

For small values of $\theta = \tilde{\theta}$ we consider up to 2nd order correction, i.e., by ignoring $\mathcal{O}(\theta^2)$. This approximates Eqs. (4.26) and (4.27) in the main text as $r(\boldsymbol{\nu}) \approx 1 - n_2^2\tilde{\theta}^2(1-s_y^2)/2$ and $f(\boldsymbol{\nu}) \approx n_2 s_y \tilde{\theta} - n_2\tilde{\theta}^2(n_3 s_x - n_1 s_z)/2$. Consequently, we have $\dot{r}(\boldsymbol{\nu}) = n_2^2\tilde{\theta}(1-s_y^2)$ and $\dot{f}(\boldsymbol{\nu}) = n_2 s_y - n_2\tilde{\theta}(n_3 s_x - n_1 s_z)$. Putting these values alongwith $\theta_c \neq 0$ in Eq. (4.21) in the main text we get

$$
\begin{aligned}
\mathcal{F}_{\tilde{\theta}} \approx\ & N^2\left(1 - \frac{n_2^2(1-s_y^2)\tilde{\theta}^2}{2}\right)^{2N-2}\Bigg[-\tilde{\theta}n_2^2(1-s_y^2)\cos\Big(N\{n_2 s_y\tilde{\theta} + \mathcal{O}(\theta^2)\} + \theta_c\Big) \\
& -\left(1 - \frac{n_2^2(1-s_y^2)\tilde{\theta}^2}{2}\right)\Big(n_2 s_y + \mathcal{O}(\theta)\Big)\sin\Big(N\{n_2 s_y\tilde{\theta} + \mathcal{O}(\theta^2)\} + \theta_c\Big)\Bigg]^2 \\
& \Bigg/\left[1 - \left(1 - \frac{n_2^2(1-s_y^2)\tilde{\theta}^2}{2}\right)^{2N}\cos^2\Big(N\{n_2 s_y\tilde{\theta} + \mathcal{O}(\theta^2)\} + \theta_c\Big)\right], \\
\approx\ & N^2\Bigg[-\tilde{\theta}n_2^2(1-s_y^2)\Big(\cos\theta_c - \{Nn_2 s_y\tilde{\theta} + \mathcal{O}(\theta^2)\}\sin\theta_c\Big) - \left(1 - \frac{n_2^2(1-s_y^2)\tilde{\theta}^2}{2}\right) \\
& \times\Big(n_2 s_y + \mathcal{O}(\theta)\Big)\left(\sin\theta_c + N\{n_2 s_y\tilde{\theta} + \mathcal{O}(\theta^2)\}\cos\theta_c - \frac{\sin\theta_c}{2}N^2\{n_2 s_y\tilde{\theta} + \mathcal{O}(\theta^2)\}^2\right)\Bigg]^2 \\
& \Bigg/\Bigg[1 - \Big(1 - Nn_2^2(1-s_y^2)\tilde{\theta}^2\Big)\Big(\cos^2\theta_c - N\{n_2 s_y\tilde{\theta} + \mathcal{O}(\theta^2)\}\sin 2\theta_c \\
& \qquad - N^2\{n_2 s_y\tilde{\theta} + \mathcal{O}(\theta^2)\}^2\cos 2\theta_c\Big)\Bigg] \\
\approx\ & \frac{N^2 n_2^2 s_y^2\sin^2\theta_c}{1-\cos^2\theta_c} = s_y^2 n_2^2 N^2.
\end{aligned} \tag{7.18}
$$

On the other hand, with $\theta_c = 0$ we have

$$
\begin{aligned}
\mathcal{F}_{\tilde{\theta}} \approx\ & N^2\left(1 - \frac{n_2^2(1-s_y^2)\tilde{\theta}^2}{2}\right)^{2N-2}\Bigg[-\tilde{\theta}n_2^2(1-s_y^2)\cos\Big(Nn_2 s_y\tilde{\theta} + \mathcal{O}(\theta^2)\Big) - \left(1 - \frac{n_2^2(1-s_y^2)\tilde{\theta}^2}{2}\right) \\
& \times\Big(n_2 s_y + \mathcal{O}(\theta)\Big)\sin\Big(Nn_2 s_y\tilde{\theta} + \mathcal{O}(\theta^2)\Big)\Bigg]^2\Bigg/\Bigg[1 - \left(1 - \frac{n_2^2(1-s_y^2)\tilde{\theta}^2}{2}\right)^{2N} \\
& \qquad \times\cos^2\Big(N\{n_2 s_y\tilde{\theta} + \mathcal{O}(\theta^2)\}\Big)\Bigg], \\
\approx\ & \frac{N^2\Big(-\tilde{\theta}n_2^2(1-s_y^2) - Nn_2^2 s_y^2\tilde{\theta} - \mathcal{O}(\theta^2)\Big)^2}{1 - (1 - Nn_2^2(1-s_y^2)\tilde{\theta}^2)(1 - N^2 n_2^2 s_y^2\tilde{\theta}^2)},
\end{aligned}
$$

$$\approx \frac{N^2 n_2^4 \tilde{\theta}^2 \left((1-s_y^2)+Ns_y^2\right)^2}{Nn_2^2\tilde{\theta}^2((1-s_y^2)+Ns_y^2)} = Nn_2^2\left((1-s_y^2)+Ns_y^2\right) = s_y^2 n_2^2 N^2 + (1-s_y^2)n_2^2 N \quad (7.19)$$

Comparing Eqs. (7.18) and (7.19) it is evident that $\theta_c = 0$ is the optimal scenario. However, $\theta_c \neq 0$ scenario also attains Heisenberg scaling.

7.7 Proof of Theorem 6

A general N-qubit state can be written as

$$|\Psi\rangle = \sum_{i=1}^{2^N} \Lambda_i |\lambda_i\rangle, \quad (7.20)$$

where $(i-1)$ is the decimal equivalent number of the ith basis vector $|\lambda_i\rangle$, represented in binary number. For example, the decimal equivalent number of the basis state $|\lambda_2\rangle = |\mathbf{0}\rangle^{\otimes N-1} \otimes |\mathbf{1}\rangle$ is 1, where $|\mathbf{0}\rangle$ and $|\mathbf{1}\rangle$ is just the representation of qubit basis. Decomposing $|\lambda_i\rangle$ as $\bigotimes_{j=1}^N |\psi_j^i\rangle$ where $|\psi_j^i\rangle$ is the ith basis state for jth qubit with $\langle\psi_j^i|\psi_j^k\rangle = \delta_{ik}$ and $\sum_{i=1}^2 |\psi_j^i\rangle\langle\psi_j^i| = I_2$ we rewrite

$$|\Psi\rangle = \sum_{i=1}^{2^N} \Lambda_i \bigotimes_{j=1}^N |\psi_j^i\rangle. \quad (7.21)$$

The encoded state can be written as

$$|\Phi\rangle = \sum_{i=1}^{2^N} \Lambda_i \left(\sqrt{p_c}\,|0\rangle \bigotimes_{j=1}^N |\chi_j^i\rangle + e^{i\theta_c}\sqrt{1-p_c}\,|1\rangle \bigotimes_{j=1}^N |\omega_j^i\rangle\right), \quad (7.22)$$

where $|\chi_j^i\rangle = U_\theta |\psi_j^i\rangle$ and $|\omega_j^i\rangle = U_\theta^T |\psi_j^i\rangle$. To calculate the QFI, we find the derivative of Eq. (7.22) above with respect to parameter θ which is given by

$$|\dot{\Phi}\rangle = \sum_{i=1}^{2^N} \Lambda_i \left[\sqrt{p_c}|0\rangle \otimes \left(\sum_{m=1}^N |\dot{\chi}_m^i\rangle \bigotimes_{j=1 j\neq m}^N |\chi_j^i\rangle\right) + e^{i\theta_c}\sqrt{1-p_c}|1\rangle \otimes \left(\sum_{m=1}^N |\dot{\omega}_m^i\rangle \bigotimes_{\substack{j=1\\ j\neq m}}^N |\omega_j^i\rangle\right)\right].$$

Therefore, we have

$$
\begin{aligned}
\langle\dot{\Phi}|\dot{\Phi}\rangle &= \sum_{i=1}^{2^N}\sum_{k=1}^{2^N}\Lambda_i\Lambda_k^*\Bigg[p_c\sum_{m=1}^{N}\Big\{\langle\dot{\chi}_m^k|\dot{\chi}_m^i\rangle\prod_{j\neq m}\langle\chi_j^k|\chi_j^i\rangle+\sum_{l\neq m}\langle\dot{\chi}_m^k|\chi_m^i\rangle\langle\chi_l^k|\dot{\chi}_l^i\rangle\prod_{j\neq m,l}\langle\chi_j^k|\chi_j^i\rangle\Big\}\\
&+(1-p_c)\sum_{m=1}^{N}\Big\{\langle\dot{\omega}_m^k|\dot{\omega}_m^i\rangle\prod_{j\neq m}\langle\omega_j^k|\omega_j^i\rangle+\sum_{l\neq m}\langle\dot{\omega}_m^k|\omega_m^i\rangle\langle\omega_l^k|\dot{\omega}_l^i\rangle\prod_{j\neq m,l}\langle\omega_j^k|\omega_j^i\rangle\Big\}\Bigg],\\
&= \sum_{i=1}^{2^N}\sum_{k=1}^{2^N}\Lambda_i\Lambda_k^*\Bigg[p_c\sum_{m=1}^{N}\Big(\dot{\chi}_m^{ki}\prod_{j\neq m}a_j^{ki}+\sum_{l\neq m}\alpha_m^{ki}\alpha_l^{ik*}\prod_{j\neq m,l}a_j^{ki}\Big)\\
&\quad+(1-p_c)\sum_{m=1}^{N}\Big(\dot{\omega}_m^{ki}\prod_{j\neq m}b_j^{ki}+\sum_{l\neq m}\beta_m^{ki}\beta_l^{ik*}\prod_{j\neq m,l}b_j^{ki}\Big)\Bigg]. \qquad (7.23)
\end{aligned}
$$

where

$$
\begin{aligned}
\langle\dot{\chi}_m^k|\dot{\chi}_m^i\rangle &= \dot{\chi}_m^{ki}, \quad \langle\chi_j^k|\chi_j^i\rangle = a_j^{ki},\\
\langle\dot{\omega}_m^k|\dot{\omega}_m^i\rangle &= \dot{\omega}_m^{ki}, \quad \langle\omega_j^k|\omega_j^i\rangle = b_j^{ki},\\
\langle\dot{\chi}_m^k|\chi_m^i\rangle &= \alpha_m^{ki}, \quad \langle\dot{\omega}_j^k|\omega_j^i\rangle = \beta_j^{ki}. \qquad (7.24)
\end{aligned}
$$

Now, $|\langle\dot{\Phi}|\Phi\rangle|^2$ being a positive number we have

$$
\begin{aligned}
\mathcal{Q}_\theta &\leq 4\sum_{i=1}^{2^N}\sum_{k=1}^{2^N}\Lambda_i\Lambda_k^*\Bigg[p_c\sum_{m=1}^{N}\Big(\dot{\chi}_m^{ki}\prod_{j\neq m}a_j^{ki}+\sum_{l\neq m}\alpha_m^{ki}\alpha_l^{ik*}\prod_{j\neq m,l}a_j^{ki}\Big)\\
&\quad+(1-p_c)\sum_{m=1}^{N}\Big(\dot{\omega}_m^{ki}\prod_{j\neq m}b_j^{ki}+\sum_{l\neq m}\beta_m^{ki}\beta_l^{ik*}\prod_{j\neq m,l}b_j^{ki}\Big)\Bigg], \qquad (7.25)\\
&= \tilde{\mathcal{Q}}_\theta.
\end{aligned}
$$

To simplify $\tilde{\mathcal{Q}}_\theta$ we observe that the terms $\prod_{j\neq m}a_j^{ki}$, and $\prod_{j\neq m}b_j^{ki}$ are the products of the inner products of $N-1$ of the qubits. Since U_θ and U_θ^T are both unitaries they preserve inner products, i.e., $a_j^{ki}=b_j^{ki}=\langle\psi_j^k|\psi_j^i\rangle=\delta_{ki}$. Hence, given a value of m, $\prod_{j\neq m}a_j^{ki}=\prod_{j\neq m}b_j^{ki}=0$, if the qubits in $|\lambda_i\rangle$ and $\langle\lambda_k|$ differ in more than one position. Similarly, if the qubits in $|\lambda_i\rangle$ and $\langle\lambda_k|$ differ in more than two positions then the terms $\prod_{j\neq m,l}b_j^{ki}=\prod_{j\neq m,l}a_j^{ki}=0$ for a given pair of values m and l.

We define, $\tilde{\mathcal{Q}}_\theta^X$, which involve contribution from N-qubit basis states where qubits differ in X number of positions only. Therefore, we can write $\tilde{\mathcal{Q}}_\theta=\sum_{X=0}^{N}\tilde{\mathcal{Q}}_\theta^X$. However, from the above discussions, we have $\tilde{\mathcal{Q}}_\theta^X=0\ \forall X\geq 3$ which implies $\tilde{\mathcal{Q}}_\theta=\sum_{X=0}^{2}\tilde{\mathcal{Q}}_\theta^X$. So we have to calculate only $\tilde{\mathcal{Q}}_\theta^0$, $\tilde{\mathcal{Q}}_\theta^1$ and $\tilde{\mathcal{Q}}_\theta^2$.

- **Upper bound of $\tilde{\mathcal{Q}}_\theta^2$:** A pair of N-qubit basis states, $|\lambda_i\rangle$ and $|\lambda_j\rangle$ which differ in exactly two qubits is given by the condition $j = i \oplus 2^k \oplus 2^l$ with $k \neq l$. Now, we can write

$$\begin{aligned}\tilde{\mathcal{Q}}_\theta^2 &= 4\sum_{i=1}^{2^N}\sum_{k=1}^{N}\sum_{\substack{l=1\\ l\neq k}}^{N}\Lambda_i\Lambda^*_{i\oplus 2^k\oplus 2^l}\Bigg[p_c\bigg(\alpha_k^{i\oplus 2^k,i}\alpha_l^{i,i\oplus d^l *}+\alpha_l^{i\oplus d^l,i}\alpha_k^{i,i\oplus 2^k *}\bigg)\\ &\quad +(1-p_c)\bigg(\beta_k^{i\oplus 2^k,i}\beta_l^{i,i\oplus d^l *}+\beta_l^{i\oplus d^l,i}\beta_k^{i,i\oplus 2^k *}\bigg)\Bigg]. \end{aligned} \tag{7.26}$$

Since for any complex number, z we have $z + z^* \leq 2|z|$ and $|\sum_i z_i| \leq \sum_i |z_i|$, we can write

$$\begin{aligned}\tilde{\mathcal{Q}}_\theta^2 &\leq 4\sum_{i=1}^{2^N}\sum_{k=1}^{N}\sum_{\substack{l=1\\ l\neq k}}^{N}|\Lambda_i\Lambda^*_{i\oplus 2^k\oplus 2^l}|p_c\bigg(\Big|\alpha_k^{i\oplus 2^k,i}\alpha_l^{i,i\oplus 2^l *}\Big|+\Big|\alpha_l^{i\oplus 2^l,i}\alpha_k^{i,i\oplus 2^k *}\Big|\bigg)\\ &+ 4\sum_{i=1}^{2^N}\sum_{k=1}^{N}\sum_{\substack{l=1\\ l\neq k}}^{N}|\Lambda_i\Lambda^*_{i\oplus 2^k\oplus 2^l}|(1-p_c)\bigg(\Big|\beta_k^{i\oplus 2^k,i}\beta_l^{i,i\oplus 2^l *}\Big|+\Big|\beta_l^{i\oplus 2^l,i}\beta_k^{i,i\oplus 2^k *}\Big|\bigg)\end{aligned} \tag{7.27}$$

Now, if $\max|\alpha_k^{i\oplus 2^k,i}| = \mathcal{A}$ and $\max|\beta_k^{i\oplus 2^k,i}| = \mathcal{B}$, where maximization is done over $|\lambda_i\rangle, \langle\lambda_{i\oplus 2^k}|$ and parameters of the unitary by which encoding is performed, then

$$\tilde{\mathcal{Q}}_\theta^2 \leq 8(p_c\mathcal{A}^2 + (1-p_c)\mathcal{B}^2)\sum_{k=1}^{N}\sum_{\substack{l=1\\ l\neq k}}^{N}\left|\sum_{i=1}^{2^N}\Lambda_i\Lambda^*_{i\oplus 2^k\oplus 2^l}\right|. \tag{7.28}$$

Defining $\vec{\Lambda} = \{\Lambda_1, \Lambda_2, \ldots, \Lambda_N\}$ as the coefficient vector and $\{k,l\}$-permuted coefficient vector as $\vec{\Lambda}_{kl} = \{\Lambda_{1\oplus 2^k\oplus 2^l}, \Lambda_{2\oplus 2^k\oplus 2^l}, \ldots, \Lambda_{N\oplus 2^k\oplus 2^l}\}$ we can write $\left|\sum_{i=1}^{2^N}\Lambda_i\Lambda^*_{i\oplus 2^k\oplus d^l}\right| = |\vec{\Lambda_{k,l}}\cdot\vec{\Lambda}| \leq \sqrt{|\vec{\Lambda}\cdot\vec{\Lambda}||\vec{\Lambda_{k,l}}\cdot\vec{\Lambda_{k,l}}|} = 1$. This implies

$$\tilde{\mathcal{Q}}_\theta^2 \leq 8(p_c\mathcal{A}^2 + (1-p_c)\mathcal{B}^2)\sum_{k=1}^{N}\sum_{\substack{l=1\\ l\neq k}}^{N}1 = 8(p_c\mathcal{A}^2 + (1-p_c)\mathcal{B}^2)N(N-1). \tag{7.29}$$

- **Upper bound of $\tilde{\mathcal{Q}}_\theta^1$:** A pair of N-qubit basis states, $|\lambda_i\rangle$ and $|\lambda_j\rangle$ which differ in exactly one qubit is characterized by the condition $j = i \oplus 2^k$ which simplifies $\tilde{\mathcal{Q}}_\theta^1$ as

$$
\begin{aligned}
\tilde{\mathcal{Q}}_\theta^1 &= 4\sum_{i=1}^{2^N}\sum_{k=1}^{N}\Lambda_i\Lambda^*_{i\oplus 2^k}\Bigg[p_c\Bigg\{\dot{\chi}_k^{i\oplus 2^k,i}+\sum_{l\neq k}\alpha_k^{i\oplus 2^k,i}\alpha_l^{i,i\oplus 2^k *}+\sum_{m\neq k}\alpha_m^{i\oplus 2^k,i}\alpha_k^{i,i\oplus 2^k *}\Bigg\} \\
&\quad +(1-p_c)\Bigg\{\dot{\omega}_k^{i\oplus 2^k,i}+\sum_{l\neq k}\beta_k^{i\oplus 2^k,i}\beta_l^{i,i\oplus 2^k *}+\sum_{m\neq k}\beta_m^{i\oplus 2^k,i}\beta_k^{i,i\oplus 2^k *}\Bigg\}\Bigg]. \qquad (7.30)\\
&\leq 4\Bigg[\sum_{i=1}^{2^N}\sum_{k=1}^{N}|\Lambda_i\Lambda^*_{i\oplus 2^k}|p_c\left|\dot{\chi}_k^{i\oplus 2^k,i}\right|+\sum_{i=1}^{2^N}\sum_{k=1}^{N}|\Lambda_i\Lambda^*_{i\oplus 2^k}|p_c\sum_{l\neq k}\left|\alpha_k^{i\oplus 2^k,i}\alpha_l^{i,i\oplus 2^k *}\right| \\
&\quad +\sum_{i=1}^{2^N}\sum_{k=1}^{N}|\Lambda_i\Lambda^*_{i\oplus 2^k}|p_c\sum_{m\neq k}\left|\alpha_m^{i\oplus 2^k,i}\alpha_k^{i,i\oplus 2^k *}\right|+\sum_{i=1}^{2^N}\sum_{k=1}^{N}|\Lambda_i\Lambda^*_{i\oplus 2^k}|(1-p_c)\left|\dot{\omega}_k^{i\oplus 2^k,i}\right| \\
&\quad +\sum_{i=1}^{2^N}\sum_{k=1}^{N}|\Lambda_i\Lambda^*_{i\oplus 2^k}|(1-p_c)\sum_{l\neq k}\left|\beta_k^{i\oplus 2^k,i}\beta_l^{i,i\oplus 2^k *}\right| \\
&\quad +\sum_{i=1}^{2^N}\sum_{k=1}^{N}|\Lambda_i\Lambda^*_{i\oplus 2^k}|(1-p_c)\sum_{m\neq k}\left|\beta_m^{i\oplus 2^k,i}\beta_k^{i,i\oplus 2^k *}\right|\Bigg] \qquad (7.31)
\end{aligned}
$$

Similar to Eqs. (7.28) and (7.29) we can write

$$\tilde{\mathcal{Q}_\theta}^{(1)} \leq 4N(p_c\mathcal{X}+(1-p_c)\mathcal{W})+8(p_c\mathcal{A}^2+(1-p_c)\mathcal{B}^2)N(N-1), \qquad (7.32)$$

where $\mathcal{X}$ and $\mathcal{W}$ are upper bounds of $\left|\dot{\chi}_k^{i\oplus 2^k,i}\right|$ and $\left|\dot{\omega}_k^{i\oplus 2^k,i}\right|$ respectively.

- **Upper bound of $\tilde{\mathcal{Q}}_\theta^0$:** Since the basis states which differ in no position is that basis state itself, the value of $\tilde{\mathcal{Q}}_\theta^0$ is upper bounded by

$$\tilde{\mathcal{Q}_\theta}^0 \leq \Big(A'N^2+B'N\Big)\sum_{i=1}^{2^N}\Lambda_i\Lambda_i^* = \Big(A'N^2+B'N\Big), \qquad (7.33)$$

where $A'N^2+B'N$ is the upper bound of $\langle\dot{\Phi}|\dot{\Phi}\rangle$ for a N-qubit product-probe state as evident from Sec. 4.2.2 in the main text.

Finally, we have

$$\tilde{\mathcal{Q}}_\theta = \tilde{\mathcal{Q}}_\theta^0+\tilde{\mathcal{Q}}_\theta^1+\tilde{\mathcal{Q}}_\theta^2 \leq \gamma N^2+\zeta N \qquad (7.34)$$

where both γ and ζ are some function of $\mathcal{X},\mathcal{W},\mathcal{A},\mathcal{B},A',B'$ only which are independent of N. Hence, we prove that no entangled state can beat Heisenberg scaling in ITDM. Note that, from the above calculation it trivially follows that this scaling is also true for general N-qudit states.

7.8 Demonstration of advantage in $N = 1$ for nonoptimal encoding

In the case of NITDM by choosing $\rho_i = \rho \forall i$ as probe state and measuring in the $\{|+\rangle, |-\rangle\}$ basis on the control qubit, the FI is given by

$$\mathcal{F}_\theta = \frac{N^2 r^{2N-2}(\boldsymbol{\nu}) \left\{ \dot{r}(\boldsymbol{\nu}) \cos\left(N f(\boldsymbol{\nu}) + \theta_c\right) - r(\boldsymbol{\nu}) \dot{f}(\boldsymbol{\nu}) \sin\left(N f(\boldsymbol{\nu}) + \theta_c\right) \right\}^2}{1 - r^{2N}(\boldsymbol{\nu}) \cos^2\left(N f(\boldsymbol{\nu}) + \theta_c\right)}. \tag{7.35}$$

where $r(\boldsymbol{\nu}) = \left| \mathrm{Tr}\left(\sum_j K_j^T \rho K_j^\dagger\right) \right|$ and $f(\boldsymbol{\nu}) = \arg\left[\mathrm{Tr}\left(\sum_j K_j^T \rho K_j^\dagger\right)\right]$. In case of $N = 1$, Eq. (7.35) reduces to

$$\mathcal{F}_\theta = \frac{\left\{ \dot{r}(\boldsymbol{\nu}) \cos\left(f(\boldsymbol{\nu}) + \theta_c\right) - r(\boldsymbol{\nu}) \dot{f}(\boldsymbol{\nu}) \sin\left(f(\boldsymbol{\nu}) + \theta_c\right) \right\}^2}{1 - r(\boldsymbol{\nu}) \cos^2\left(f(\boldsymbol{\nu}) + \theta_c\right)} = \frac{\left\{ \frac{d}{d\theta}\Big(r(\boldsymbol{\nu}) \cos\left(f(\boldsymbol{\nu}) + \theta_c\right) \Big) \right\}^2}{1 - \Big(r(\boldsymbol{\nu}) \cos\left(f(\boldsymbol{\nu}) + \theta_c\right) \Big)^2} \tag{7.36}$$

From

$$r(\boldsymbol{\nu}) = \left| \mathrm{Tr}\left(\sum_j K_j^T \rho K_j^\dagger \right) \right| = \left| \frac{1+q}{2} - n_2^2 q(1 - \cos\theta) + i q n_2 \Big((1 - \cos\theta)(n_1 r_3 - r_1 n_3) + r_2 \sin\theta \Big) \right|, \tag{7.37}$$

we have

$$r(\boldsymbol{\nu}) \cos\left(f(\boldsymbol{\nu}) + \theta_c\right) = \mathrm{Re}\left\{ \mathrm{Tr}\left(\sum_j K_j^T \rho K_j^\dagger \right) \right\} = \frac{1+q}{2} - n_2^2 q(1 - \cos\theta). \tag{7.38}$$

Putting Eq. (7.38) in Eq. (7.36) we get

$$\mathcal{F}_\theta^q = \frac{n_2^4 q^2 \sin^2\theta}{1 - \left\{ \frac{1+q}{2} - n_2^2 q(1 - \cos\theta) \right\}^2}. \tag{7.39}$$

Proof of optimality of $\hat{n}_2 = \hat{y}$ and comparison with "switched" strategy. Note that, $\mathcal{F}_\theta^q$ can be written as

$$\mathcal{F}_\theta^q = \frac{n_2^4 q^2 \sin^2\theta}{1 - \left[\left(\frac{1+q}{2}\right)^2 + n_2^2 \{ n_2^2 q^2 (1 - \cos\theta)^2 - q(1+q)(1 - \cos\theta) \} \right]}.$$

From Eq. (7.40) it is clear that the numerator is maximized at $n_2 = \pm 1$ where the denominator is minimized. Hence, $n_2 = \pm 1$ is the optimal encoding axis in this scenario.

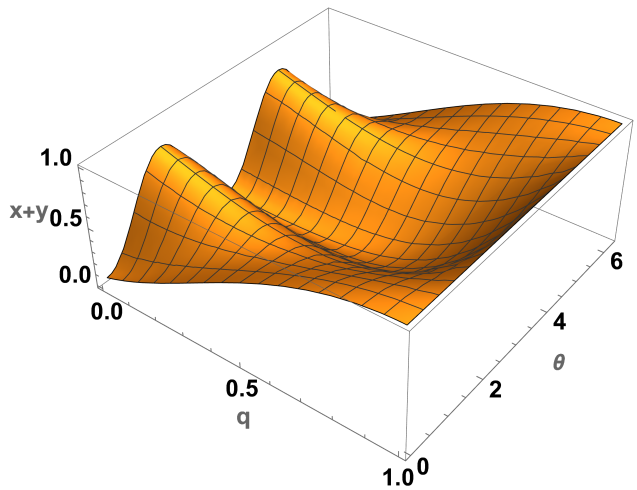

Figure 7.1: **Value of $x+y$ (ordinate) against noise strength q (abscissa), and paramater θ (abscissa)** The figure demonstrates the value of $x+y$ never goes above 1. All axes are dimensionless.

To compare with "switched" strategy let us evaluate the difference between $\mathcal{F}_\theta^q|_{\hat{n}=\hat{y}}$ and the "switched" strategy, defined as $\delta = \mathcal{F}_\theta^q|_{\hat{n}=\hat{y}} - \mathcal{F}_\theta^{q,S}$. Now, δ can be explicitly calculated as $\delta = 1 - x - y$ where $x = \frac{1}{16}\left\{(1+q)^2 - 4(-1+q)q\cos\theta\right\}^2$ and $y = (1-q)^2\sin^2\theta\left\{1 - \frac{1}{4}\left(-1+q-2q\cos\theta\right)^2\right\}$. Our numerical investigation suggests (see Fig. 7.1) that $x+y \leq 1$ which proves $\delta \geq 0\,\forall q,\theta$.

Comparing NITDM with "switched" and regular strategy with non-optimal encoding. Here, we demonstrate that, beyond the optimal encoding procedure, NITDM can also be advantageous in certain scenarios even under non-optimal encoding (see Fig. 7.2), outperforming both the "switched" and regular strategies. Specifically, when selecting $\hat{n} = [0.8, 0.6, 0]$ instead of $n_2 = 1$, NITDM proves to be more effective than the "switched" strategy in the region $q \gtrsim 0.73$, corresponding to the low-noise regime.

Conversely, maintaining n_2 constant while varying n_1, n_3, and the probe state can reduce the advantage of the time-flip approach compared to regular strategy, as illustrated in Fig. 7.2. While for $\hat{n} = [0.8, 0.6, 0]$ and $\hat{s} = [0.2, 0.7, 0.5]$ NITDM always excels regular strategy, in case of $\hat{n} = [0, 0.6, 0.8]$ and $\hat{s} = [0.4, 0.3, 0.0]$ only for $q \gtrsim 0.85$ $\mathcal{F}_\theta^q$ is higher. Nevertheless, in many cases within the low-noise regime, NITDM exhibits superior performance.

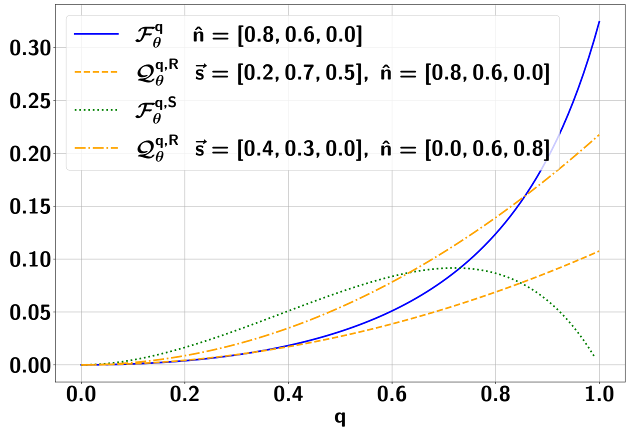

Figure 7.2: **Fisher information, $\mathcal{F}_\theta^q, \mathcal{F}_\theta^{q,S}$ and QFI, $\mathcal{Q}_\theta^{q,R}$ (ordinate) with respect to noise parameter q (abscissa). Comparison between Flip, Switch, and regular strategies for $n_2 \neq 1$.** We choose $\theta = \pi/4$. The figure demonstrates the advantage of time flip over "switched" and regular strategies in non-ideal encoding scenarios. All axes are dimensionless.

7.9 θ-averaged performance of single qubit-NITDM

Since both $\mathcal{F}_\theta^q$ and $\mathcal{F}_\theta^{q,S}$ are θ-dependent, to compare the performance of protocols with the aid of switch and flip, we evaluate the difference of the average FI obtained through these strategies, i.e., $\langle \mathcal{F}_\theta^q \rangle - \langle \mathcal{F}_\theta^{q,S} \rangle = \frac{\sqrt{3}}{8}(1-q)\sqrt{(1-q)(3+5q)} + \frac{1}{8}\sqrt{(5+6q-3q^2)(5-2q+5q^2)} - \frac{1}{4}\sqrt{(3+q)(3+q-4qn_2^2)} - \frac{1}{4}\sqrt{(1-q)(1-q+4qn_2^2)}$. Analyzing this particular equation is nontrivial because of the associated square roots. Hence, we opt for a numerical approach instead. One thing we know is that for $n_2 = \pm 1$, NITDM always outperforms the "switched" one at all q and θ values. Therefore, it always beats the switched method on average for all q values. For a given value of q we analyze the range of n_2 values $\pm n_2^{\min} \leq n_2 \leq \pm 1$ where flip strategy is better, i.e., $\langle \mathcal{F}_\theta^q \rangle > \langle \mathcal{F}_\theta^{q,S} \rangle$ and fit $n_2^{\min}$ with, $n_2^{\min} = n_2^0[1 - q^g]^{h^{-1}}$. Fig. 7.3 represents the χ^2-fitted [108, 109] curve of $n_2^{\min}$ with $g = 1.14147 \pm (0.48\%)$ and $h = 2.38455 \pm (0.25\%)$ as fitting parameters and the constant $n_2^0 = 0.945742$. Although the magnitude of the advantage decreases significantly as n_2 and q deviate from unity, in low-noise regimes, metrology employing time-flip exhibits superior performance compared to that using switch over a broad range of n_2.

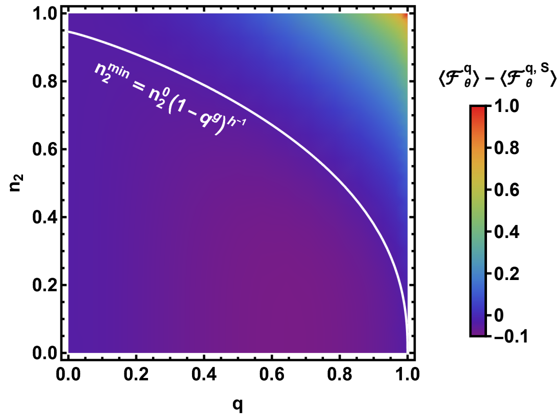

Figure 7.3: **Comparison between Flip and switch strategy on average. Variation of $\langle \mathcal{F}_\theta^q \rangle - \langle \mathcal{F}_\theta^{q,S} \rangle$ (heatmap) against n_2 (vertical axis) and noise strength q (horizontal axis).** The white contour is the χ^2-fitted line of $n_2^{\min}$ where the difference $\langle \mathcal{F}_\theta^q \rangle - \langle \mathcal{F}_\theta^{q,S} \rangle = 0$. Fitted curve is $n_2^{\min} = n_2^0[1 - q^g]^{h^{-1}}$ with $g = 1.14147 \pm (0.48\%)$ and $h = 2.38455 \pm (0.25\%)$ as fitting parameters and a constant $n_2^0 = 0.945742$. In the regions above the curve flip outperforms switch. All axes are dimensionless.

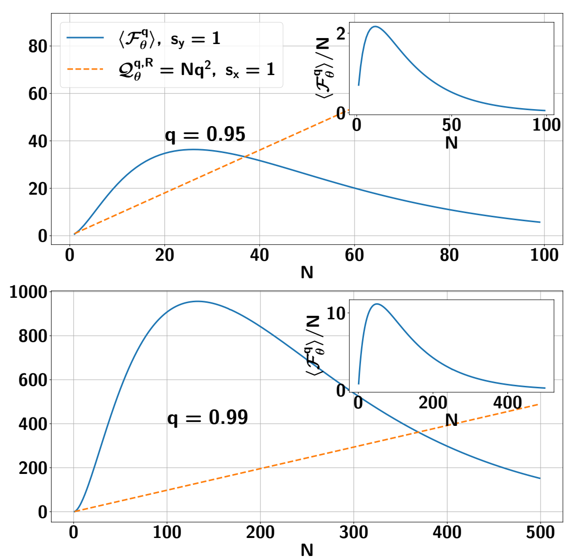

Figure 7.4: **Advantage of average performance of multi-qubit NITDM and regular strategy.** Average FI, $\langle \mathcal{F}_\theta^q \rangle$ (blue lines) with respect to number or qubits N (abscissa) for different noise strength q. QFI in regular strategy, $\mathcal{Q}_\theta^{q,R}$ (orange dashed lines) against N. Inset: Average Fisher information per qubit, $\langle \mathcal{F}_\theta^q \rangle / N$ (ordinate) against number or qubits N (abscissa). Here, we fix the parameter value $\theta = \pi/4$ and the encoding axis as $\hat{n}_2 = 1$. All axes are dimensionless.

7.10 θ-averaged performance of multiqubit-NITDM

Similar to the case where θ is fixed, in θ-averaged scenario we define $\{\langle\tilde{\mathcal{F}}_\theta^q\rangle, \tilde{N}\}$ corresponding to which $\langle\mathcal{F}_\theta^q/N\rangle$ is maximized at $N = \tilde{N}$. Given $q = 0.99$ and 0.95, in Fig. 7.4 we demonstrate the behavior of θ-averaged FI with respect to the number of qubits and corresponding quantities are listed in Table 7.1.

q	$\langle\tilde{\mathcal{F}}_\theta^q\rangle/\tilde{N}$	$\tilde{N}$	$\max_N \langle\mathcal{F}_\theta^q\rangle$	N corresponding to $\max_N \langle\mathcal{F}_\theta^q\rangle$
0.95	2.17	10	36.4	26
0.99	11.16	50	956.4	133

Table 7.1: Given two values of q, the maximum value of both θ-averaged FI, $\max_N \langle\mathcal{F}_\theta^q\rangle$ and θ-averaged FI per qubit, $\langle\tilde{\mathcal{F}}_\theta^q\rangle/\tilde{N}$, and the corresponding number of qubits for each maximum value are listed from Fig. 7.4.

From Table 7.1, it is evident that given $N = 1000$ and $q = 0.99$, it is better to use 20 number of 50-qubit NITDM circuits to get $20\langle\tilde{\mathcal{F}}_\theta^{0.99}\rangle = 11160$ where $Nq^2 = 980.1$. Similarly, for $q = 0.95$ we can use 10-qubit circuits 100 times which leads to $100\langle\tilde{\mathcal{F}}_\theta^{0.95}\rangle = 2170$, but $Nq^2 = 902.5$.

Bibliography

[1] Gaurang Agrawal, Pritam Halder, and Aditi Sen De. Indefinite Time Directed Quantum Metrology. *arXiv*, February 2025.

[2] Xiaobin Zhao, Yuxiang Yang, and Giulio Chiribella. Quantum Metrology with Indefinite Causal Order. *Phys. Rev. Lett.*, 124(19):190503, May 2020.

[3] Giulio Chiribella, Giacomo Mauro D'Ariano, Paolo Perinotti, and Benoit Valiron. Quantum computations without definite causal structure. *Physical Review A*, 88:022318, 8 2013.

[4] Ognyan Oreshkov, Fabio Costa, and Časlav Brukner. Quantum correlations with no causal order. *Nat. Commun.*, 3(1092):1–8, October 2012.

[5] Mateus Araújo, Cyril Branciard, Fabio Costa, Adrien Feix, Christina Giarmatzi, and Časlav Brukner. Witnessing causal nonseparability. *New J. Phys.*, 17(10):102001, October 2015.

[6] Giulio Chiribella. Perfect discrimination of no-signalling channels via quantum superposition of causal structures. *Phys. Rev. A*, 86(4):040301, October 2012.

[7] Jessica Bavaresco, Mio Murao, and Marco Túlio Quintino. Strict Hierarchy between Parallel, Sequential, and Indefinite-Causal-Order Strategies for Channel Discrimination. *Phys. Rev. Lett.*, 127(20):200504, November 2021.

[8] Jessica Bavaresco, Mio Murao, and Marco Túlio Quintino. Unitary channel discrimination beyond group structures: Advantages of sequential and indefinite-causal-order strategies. *J. Math. Phys.*, 63(4):042203, April 2022.

[9] Spiros Kechrimparis, James Moran, Athena Karsa, Changhyoup Lee, and Hyukjoon

Kwon. Enhancing quantum state discrimination with indefinite causal order. *New J. Phys.*, December 2024.

[10] Daniel Ebler, Sina Salek, and Giulio Chiribella. Enhanced communication with the assistance of indefinite causal order. *Physical Review Letters*, 120:120502, 3 2018.

[11] Sina Salek, Daniel Ebler, and Giulio Chiribella. Quantum communication in a superposition of causal orders. *arXiv*, September 2018.

[12] Zhen Wu, James Fullwood, Zhihao Ma, Siqi Zhou, Qi Zhao, and Giulio Chiribella. General Communication Enhancement via the Quantum Switch. *arXiv*, July 2024.

[13] Hlér Kristjánsson, Giulio Chiribella, Sina Salek, Daniel Ebler, and Matthew Wilson. Resource theories of communication. *New J. Phys.*, 22(7):073014, July 2020.

[14] Matt Wilson and Giulio Chiribella. A Diagrammatic Approach to Information Transmission in Generalised Switches. *arXiv*, March 2020.

[15] Giulio Chiribella, Matt Wilson, and H. F. Chau. Quantum and Classical Data Transmission through Completely Depolarizing Channels in a Superposition of Cyclic Orders. *Phys. Rev. Lett.*, 127(19):190502, November 2021.

[16] Nicolas Loizeau and Alexei Grinbaum. Channel capacity enhancement with indefinite causal order. *Phys. Rev. A*, 101(1):012340, January 2020.

[17] Sk Sazim, Michal Sedlak, Kratveer Singh, and Arun Kumar Pati. Classical communication with indefinite causal order for N completely depolarizing channels. *Phys. Rev. A*, 103(6):062610, June 2021.

[18] David Felce and Vlatko Vedral. Quantum Refrigeration with Indefinite Causal Order. *Phys. Rev. Lett.*, 125(7):070603, August 2020.

[19] Tamal Guha, Mir Alimuddin, and Preeti Parashar. Thermodynamic advancement in the causally inseparable occurrence of thermal maps. *Phys. Rev. A*, 102(3):032215, September 2020.

[20] Kyrylo Simonov, Saptarshi Roy, Tamal Guha, Zoltán Zimborás, and Giulio Chiribella. Activation of thermal states by coherently controlled thermalization processes. *arXiv*, August 2022.

[21] Kyrylo Simonov, Gianluca Francica, Giacomo Guarnieri, and Mauro Paternostro. Work extraction from coherently activated maps via quantum switch. *Phys. Rev. A*, 105(3):032217, March 2022.

[22] Qiushi Liu, Zihao Hu, Haidong Yuan, and Yuxiang Yang. Optimal Strategies of Quantum Metrology with a Strict Hierarchy. *Phys. Rev. Lett.*, 130(7):070803, February 2023.

[23] François Chapeau-Blondeau. Noisy quantum metrology with the assistance of indefinite causal order. *Physical Review A*, 103:032615, 3 2021.

[24] Michael Frey. Indefinite causal order aids quantum depolarizing channel identification. *Quantum Inf. Process.*, 18(4):1–20, April 2019.

[25] Masashi Ban. Quantum Fisher information of phase estimation in the presence of indefinite causal order. *Phys. Lett. A*, 468:128749, April 2023.

[26] Raphaël Mothe, Cyril Branciard, and Alastair A. Abbott. Reassessing the advantage of indefinite causal orders for quantum metrology. *Phys. Rev. A*, 109(6):062435, June 2024.

[27] Min An, Shihao Ru, Yunlong Wang, Yu Yang, Feiran Wang, Pei Zhang, and Fuli Li. Noisy quantum parameter estimation with indefinite causal order. *Phys. Rev. A*, 109(1):012603, January 2024.

[28] Peng Yin, Xiaobin Zhao, Yuxiang Yang, Yu Guo, Wen-Hao Zhang, Gong-Chu Li, Yong-Jian Han, Bi-Heng Liu, Jin-Shi Xu, Giulio Chiribella, Geng Chen, Chuan-Feng Li, and Guang-Can Guo. Experimental super-Heisenberg quantum metrology with indefinite gate order. *Nat. Phys.*, 19:1122–1127, August 2023.

[29] Qiushi Liu, Zihao Hu, Haidong Yuan, and Yuxiang Yang. Fully-Optimized Quantum Metrology: Framework, Tools, and Applications. *Adv. Quantum Technol.*, 7(12):2400094, December 2024.

[30] Lorenzo M. Procopio, Amir Moqanaki, Mateus Araújo, Fabio Costa, Irati Alonso Calafell, Emma G. Dowd, Deny R. Hamel, Lee A. Rozema, Časlav Brukner, and Philip Walther. Experimental superposition of orders of quantum gates. *Nat. Commun.*, 6(7913):1–6, August 2015.

[31] Giulia Rubino, Lee A. Rozema, Adrien Feix, Mateus Araújo, Jonas M. Zeuner, Lorenzo M. Procopio, Časlav Brukner, and Philip Walther. Experimental verification of an indefinite causal order. *Sci. Adv.*, 3(3), March 2017.

[32] K. Goswami, C. Giarmatzi, M. Kewming, F. Costa, C. Branciard, J. Romero, and A. G. White. Indefinite Causal Order in a Quantum Switch. *Phys. Rev. Lett.*, 121(9):090503, August 2018.

[33] Teodor Strömberg, Peter Schiansky, Robert W. Peterson, Marco Túlio Quintino, and Philip Walther. Demonstration of a Quantum Switch in a Sagnac Configuration. *Phys. Rev. Lett.*, 131(6):060803, August 2023.

[34] Kejin Wei, Nora Tischler, Si-Ran Zhao, Yu-Huai Li, Juan Miguel Arrazola, Yang Liu, Weijun Zhang, Hao Li, Lixing You, Zhen Wang, Yu-Ao Chen, Barry C. Sanders, Qiang Zhang, Geoff J. Pryde, Feihu Xu, and Jian-Wei Pan. Experimental Quantum Switching for Exponentially Superior Quantum Communication Complexity. *Phys. Rev. Lett.*, 122(12):120504, March 2019.

[35] Yu Guo, Xiao-Min Hu, Zhi-Bo Hou, Huan Cao, Jin-Ming Cui, Bi-Heng Liu, Yun-Feng Huang, Chuan-Feng Li, Guang-Can Guo, and Giulio Chiribella. Experimental Transmission of Quantum Information Using a Superposition of Causal Orders. *Phys. Rev. Lett.*, 124(3):030502, January 2020.

[36] K. Goswami, Y. Cao, G. A. Paz-Silva, J. Romero, and A. G. White. Increasing communication capacity via superposition of order. *Phys. Rev. Res.*, 2(3):033292, August 2020.

[37] Xinfang Nie, Xuanran Zhu, Keyi Huang, Kai Tang, Xinyue Long, Zidong Lin, Yu Tian, Chudan Qiu, Cheng Xi, Xiaodong Yang, Jun Li, Ying Dong, Tao Xin, and Dawei Lu. Experimental Realization of a Quantum Refrigerator Driven by Indefinite Causal Orders. *Phys. Rev. Lett.*, 129(10):100603, September 2022.

[38] Gaoyan Zhu, Yuanbo Chen, Yoshihiko Hasegawa, and Peng Xue. Charging Quantum Batteries via Indefinite Causal Order: Theory and Experiment. *Phys. Rev. Lett.*, 131(24):240401, December 2023.

[39] Lee A. Rozema, Teodor Strömberg, Huan Cao, Yu Guo, Bi-Heng Liu, and Philip

Walther. Experimental aspects of indefinite causal order in quantum mechanics. *Nat. Rev. Phys.*, 6:483–499, August 2024.

[40] Giulio Chiribella and Zixuan Liu. Quantum operations with indefinite time direction. *Commun. Phys.*, 5(190):1–8, July 2022.

[41] Giulia Rubino, Gonzalo Manzano, and Časlav Brukner. Quantum superposition of thermodynamic evolutions with opposing time's arrows. *Commun. Phys.*, 4(251):1–10, November 2021.

[42] Zixuan Liu, Ming Yang, and Giulio Chiribella. Quantum communication through devices with indefinite input-output direction. *New J. Phys.*, 25(4):043017, April 2023.

[43] Teodor Strömberg, Peter Schiansky, Marco Túlio Quintino, Michael Antesberger, Lee A. Rozema, Iris Agresti, Časlav Brukner, and Philip Walther. Experimental superposition of a quantum evolution with its time reverse. *Phys. Rev. Res.*, 6(2):023071, April 2024.

[44] Göktuğ Karpat and Barış Çakmak. Memory in quantum processes with indefinite time direction and causal order. *Phys. Rev. A*, 110(1):012446, July 2024.

[45] Binke Xia, Jingzheng Huang, Hongjing Li, Zhongyuan Luo, and Guihua Zeng. Nanoradian-scale precision in light rotation measurement via indefinite quantum dynamics. *Sci. Adv.*, 10(28), July 2024.

[46] Yu Guo, Zixuan Liu, Hao Tang, Xiao-Min Hu, Bi-Heng Liu, Yun-Feng Huang, Chuan-Feng Li, Guang-Can Guo, and Giulio Chiribella. Experimental Demonstration of Input-Output Indefiniteness in a Single Quantum Device. *Phys. Rev. Lett.*, 132(16):160201, April 2024.

[47] Giulia Rubino, Gonzalo Manzano, Lee A. Rozema, Philip Walther, Juan M. R. Parrondo, and Časlav Brukner. Inferring work by quantum superposing forward and time-reversal evolutions. *Phys. Rev. Res.*, 4(1):013208, March 2022.

[48] Man-Duen Choi. Completely positive linear maps on complex matrices. *Linear Algebra Appl.*, 10(3):285–290, June 1975.

[49] *States, Effects, and Operations.* Springer, Berlin, Germany.

[50] Giulio Chiribella, Giacomo Mauro D'Ariano, and Paolo Perinotti. Theoretical framework for quantum networks. *Phys. Rev. A*, 80(2):022339, August 2009.

[51] Alessandro Bisio and Paolo Perinotti. Theoretical framework for higher-order quantum theory. *Proceedings of the Royal Society A: Mathematical, Physical and Engineering Sciences*, 475:20180706, 5 2019.

[52] Aleks Kissinger and Sander Uijlen. A categorical semantics for causal structure. *arXiv*, January 2017.

[53] G. Chiribella, G. M. D'Ariano, and P. Perinotti. Quantum Circuit Architecture. *Phys. Rev. Lett.*, 101(6):060401, August 2008.

[54] Aleks Kissinger and Sander Uijlen. Picturing Indefinite Causal Structure. *arXiv*, January 2017.

[55] Hlér Kristjánsson, Tatsuki Odake, Satoshi Yoshida, Philip Taranto, Jessica Bavaresco, Marco Túlio Quintino, and Mio Murao. Exponential separation in quantum query complexity of the quantum switch with respect to simulations with standard quantum circuits. *arXiv*, September 2024.

[56] Mateus Araújo, Fabio Costa, and Časlav Brukner. Computational Advantage from Quantum-Controlled Ordering of Gates. *Phys. Rev. Lett.*, 113(25):250402, December 2014.

[57] Mateus Araújo, Philippe Allard Guérin, and Ämin Baumeler. Quantum computation with indefinite causal structures. *Phys. Rev. A*, 96(5):052315, November 2017.

[58] Martin J. Renner and Časlav Brukner. Reassessing the computational advantage of quantum-controlled ordering of gates. *Phys. Rev. Res.*, 3(4):043012, October 2021.

[59] Martin J. Renner and Časlav Brukner. Computational Advantage from a Quantum Superposition of Qubit Gate Orders. *Phys. Rev. Lett.*, 128(23):230503, June 2022.

[60] Alastair A. Abbott, Mehdi Mhalla, and Pierre Pocreau. Quantum query complexity of Boolean functions under indefinite causal order. *Phys. Rev. Res.*, 6(3):L032020, July 2024.

[61] Márcio M. Taddei, Jaime Cariñe, Daniel Martínez, Tania García, Nayda Guerrero, Alastair A. Abbott, Mateus Araújo, Cyril Branciard, Esteban S. Gómez, Stephen P.

Walborn, Leandro Aolita, and Gustavo Lima. Computational Advantage from the Quantum Superposition of Multiple Temporal Orders of Photonic Gates. *PRX Quantum*, 2(1):010320, February 2021.

[62] Philippe Allard Guérin, Giulia Rubino, and Časlav Brukner. Communication through quantum-controlled noise. *Phys. Rev. A*, 99(6):062317, June 2019.

[63] Gianluca Francica. Causal games of work extraction with indefinite causal order. *Phys. Rev. A*, 106:042214, Oct 2022.

[64] Vittorio Giovannetti, Seth Lloyd, and Lorenzo Maccone. Quantum Metrology. *Phys. Rev. Lett.*, 96(1):010401, January 2006.

[65] Matteo G. A. Paris. QUANTUM ESTIMATION FOR QUANTUM TECHNOLOGY. *Int. J. Quantum Inform.*, 07(supp01):125–137, January 2009.

[66] Vittorio Giovannetti, Seth Lloyd, and Lorenzo Maccone. Advances in quantum metrology. *Nat. Photonics*, 5:222–229, April 2011.

[67] Géza Tóth and Iagoba Apellaniz. Quantum metrology from a quantum information science perspective. *J. Phys. A: Math. Theor.*, 47(42):424006, October 2014.

[68] C. L. Degen, F. Reinhard, and P. Cappellaro. Quantum sensing. *Rev. Mod. Phys.*, 89(3):035002, July 2017.

[69] Luca Pezzè, Augusto Smerzi, Markus K. Oberthaler, Roman Schmied, and Philipp Treutlein. Quantum metrology with nonclassical states of atomic ensembles. *Rev. Mod. Phys.*, 90(3):035005, September 2018.

[70] S. Pirandola, B. R. Bardhan, T. Gehring, C. Weedbrook, and S. Lloyd. Advances in photonic quantum sensing. *Nat. Photonics*, 12:724–733, December 2018.

[71] Stanisław Kurdziałek, Wojciech Górecki, Francesco Albarelli, and Rafał Demkowicz-Dobrzański. Using Adaptiveness and Causal Superpositions Against Noise in Quantum Metrology. *Phys. Rev. Lett.*, 131(9):090801, August 2023.

[72] Stanisław Kurdziałek, Piotr Dulian, Joanna Majsak, Sagnik Chakraborty, and Rafał Demkowicz-Dobrzański. Quantum metrology using quantum combs and tensor network formalism. *New J. Phys.*, 27(1):013019, January 2025.

[73] Rafał Demkowicz-Dobrzański, Jan Kołodyński, and Mădălin Guţă. The elusive Heisenberg limit in quantum-enhanced metrology. *Nat. Commun.*, 3(1063):1–8, September 2012.

[74] Michael A. Taylor and Warwick P. Bowen. Quantum metrology and its application in biology. *Phys. Rep.*, 615:1–59, February 2016.

[75] N. P. Mauranyapin, L. S. Madsen, M. A. Taylor, M. Waleed, and W. P. Bowen. Evanescent single-molecule biosensing with quantum-limited precision. *Nat. Photonics*, 11:477–481, August 2017.

[76] M. Malnou, D. A. Palken, B. M. Brubaker, Leila R. Vale, Gene C. Hilton, and K. W. Lehnert. Squeezed Vacuum Used to Accelerate the Search for a Weak Classical Signal. *Phys. Rev. X*, 9(2):021023, May 2019.

[77] Steven D. Bass and Michael Doser. Quantum sensing for particle physics. *Nat. Rev. Phys.*, 6:329–339, May 2024.

[78] Carlton M. Caves. Quantum-mechanical noise in an interferometer. *Phys. Rev. D*, 23(8):1693–1708, April 1981.

[79] Roman Schnabel, Nergis Mavalvala, David E. McClelland, and Ping K. Lam. Quantum metrology for gravitational wave astronomy. *Nat. Commun.*, 1(121):1–10, November 2010.

[80] A gravitational wave observatory operating beyond the quantum shot-noise limit, December 2011. [Online; accessed 1. Feb. 2025].

[81] J. Appel, P. J. Windpassinger, D. Oblak, U. B. Hoff, N. Kjærgaard, and E. S. Polzik. Mesoscopic atomic entanglement for precision measurements beyond the standard quantum limit. *Proc. Natl. Acad. Sci. U.S.A.*, 106(27):10960–10965, July 2009.

[82] Hidetoshi Katori. Optical lattice clocks and quantum metrology. *Nat. Photonics*, 5:203–210, April 2011.

[83] Andrew D. Ludlow, Martin M. Boyd, Jun Ye, E. Peik, and P. O. Schmidt. Optical atomic clocks. *Rev. Mod. Phys.*, 87(2):637–701, June 2015.

[84] B. C. Nichol, R. Srinivas, D. P. Nadlinger, P. Drmota, D. Main, G. Araneda, C. J.

Ballance, and D. M. Lucas. An elementary quantum network of entangled optical atomic clocks. *Nature*, 609:689–694, September 2022.

[85] Jonathan A. Jones, Steven D. Karlen, Joseph Fitzsimons, Arzhang Ardavan, Simon C. Benjamin, G. Andrew D. Briggs, and John J. L. Morton. Magnetic Field Sensing Beyond the Standard Quantum Limit Using 10-Spin NOON States. *Science*, 324(5931):1166–1168, April 2009.

[86] W. Wasilewski, K. Jensen, H. Krauter, J. J. Renema, M. V. Balabas, and E. S. Polzik. Quantum Noise Limited and Entanglement-Assisted Magnetometry. *Phys. Rev. Lett.*, 104(13):133601, March 2010.

[87] Carlos A. Pérez-Delgado, Mark E. Pearce, and Pieter Kok. Fundamental Limits of Classical and Quantum Imaging. *Phys. Rev. Lett.*, 109(12):123601, September 2012.

[88] Marco Genovese. Real applications of quantum imaging. *J. Opt.*, 18(7):073002, June 2016.

[89] Paul-Antoine Moreau, Ermes Toninelli, Thomas Gregory, and Miles J. Padgett. Imaging with quantum states of light. *Nat. Rev. Phys.*, 1:367–380, June 2019.

[90] Samuel L. Braunstein and Carlton M. Caves. Statistical distance and the geometry of quantum states. *Phys. Rev. Lett.*, 72(22):3439–3443, May 1994.

[91] D. J. Wineland, J. J. Bollinger, W. M. Itano, F. L. Moore, and D. J. Heinzen. Spin squeezing and reduced quantum noise in spectroscopy. *Phys. Rev. A*, 46(11):R6797–R6800, December 1992.

[92] D. Leibfried, M. D. Barrett, T. Schaetz, J. Britton, J. Chiaverini, W. M. Itano, J. D. Jost, C. Langer, and D. J. Wineland. Toward Heisenberg-Limited Spectroscopy with Multiparticle Entangled States. *Science*, 304(5676):1476–1478, June 2004.

[93] Luca Pezzé and Augusto Smerzi. Entanglement, Nonlinear Dynamics, and the Heisenberg Limit. *Phys. Rev. Lett.*, 102(10):100401, March 2009.

[94] R. Augusiak, J. Kołodyński, A. Streltsov, M. N. Bera, A. Acín, and M. Lewenstein. Asymptotic role of entanglement in quantum metrology. *Phys. Rev. A*, 94(1):012339, July 2016.

[95] Julian Wechs, Hippolyte Dourdent, Alastair A. Abbott, and Cyril Branciard. Quantum

Circuits with Classical Versus Quantum Control of Causal Order. *PRX Quantum*, 2(3):030335, August 2021.

[96] Michael A. Nielsen and Isaac L. Chuang. *Quantum Computation and Quantum Information*. Cambridge University Press, 6 2012.

[97] John Preskill. Lecture notes for physics 229: Quantum information and computation. *California institute of technology*, 16(1):1–8, 1998.

[98] Benjamin Schumacher and Michael Westmoreland. *Quantum Processes Systems, and Information*. Cambridge University Press, Cambridge, England, UK, March 2010.

[99] Graeme Smith. Quantum Channel Capacities. *arXiv*, July 2010.

[100] A. S. Holevo. Quantum channel capacities. *Quantum Electron.*, 50(5):440, May 2020.

[101] A. S. Holevo. The capacity of the quantum channel with general signal states. *IEEE Trans. Inf. Theory*, 44(1):269–273, August 2002.

[102] Benjamin Schumacher and Michael D. Westmoreland. Sending classical information via noisy quantum channels. *Phys. Rev. A*, 56(1):131–138, July 1997.

[103] Seth Lloyd. Capacity of the noisy quantum channel. *Phys. Rev. A*, 55(3):1613–1622, March 1997.

[104] Alastair A. Abbott, Julian Wechs, Dominic Horsman, Mehdi Mhalla, and Cyril Branciard. Communication through coherent control of quantum channels. *Quantum*, 4:333, September 2020.

[105] Mateus Araújo, Adrien Feix, Fabio Costa, and Časlav Brukner. Quantum circuits cannot control unknown operations. *New J. Phys.*, 16(9):093026, September 2014.

[106] Giulio Chiribella and Hlér Kristjánsson. Quantum Shannon theory with superpositions of trajectories. *Proc. R. Soc. A.*, 475(2225), May 2019.

[107] Bob Coecke, Tobias Fritz, and Robert W. Spekkens. A mathematical theory of resources. *Inform. And Comput.*, 250:59–86, October 2016.

[108] Karl Pearson. X. on the criterion that a given system of deviations from the probable in the case of a correlated system of variables is such that it can be reasonably supposed to

have arisen from random sampling. *The London, Edinburgh, and Dublin Philosophical Magazine and Journal of Science*, 50:157–175, 7 1900.

[109] William G. Cochran. The χ^2 test of goodness of fit. *The Annals of Mathematical Statistics*, 23:315–345, 9 1952.